The structure and mechanism of SAICAR synthetase

by

Nathaniel Daum Ginder

A dissertation submitted to the graduate faculty

in partial fulfillment of the requirements for the degree of

DOCTOR OF PHILOSOPHY

Major: Biochemistry

Program of Study Committee:
Richard Honzatko, Major Professor
Herbert Fromm
Mark Hargrove
Nicola Pohl
Edward Yu

Iowa State University

Ames, Iowa

2008

UMI Number: 3308991

ProQuest Information and Learning Company
300 North Zeeb Road
P.O. Box 1346
Ann Arbor, MI 48106-1346

TABLE OF CONTENTS

Abbreviations

AICAR	5-aminoimidazole-4-carboxamide ribonucleotide
AIR	5-amino-imidazole- ribonucleotide
AMP, ADP, ATP	adenosine mono-, di-, triphosphate
CAIR	5-aminoimidazole-4-carboxy ribonucleotide
E. coli	Escherichia coli
eSS	E. coli SAICAR synthetase
GMP, GDP, GTP	guanosine mono-, di-, triphosphate
hSS	human SAICAR synthetase/AIR Carboxylase
IMP	Inosine monophosphate
k_{cat}	catalytic constant
K_I	inhibition dissociation constant
K_m	Michaelis constant
NADH	nicotinamide adenine dinucleotide (reduced)
1-PIMP	1- phosphoryl-IMP
N^5-CAIR	N^5-carboxy-5-aminoimidazole ribonucleotide
PAICAR	N-phosphoryl aicar
P_i	inorganic phosphate
6-PIMP	6-phosphoryl-IMP
PIX	Positional Isotope Exchange
PK/LDH	pyruvate kinase, lactate dehydrogenase
PRPP	5-phospho-α-D-ribosyl-1-pyrophosphate
SAICAR	5-aminoimidazole-4(N-succinylcarboxamide) ribonucleotide

tSS	Thermatoga maritima SAICAR Synthetase
ySS	Saccharomyces cerevisiae SAICAR synthetase

Abstract

SAICAR synthetase catalyzes the eighth step in bacterial de novo purine nucleotide biosynthesis: ATP + L-aspartate + CAIR → ADP + P_i + SAICAR Enzymes involved in nucleotide synthesis are common targets for chemotherapeutic and antimicrobial drugs. They work by reducing the rate of growth of rapidly proliferating cells, thus preventing tumor growth and microbial fecundity. L-Alanosine, an L-aspartate analogue that acts as a substrate for SAICAR synthetase, is a natural product with antiviral and antitumor activities. The product of the reaction is a potent inhibitor of adenylosuccinate synthetase and adenylosuccinate lyase and is responsible for L-alanosine toxicity. L-Alanosine may be effective as a chemotherapeutic agent in combination with other drugs for certain T-Cell lymphocyte tumors.

Crystal structures of E. coli SAICAR synthetase with CAIR revealed two new Mg^{2+} binding sites. The binding of CAIR and metals orders a loop (residues 35-39). Site-directed mutagenesis experiments and crystal structures reveal a role in L-aspartate binding for this loop. Analogs of CAIR (AICAR and IMP) are phosphorylated, as revealed by crystal structures, and likely mimic a putative phosphoryl intermediate of the substrate. Positional Isotope Exchange (PIX) experiments show migration of ^{18}O from the bridging position of γ-^{18}O-ATP to terminal positions of the β-phosphoryl group only in the presence of CAIR, indicative of the formation of a phosphoryl intermediate.

The enzyme from humans combines SAICAR synthetase and AIR carboxylase activities. The kinetic mechanism of human SAICAR synthetase was Steady State Ordered (CAIR first, ATP second, and L-aspartate last.) Elimination of AIR carboxylase activity by mutation or by direct inhibition causes a 10-fold difference in the “on” rate

constant for CAIR, suggesting a functional linkage between the AIR carboxylase and SAICAR synthetase active sites.

Chapter I. Introduction

Phosphoribosyl-aminoimidazole-succinocarboxamide synthetase [EC.6.3.2.6, 5'-phosphoribosyl-4-carboxy-5-aminoimidazole:L-aspartate ligase (ADP)] (SAICAR[1] synthetase) catalyzes the eighth step in bacterial de novo purine nucleotide biosynthesis:

ATP + L-aspartate + CAIR → SAICAR + ADP + P_i.

Lukens and Buchanan (1) first reported the enzymatic activity in 1959, and subsequently Miller and Buchanan (2) purified and reported properties of the enzyme from chicken liver. Patey and Shaw later determined that AIR carboxylase activity co-purified with SAICAR synthetase activity (3). More recently, the Davisson laboratory has determined kinetic parameters for the enzyme from chicken (4), and the Stubbe laboratory has done the same for the enzyme from E. coli (5). Nelson et al. marks the first time that a detailed kinetic study was performed and reports the kinetic mechanism to be Rapid Equilibrium Random (6). Structures have been reported of the unligated and adenine nucleotide complexes from Saccharomyces cerevisiae (7-10), adenine nucleotide complexes from Methanocaldococcus jannaschii (PDB identifiers 2YZL and 2ZO2), and unligated

[1] The abbreviations used are: SAICAR, 5-aminoimidazole-4(N-succinylcarboxamide) ribonucleotide; CAIR, 5-aminoimidazole-4-carboxy ribonucleotide; CAIRs, 5-aminoimidazole-4-carboxy ribonucleoside; AICARs, 5-aminoimidazole-4-carboxamide ribonucleoside; AICAR, 5-aminoimidazole-4-carboxamide ribonucleotide; AIR, 5-aminoimidazole ribonucleotide; N^5-CAIR, N^5-carboxy-5-aminoimidazole-4-carboxy ribonucleotide; aspartate, L-aspartate; Asp, L-aspartate; NAIR, 5-aminoimidazole-4-nitro ribonucleotide; PRPP, phosphoribosyl pyrophosphate eSS, Escherichia coli SAICAR synthetase; tSS, Thermatoga maritime SAICAR synthetase; ySS, Saccharomyces cerevisiae SAICAR synthetase; hSS, human SAICAR synthetase.

structures from Thermatoga maritima (11), Homo sapiens (12), and Geobacillus kaustophilus (PDB identifier 2YWV.)

The role of SAICAR synthetase in central metabolism makes it an important enzyme to most life forms. In fact all organisms, except some parasitic protozoa, have a de novo purine biosynthesis pathway with SAICAR synthetase activity. Some tumor cell lines do not have an intact salvage pathway and rely solely on de novo purine biosynthesis (13). Moreover, cells undergoing rapid growth such as tumors and bacterial infections rely on de novo nucleotide synthesis and inhibition of these enzymes has proven a useful strategy for chemotherapeutic drugs and antibiotics (13).

De novo Purine Biosynthesis:

The de novo purine biosynthesis pathway transforms PRPP to IMP, where it branches to steps specific for AMP and GMP synthesis. The pathway was first elucidated in the 1950s and early 1960s in the avian system by Buchanan and co-workers (1,2,14-16). Buchanan reported 10 enzymatic activities that were necessary for the conversion of PRPP to IMP. In contrast, 12 activities are involved in the pathway of micro-organisms (17,18). Using the E. coli gene nomenclature, PurT and PurK are the two additional activities. PurT and PurN appear redundant (the conversion of GAR to FGAR), but PurT uses formate as the formyl donor as opposed to N^{10}-formyl tetrahydrofolate (19-21). PurK was long thought to merely enhance CO_2 binding in micro-organisms; and in fact, cells are still able to grow with PurK knocked out under conditions of high CO_2 (22,23). In 1992, Stubbe found out that a stoichiometric ATP requirement was needed for PurK functionality (5) and later identified a new intermediate N^5-CAIR (24). Despite the

sequence homology of the enzymes that catalyze the formation of CAIR in microbial versus vertebrate systems, the enzymes catalyze different reactions. The enzyme is an N^5-CAIR mutase in microbial systems and an AIR carboxylase in the avian system.

Significance to Human Health

SAICAR synthetase is already a target in the treatment of cancer. L-Alanosine is a natural product of Streptomyces alanosinicus with antiviral and antitumor activities. L-Alanosine is a substrate analogue of L-aspartate in vitro and in vivo for SAICAR synthetase (6,25). The product of the L-alanosine reaction is L-alanosyl-5-amino-4-imidazolecarboxylic acid ribonucleotide, the compound responsible for L-alanosine toxicity and a potent inhibitor of adenylosuccinate synthetase and adenylosuccinate lyase (enzymes participating in de novo purine nucleotide biosynthesis) (25-27).

A complication of L-alanosine therapy is its comparable toxicity toward healthy and cancerous cells; however, specific cancers show enhanced susceptibility toward the toxic effects of L-alanosine. Methylthioadenosine phosphorylase (MTAP) is an important salvage enzyme for adenine nucleotides. The gene for MTAP in humans is proximal to tumor suppressor genes p15 and p16, and as a consequence, many tumor cells that lack one or more suppressor genes also have no gene for MTAP. Approximately 30% of T-cell acute lymphocytic leukemia lack the MTAP salvage pathway and rely entirely on de novo purine nucleotide biosynthesis for adenine nucleotides (13,28-31). L-Alanosine is toxic to cell lines of such cancers at concentrations well below those that poison cells with intact salvage pathways. Hence,

L-alanosine in combination with salvage pathway precursors of adenine nucleotides offers an effective therapy for these cancers (13,29-32).

Genetic Properties and Subunit Assembly of SAICAR synthetase

Because of the presence of gene fusions in purine biosynthesis in some organisms, it is useful to also consider the PurK and PurE activities when discussing the genetic properties of the SAICAR synthetase activity (PurC). In E. coli, and many other micro-organisms, PurK, PurE, and PurC all are individual peptides (18). PurK crystallizes as a homodimer (33) and PurE crystallizes as a homo-octamer (34). PurC was reported by Stubbe to be a homotrimer by analytical ultracentrifugation (5), but it was found to be a dimer when crystallized (35). The S. cerevisiae homologue crystallizes as a monomer (8,9).

In yeast and fungi, two genes, Ade1 and Ade2, are responsible for the transformation of AIR to CAIR. Ade1 has sequence homology to PurC, and the purified protein has SAICAR synthetase activity in in vitro experiments on purified proteins (36,37). Sequence homology indicates Ade2 is a gene fusion of PurK and PurE and has both activities in in vitro experiments conducted with purified protein (38,39). The same study showed that Ade2 has a native mass of 490 kDa, implying an octamer of 62 kDa subunits. This matches the oligomeric state of E. coli PurE (34) and the human bifunctional enzyme (12) and suggests a general scheme for subunit assembly around the PurE domain.

In 1973, Patey and Shaw observed that AIR carboxylase activity co-purified with SAICAR synthetase activity (3). Subsequently, functional complementation screening

showed that the gene in vertebrates is a fusion of SAICAR synthetase) and AIR carboxylase activities (40-43). The enzyme from chicken has a mass in excess of 330 kDa and possesses 6–8 identical subunits of 47 kDa (3,4). The human homologue of the protein has recently been crystallized as a homo-octamer (12).

Regulation of purine biosynthetic genes varies greatly among micro-organisms (18). The genes necessary to transform PRPP to IMP in E. coli are contained in seven operons. All, except for purA, have a common control site and are co-regulated by the repressor protein PurR. The free bases hypoxanthine and guanine bind directly to PurR and enhance its DNA binding properties, while nucleotides and other bases have no effect. Similar repression was observed in Salmonella typhimurium.

Bacillus subtilis, on the other hand, encodes all of the genes necessary to synthesize IMP from PRPP in a single operon (18). A PurR protein has also been identified for this organism, but it bears no structural or mechanistic similarities to the E. coli protein. It is regulated by specifically binding to PRPP which reduces the affinity of the protein for its DNA binding site.

The genes required for de novo AMP biosynthesis in Saccharomyces cerevisiae are called the ADE genes and are repressed at the transcriptional level by the presence of extracellular hypoxanthine and adenine (44). The proteins Bas1 and Bas2 activate transcription in vivo in the absence of these regulatory purine bases. A study by Som et al. (44) implicates the purine biosynthesis intermediate SAICAR in the Bas1 and Bas2 mediated activation of ADE transcription. When genes upstream of SAICAR synthetase in the pathway were knocked out, ADE gene repression was not reversed even when low levels of inhibitory purine bases were present in the media. When genes upstream of

SAICAR synthetase were knocked out, ADE genes were de-repressed even when high levels of inhibitory purines were present in the media. This suggests that SAICAR might be a signaling molecule for gene transcription, though no information was reported regarding the in vivo concentration of the molecule under the various experimental states. Moreover, in vitro experiments failed to show enhanced binding of Bas1 and Bas2 to their chromosomal binding sites in the presence of SAICAR. This could be because SAICAR is chemically transformed to a different metabolite or exists in a metal nucleotide complex. Alternately, a different protein might help to mediate the interaction. Only SAICAR synthetase and adenylosuccinate lyase are currently known to bind SAICAR.

Properties of the Chemical Reaction:

The reaction catalyzed by SAICAR synthetase is as follows:

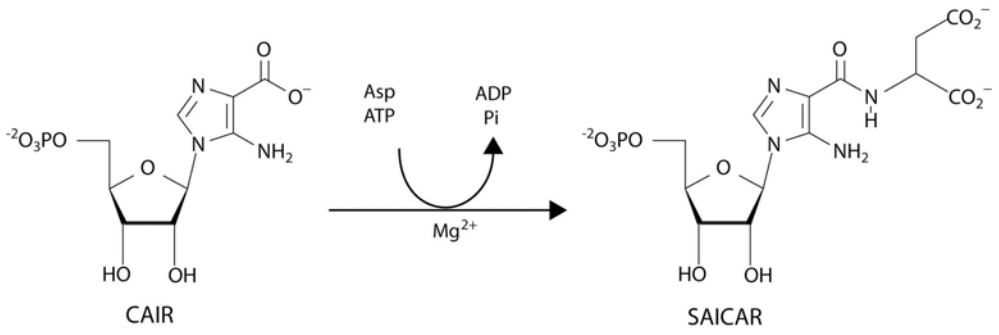

An extensive survey using analogues of CAIR demonstrated considerable promiscuity for this substrate (37). Some notable results were that 2'-deoxy-CAIR, 3'-deoxy-CAIR, and 5'-deamino-CAIR were all substrates. GTP and 2'-dATP can substitute for ATP in the reaction, while CTP and UTP inhibit the enzyme (36). Catalysis is supported by magnesium and manganese but is not supported by calcium (6). L-Aspartate and L-

alanosine are the only substrates for ligation that have been reported for the E. coli enzyme (6). L-malate is a substrate for the S. cerevisiae enzyme but not the E. coli enzyme (37).

Nelson et al. (6) determined the kinetic mechanism of the E. coli enzyme to be Rapid-Equilibrium Random. The K_m values for CAIR, ATP, and L-aspartate were 6.6 µM, 60 µM, and 790 µM, respectively, and k_{cat} was 9.0 s^{-1}. These values were all comparable to previous values published for E. coli PurC except that the K_m for CAIR is 6-fold lower (5,6). Two facts that could explain the discrepancy are that CAIR spontaneously decarboxylates (45), and the product, AIR inhibits SAICAR synthetase (6). V_{max} was achieved with 6 mM Mg^{2+}, which is in excess of the amount necessary to put all of the ATP into an $MgATP^{2-}$ complex (6). There are several possible explanations for this: 1) The enzyme could place the ATP in an unfavorable conformation for binding metal; 2) The enzyme might recognize a Mg^{2+}•CAIR complex for catalysis; 3) An additional Mg^{2+} binding site might exist on the enzyme; 4) Mg^{2+} might bind to the product SAICAR increasing the rate of release from the enzyme.

Kinetic constants from other organisms have also been reported. For yeast, the K_m values for CAIR, ATP, and L-aspartate were 1.6 µM, 14 µM, and 960 µM, respectively (36). The kinetic constants for the SAICAR synthetase activity of the bifunctional AIR Carboxylase/SAICAR synthetase enzyme from chicken have also been reported (4). This system provides problems for assaying the transformation of CAIR to SAICAR because AIR carboxylase rapidly decarboxylates CAIR to AIR. Firestine et al. (4) used NAIR, the 4-nitro analogue of CAIR, with the aim of specifically inhibiting the PurE activity so that PurC activity could be measured. In the presence of NAIR, the K_m

values for CAIR, ATP, and L-aspartate were 3 μM, 10 μM, and 1.4 mM, respectively, and k_{cat} was 3.6 s^{-1}.

Possible Chemical Mechanisms:

Coupling the hydrolysis of a nucleoside triphosphate to a ligation reaction is a common strategy in nature. The enzyme adenylosuccinate synthetase catalyzes one of the two reactions specific to de novo AMP biosynthesis (46-49):

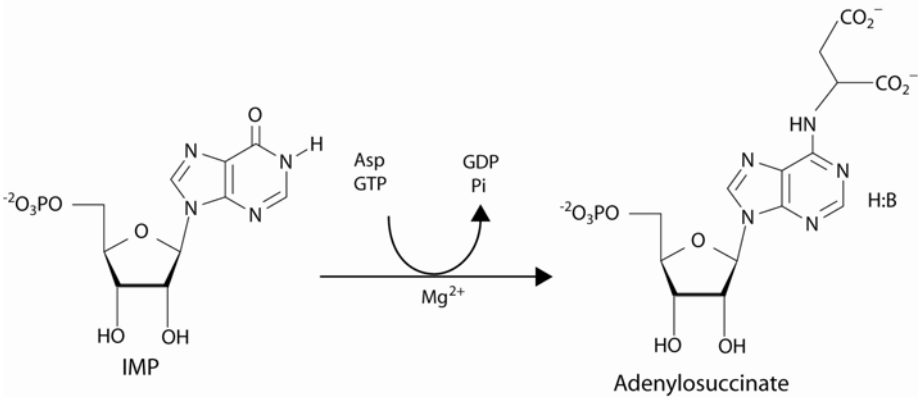

Adenylosuccinate synthetase putatively transfers the γ-phosphoryl group of GTP to the O-6 atom of IMP. The α-amino group of L-aspartate then attacks the resulting intermediate of 6-phosphoryl-IMP (6-PIMP), forming adenylosuccinate. 6-PIMP has been trapped in crystal structures of adenylosuccinate synthetases from several sources (50-52). Positional Isotope Exchange (PIX) experiments have provided evidence for the creation of a 6-PIMP (53), and a preferred flux through the random mechanism with IMP and GTP binding first was demonstrated with isotope exchange at equilibrium (54). Markham and Reed have suggested an alternative mechanism in which L-aspartate first reacts with IMP (55). The resulting intermediate has a nucleophilic 6-oxyanion that attacks the γ-phosphoryl group of GTP, forming a phosphoryl intermediate identical to

that created by the reaction of L-aspartate with 6-phosphoryl-IMP. No evidence exists, however, for a coupled L-aspartate-IMP intermediate.

Chemical Properties of CAIR:

A considerable amount of research has been done on the chemical and thermodynamic properties of CAIR and related compounds. Some of the results are useful in considering the chemical mechanism and natural substrates for SAICAR synthetase. CAIR is prone to decarboxylation to AIR, a precursor in de novo purine biosynthesis. This decarboxylation is catalyzed by acid and inhibited by the presence of transition metals (45). These crystalline transition metal complexes were later characterized, though their crystal structures were never solved (56,57). Shaw did not find Mg^{2+} to inhibit the decarboxylation, nor did he crystallize any nucleotide complexes with it. Some data regarding the effects of Mg^{2+} on the AIR carboxylase reaction may provide indirect data for an Mg^{2+}•CAIR complex in solution. In the AIR carboxylase reaction, the presence of Mg^{2+} both shifted the AIR/CAIR equilibrium away from AIR and decreased the rate of decarboxylation of CAIR to AIR, while having little impact on the rate of conversion of AIR to CAIR (4).

Studies reporting the tautomeric state of the exocyclic amine in 5'-aminoimidazole ribonucleotide (AIR) are also of interest. NMR studies of AIR give evidence for a 5-imino resonance form in aqueous solution. The resonances of atom H4 in ^{1}H NMR and of atom C4 in ^{13}C NMR are at unusually high field strengths, consistent with significant levels of the imino form of AIR (58). Slow chemical exchange of H4 hydrogen atoms with solvent deuterium further supports the presence of the imino form

of AIR. Although no data have been presented regarding resonance states of CAIR, a similar labilization of the C4 bond is observed in the facile decarboxylation of CAIR (45,59). Among researchers studying the AIR carboxylase reaction, there is interest in a proposed isoCAIR intermediate in the reaction (the tautomer of CAIR with an imino nitrogen in the 5 position and a tetrahedral carbon at C4) (60). Recently, discrete Fourier transform calculations were performed on CAIR and isoCAIR analogs (both bases had a methyl at the N1 position instead of a ribotide) and showed only a 3.1 kcal/mol higher value for the ground state energy for isoCAIR than CAIR (61). This shows that the formation of an imino might be on the same energy magnitude as the formation of a hydrogen bond. Such an imino resonance form could put more charge on the carboxyl group of CAIR increasing its nucleophilicity. This is illustrated in the proposed mechanism of Nelson et al. (6).

Structures of SAICAR Synthetases from other organisms:

Structures have been reported for the SAICAR synthetases of S. cerevisiae and T. maritima. The enzyme from yeast was first crystallized in 1996 (8). The fold was novel, but the domains bore similarities to other nucleotide binding proteins and are compared in detail in a subsequent publication (9). Interestingly, Domain B has similarities with other enzymes that couple peptide-formation to nucleoside triphosphate cleavage.

Complexes of the yeast enzyme with adenine nucleotides were subsequently reported (7). 1OBG was co-crystallized with ATP and Mg^{2+}, and the resulting complex had different crystal packing from the unligated structure, 1A48, and had AMP and sulfate bound to the enzyme. It is unclear why AMP was present because the hydrolysis

product of the enzyme is ADP. One possibility is that ADP was present but the adjacent sulfate ion competes with the β-phosphoryl group. 1OBD resulted from the soaking of ATP and Mg^{2+} into the 1A48 crystal form, and Mg^{2+}•ATP was observed in the active site. It is unclear whether this structure accurately represents the correct adenine-nucleotide-enzyme complex because the loop that is involved in phosphoryl binding also participates in a lattice contact in the unligated 1A48 structure, and its position was unchanged after the soak. An additional binding site for AMP distal from the active site was modeled into both structures. Generation of electron density maps revealed density for the nucleotide only in the 1OBG structure, and the generation of symmetry molecules showed that a lattice neighbor was hydrogen-bonded to the nucleotide. The different packing of 1OBD would preclude the formation of this interaction. There is no evidence from solution studies for an allosteric adenine binding site.

In all three structures, sulfate binds to several conserved residues in a location on the opposite side of the active site cleft from the adenine nucleotide. Two arginines and the positive dipole of a helix are oriented towards the sulfate. If the 5'-phosphoryl group of CAIR was positioned in this location, its carboxyl group would be placed near the phosphoryl chain of the adenine nucleotide. Attempts to crystallize in the presence of AICAR yielded significant density in this region, indicative of a phosphoryl group, but the density was weak for the ribose and absent for the base (10).

The structure of SAICAR synthetase from T. maritima has also been deposited as a part of the T. maritima structural genomics project (11). Different from yeast, the T. maritima enzyme is a dimer and is approximately 75 amino acids shorter. The chain length difference is clustered in four insertions. Notably, one of the insertions occurs in

the region of subunit association of T. maritima, possibly interfering with it, and another is in the C-terminal domain where significant conformational differences occur. The differences in the C-terminal domain of T. maritima place several conserved residues, which comprise the putative 5' phosphoryl binding site in yeast, away from the active site.

The crystal structure of human AIR carboxylase/SAICAR synthetase bifunctional enzyme revealed a. homo-octamer with the central organization around AIR carboxylase domains, similar to that of the E. coli PurE enzyme (12). SAICAR synthetase subdomains are at the periphery of the octamer and link up with neighboring subunits as observed for the E. coli SAICAR synthetase dimer. The AIR carboxylase/SAICAR synthetase octamer, however, has a set of channels that interconnect active sites, though there has been no biochemical evidence for channeling. In fact when the human bifunctional enzyme was incubated with AIR, HCO_3^-, L-aspartate, ATP, and Mg^{2+}, the rate of SAICAR production was increased 6-fold with the addition of eSS (4). This suggests that CAIR from the AIR carboxylase was released into the bulk solvent so that the added eSS could interact with it. The human enzyme is highly disordered in the SAICAR synthetase active site. Residues corresponding to 34–56 and 199–220 of the E. coli enzyme are without electron density in the human bifunctional enzyme, and many of these absent residues correspond to those that interact with CAIR. Additionally the average B-factor for residues 1-265 (corresponding to the SAICAR synthetase domain) is 63.4; while the B-factor for residues 266-425 (corresponding to the AIR carboxylase domain) is 35.6. This indicates an average B-factor that is nearly 2-fold larger for the

SAICAR synthetase domain. It is unclear what the source of this disorder is.

Thesis Organization

This thesis contains six chapters. Chapter I contains a literature review with some general information regarding the steps involved in converting AIR to SAICAR. Chapter II presents the structure of the E. coli enzyme with bound ligands and relates these findings to the proposed chemical mechanism. Chapter III presents a study of the kinetic mechanism of human SAICAR synthetase and demonstrates a linkage of functions in the bifunctional enzyme. Chapter IV includes structural and PIX data that supports a mechanism in which a phosphoryl intermediate is created prior to the attack by L-aspartate. Chapter V shows kinetic, as well as structural, evidence for the importance of the 30s loop in the role of binding aspartate. General conclusions from the research are presented in Chapter VI.

References

1. Nelson, S. W., Binkowski, D. J., Honzatko, R. B., and Fromm, H. J. (2005) Biochemistry 44(2), 766-774
2. Tyagi, A. K., and Cooney, D. A. (1980) Cancer Res 40(12), 4390-4397
3. Lukens, L. N., and Buchanan, J. M. (1959) J Biol Chem 234(7), 1791-1798
4. Miller, R. W., and Buchanan, J. M. (1962) J Biol Chem 237, 485-490
5. Patey, C. A., and Shaw, G. (1973) Biochem J 135(3), 543-545
6. Firestine, S. M., and Davisson, V. J. (1994) Biochemistry 33(39), 11917-11926
7. Meyer, E., Leonard, N. J., Bhat, B., Stubbe, J., and Smith, J. M. (1992) Biochemistry 31(21), 5022-5032
8. Antonyuk, S. V., Grebenko, A. I., Levdikov, V. M., Urusova, D. V., Melik-Adamyan, V. R., Lamzin, V. S., and Wilson, K. S. (2001) Crystallography Reports 46(4), 687-691
9. Levdikov, V. M., Grebenko, A. I., Barynin, V. V., Melik-Adamyan, W. R., Lamzin, V. S., and Wilson, K. S. (1996) Crystallography Reports 41(2), 275-286
10. Levdikov, V. M., Barynin, V. V., Grebenko, A. I., Melik-Adamyan, W. R., Lamzin, V. S., and Wilson, K. S. (1998) Structure 6(3), 363-376

11. Urusova, D. V., Antonyuk, S. V., Grebenko, A. I., Lamzin, V. S., and Melik-Adamyan, V. R. (2003) Crystallography Reports 48(5), 763-767
12. Zhang, R., Skarina, T., Evdokimova, E., Edwards, A., Savchenko, A., Laskowski, R., Cuff, M. E., and Joachimiak, A. (2006) Acta Crystallograph Sect F Struct Biol Cryst Commun 62(Pt 4), 335-339
13. Li, S. X., Tong, Y. P., Xie, X. C., Wang, Q. H., Zhou, H. N., Han, Y., Zhang, Z. Y., Gao, W., Li, S. G., Zhang, X. C., and Bi, R. C. (2007) J Mol Biol 366(5), 1603-1614
14. Batova, A., Diccianni, M. B., Omura-Minamisawa, M., Yu, J., Carrera, C. J., Bridgeman, L. J., Kung, F. H., Pullen, J., Amylon, M. D., and Yu, A. L. (1999) Cancer Res 59(7), 1492-1497
15. Levenberg, B., and Buchanan, J. M. (1957) J Biol Chem 224(2), 1019-1027
16. Hartman, S. C., and Buchanan, J. M. (1958) J Biol Chem 233(2), 451-455
17. Hartman, S. C., and Buchanan, J. M. (1959) J Biol Chem 234(7), 1812-1816
18. Kappock, T. J., Ealick, S. E., and Stubbe, J. (2000) Curr Opin Chem Biol 4(5), 567-572
19. Zalkin, H., and Dixon, J. E. (1992) Prog Nucleic Acid Res Mol Biol 42, 259-287
20. Nygaard, P., and Smith, J. M. (1993) J Bacteriol 175(11), 3591-3597
21. Thoden, J. B., Firestine, S., Nixon, A., Benkovic, S. J., and Holden, H. M. (2000) Biochemistry 39(30), 8791-8802
22. Marolewski, A., Smith, J. M., and Benkovic, S. J. (1994) Biochemistry 33(9), 2531-2537
23. Gots, J. S., Benson, C. E., Jochimsen, B., and Koduri, K. R. (1977) Ciba Found Symp (48), 23-41
24. Gots, J. S., Benson, C. E., Jochimson, B., and Koduri, K. R. (1976) Purine and Pyrimidine Metabolism, Elsevier, Amsterdam
25. Mueller, E. J., Meyer, E., Rudolph, J., Davisson, V. J., and Stubbe, J. (1994) Biochemistry 33(8), 2269-2278
26. Anandaraj, S. J., Jayaram, H. N., Cooney, D. A., Tyagi, A. K., Han, N., Thomas, J. H., Chitnis, M., and Montgomery, J. A. (1980) Biochem Pharmacol 29(2), 227-245
27. Casey, P. J., and Lowenstein, J. M. (1987) Biochem Pharmacol 36(5), 705-709
28. Illei, P. B., Rusch, V. W., Zakowski, M. F., and Ladanyi, M. (2003) Clin Cancer Res 9(6), 2108-2113
29. Batova, A., Diccianni, M. B., Nobori, T., Vu, T., Yu, J., Bridgeman, L., and Yu, A. L. (1996) Blood 88(8), 3083-3090
30. Efferth, T., Gebhart, E., Ross, D. D., and Sauerbrey, A. (2003) Biochem Pharmacol 66(4), 613-621
31. Li, W., Su, D., Mizobuchi, H., Martin, D. S., Gu, B., Gorlick, R., Cole, P., and Bertino, J. R. (2004) Oncol Res 14(7-8), 373-379
32. Efferth, T., Miyachi, H., Drexler, H. G., and Gebhart, E. (2002) Blood Cells Mol Dis 28(1), 47-56
33. Thoden, J. B., Kappock, T. J., Stubbe, J., and Holden, H. M. (1999) Biochemistry 38(47), 15480-15492
34. Mathews, II, Kappock, T. J., Stubbe, J., and Ealick, S. E. (1999) Structure 7(11), 1395-1406

35. Ginder, N. D., Binkowski, D. J., Fromm, H. J., and Honzatko, R. B. (2006) J Biol Chem 281(30), 20680-20688
36. Ostanin, K. V., Alenin, V. V., Domkin, V. D., and Smirnov, M. N. (1989) Biokhimiia 54(8), 1265-1273
37. Alenin, V. V., Ostanin, K. V., Kostikova, T. R., Domkin, V. D., Zubova, V. A., and Smirnov, M. N. (1992) Biokhimiia 57(6), 845-855
38. Firestine, S. M., Misialek, S., Toffaletti, D. L., Klem, T. J., Perfect, J. R., and Davisson, V. J. (1998) Arch Biochem Biophys 351(1), 123-134
39. Schmuke, J. J., Davisson, V. J., Bonar, S. L., Gheesling Mullis, K., and Dotson, S. B. (1997) Yeast 13(8), 769-776
40. Minet, M., and Lacroute, F. (1990) Curr Genet 18(4), 287-291
41. Chen, Z. D., Dixon, J. E., and Zalkin, H. (1990) Proc Natl Acad Sci U S A 87(8), 3097-3101
42. Schild, D., Brake, A. J., Kiefer, M. C., Young, D., and Barr, P. J. (1990) Proc Natl Acad Sci U S A 87(8), 2916-2920
43. Iwahana, H., Honda, S., Tsujisawa, T., Takahashi, Y., Adzuma, K., Katashima, R., Yamaoka, T., Moritani, M., Yoshimoto, K., and Itakura, M. (1995) Biochim Biophys Acta 1261(3), 369-380
44. Som, I., Mitsch, R. N., Urbanowski, J. L., and Rolfes, R. J. (2005) Eukaryot Cell 4(10), 1725-1735
45. Litchfield, G. J., and Shaw, G. (1971) J Chem Soc (B), 1474-1484
46. Honzatko, R. B., Stayton, M. M., and Fromm, H. J. (1999) Adv Enzymol Relat Areas Mol Biol 73, 57-102, ix-x
47. Lieberman, I. (1956) J Biol Chem 223(1), 327-339
48. Fromm, H. J. (1958) Biochim Biophys Acta 29(2), 255-262
49. Honzatko, R. B., and Fromm, H. J. (1999) Arch Biochem Biophys 370(1), 1-8
50. Poland, B. W., Bruns, C., Fromm, H. J., and Honzatko, R. B. (1997) J Biol Chem 272(24), 15200-15205
51. Choe, J. Y., Poland, B. W., Fromm, H. J., and Honzatko, R. B. (1999) Biochemistry 38(21), 6953-6961
52. Iancu, C. V., Borza, T., Fromm, H. J., and Honzatko, R. B. (2002) J Biol Chem 277(30), 26779-26787
53. Bass, M. B., Fromm, H. J., and Rudolph, F. B. (1984) J Biol Chem 259(20), 12330-12333
54. Cooper, B. F., Fromm, H. J., and Rudolph, F. B. (1986) Biochemistry 25(23), 7323-7327
55. Markham, G. D., and Reed, G. H. (1978) J Biol Chem 253(17), 6184-6189
56. Chipperfield, J. R., Humble, R. W., Iveson, G., Kadir, K., Mackenzie, G., and Shaw, G. (1987) Nucleosides and Nucleotides 6(1&2), 353-358
57. Chipperfield, J. R., Humble, R. W., Iveson, G., Kadir, K., Mackenzie, G., and Shaw, G. (1988) Nucleosides and Nucleotides 7(5&6), 571-576
58. Groziak, M. P., Bhat, B., and Leonard, N. J. (1988) Proc Natl Acad Sci U S A 85(19), 7174-7176
59. Groziak, M. P., Huan, Z. W., Ding, H., Meng, Z., Stevens, W. C., and Robinson, P. D. (1997) J Med Chem 40(21), 3336-3345

60. Constantine, C. Z., Starks, C. M., Mill, C. P., Ransome, A. E., Karpowicz, S. J., Francois, J. A., Goodman, R. A., and Kappock, T. J. (2006) Biochemistry 45(27), 8193-8208
61. Hoskins, A. A., Morar, M., Kappock, T. J., Mathews, II, Zaugg, J. B., Barder, T. E., Peng, P., Okamoto, A., Ealick, S. E., and Stubbe, J. (2007) Biochemistry 46(10), 2842-2855

Chapter II. Nucleotide Complexes of *Escherichia coli* Phosphoribosyl-Aminoimidazole-Succinocarboxamide Synthetase[†]

A paper Published in The Journal of Biological Chemistry[*]

Nathaniel D. Ginder, Daniel J. Binkowski, Herbert J. Fromm, and Richard B. Honzatko[‡]

Abstract

Phosphoribosyl-aminoimidazole-succinocarboxamide synthetase (SAICAR synthetase) converts 4-carboxy-5-aminoimidazole ribonucleotide (CAIR) to 4-(N-succinylcarboxamide)-5-aminoimidazole ribonucleotide (SAICAR). The enzyme is a target of natural products that impair cell growth. Reported here are the crystal structures of the ADP and the ADP•CAIR complexes of SAICAR synthetase from Escherichia coli, the latter being the first instance of a CAIR-ligated SAICAR synthetase. ADP and CAIR bind to the active site in association with three Mg^{2+}, two of which coordinate the same oxygen atom of the 4-carboxyl group of CAIR; whereas, the third coordinates the α- and β-phosphoryl groups of ADP. The ADP•CAIR complex is the basis for a transition-state model of a phosphoryl-transfer reaction involving CAIR and ATP, but also supports an alternative chemical pathway in which the nucleophilic attack of L-aspartate precedes the phosphoryl-transfer reaction. The polypeptide fold for residues 204–221 of the E. coli structure differs significantly from those of the ligand-free SAICAR synthetase from Thermatoga maritima and the adenine nucleotide complexes of the synthetase from Saccharomyces cerevisiae. Conformational differences between the E. coli, T. maritima,

and yeast synthetases suggest the possibility of selective inhibition of de novo purine nucleotide biosynthesis in microbial organisms.

[†]This work was supported in part by National Institutes of Health Research Grant NS 10546. We thank Dr. Jay Nix, who assisted with data acquisition and processing at Beamline 4.2.2 of the Advanced Light Source, Lawrence Berkeley Laboratory, and Professor S. Ramaswamy, Department of Biochemistry, University of Iowa, for providing synchrotron resources of the Molecular Biology Consortium. Coordinates and structure factors (accession labels 2GQR and 2GQS) for the structures described in this paper have been deposited in the Protein Data Bank, Research Collaboratory for Structural Bioinformatics (RCSB).

[*]Permission was not required for reprint of J. Biol. Chem., Vol. 281, Issue 30, 20680-20688
[‡]Corresponding author. Telephone: (515) 294-6116. Fax: (515) 294-0453. E-mail: honzatko@iastate.edu.

Abbreviations: SAICAR, 4-(N-succinylcarboxamide)-5-aminoimidazole ribonucleotide; CAIR, 4-carboxy-5-aminoimidazole ribonucleotide; AICAR, 5-aminoimidazole-4-carboxamide ribonucleotide; AIR, 5-aminoimidazole ribonucleotide; eSS, Escherichia coli SAICAR synthetase; tSS, Thermatoga maritima SAICAR synthetase; ySS, Saccharomyces cerevisiae SAICAR synthetase.

[2]Daniel J. Binkowski and Richard B. Honzatko, unpublished observations.

Introduction

Phosphoribosyl-aminoimidazole-succinocarboxamide synthetase [EC.6.3.2.6, 5'-phosphoribosyl-4-carboxy-5-aminoimidazole:L-aspartate ligase (ADP)] (SAICAR[1] synthetase) catalyzes the eighth step in bacterial de novo purine nucleotide biosynthesis:

ATP + L-aspartate + CAIR → ADP + P_i + SAICAR

Lukens and Buchanan (1) first described the enzyme in 1959. In 1962 Miller and Buchanan (2) demonstrated its presence in a variety of life forms and reported the purification and properties of the synthetase from chicken liver. More recently, the Stubbe laboratory purified SAICAR synthetase from Escherichia coli (3). The E. coli enzyme exhibits a rapid-equilibrium random kinetic mechanism (4). In contrast, the SAICAR synthetase from Saccharomyces cerevisiae is a monomer (5-8) and that from Thermatoga maritima a dimer (9). Comparable enzymes from vertebrates have masses in excess of 330 kDa and possess 6–8 identical subunits of 47 kDa (10,11). The vertebrate systems are bifunctional, combining 5-aminoimidazole ribonucleotide carboxylase (AIR carboxylase) and SAICAR synthetase activities (10-12).

L-Alanosine can replace L-aspartate as a substrate both in vitro and in vivo for SAICAR synthetase (4,13,14). The product of the SAICAR synthetase reaction, L-alanosyl-5-amino-4-imidazolecarboxylic acid ribonucleotide, is a potent inhibitor of adenylosuccinate synthetase and adenylosuccinate lyase, being the compound responsible for L-alanosine toxicity (13). Many cancers (approximately 30% of all T-cell acute lymphocytic leukemia, for instance) lack a salvage pathway for adenine nucleotides and rely entirely on de novo biosynthesis (15). L-Alanosine is toxic to cell lines of such cancers at concentrations well below those that poison cells with intact salvage pathways. Hence, L-alanosine may be effective as a chemotherapeutic agent in combination with other drugs (15).

Differences in subunit size, function, and assembly of microbial and vertebrate SAICAR synthetases suggest the potential for selective inhibition of SAICAR synthetases and, hence, the possibility of new antibiotics. Efforts to further develop

specific inhibitors of microbial SAICAR synthetases would benefit from a basic understanding of structure-function relations; however, for SAICAR synthetase such information is lacking. To this end, we report the structures of the ADP and ADP•CAIR complexes of E. coli SAICAR synthetase (hereafter, eSS). The latter complex is the first structure of a CAIR-bound SAICAR synthetase and reveals a previously unsuspected requirement for Mg^{2+} in the recognition of CAIR by the synthetase. (A total of three metal ions bind to the active site). The CAIR•ADP complex is consistent with a chemical mechanism composed of two partial reactions, a phosphoryl transfer from ATP and a nucleophilic attack by L-aspartate, but the relative order of the two reactions is unclear. Moreover, the conformation of eSS differs significantly from that of ligand-free SAICAR synthetase from T. maritima in the region of the CAIR binding site, suggesting the possibility of substrate-induced conformational changes in microbial synthetases.

Experimental Procedures

Materials— ATP, L-aspartate, NADH, phosphoenolpyruvate, pyruvate kinase, and lactate dehydrogenase were purchased from Sigma. CAIR was synthesized as described previously (4). E. coli strain BL21(DE3) came from Invitrogen.

Enzyme Preparation— Selenomethionine-substitution in eSS employed the inhibition of methionine biosynthesis coupled with selenomethionine supplementation (16). BL21 DE3 cells were transformed with a pET 28b vector containing the eSS insert with an N-terminal hexahistidyl tag (4). All bacterial cultures contained 30 μg/mL kanamycin sulfate (Gibco). An overnight culture was prepared in LB media (Sigma), and the cells isolated by centrifugation (1500xg for 10 min). The pellet was resuspended in 24 mL of

M9 media, supplemented with 1 mM $MgSO_4$, 0.3 mM $FeSO_4$, and 0.5 µM thiamin. Four mL of inoculant were added to each of 6 flasks containing 650 mL of M9 media with the same supplements. The flasks were shaken at 37 °C to an OD_{600} of 0.8. The temperature was adjusted to 16 °C, and 35 mg each of L-leucine, L-isoleucine, and L-valine, and 65 mg each of L-phenylalanine, L-lysine, and L-threonine were added as solids to each flask. After shaking for 20 minutes, 2 mL of a 20 mg/mL solution of L-selenomethionine was added to each flask. IPTG was added to a final concentration of 0.5 mM after an additional 15 minutes of agitation. Cells were isolated after 18 hrs. by centrifugation (1500xg, 10 min), resuspended in 10 mM KP_i (pH 7.0), centrifuged again, and finally resuspended in 100 mL lysis buffer containing 50 mM KP_i, 300 mM NaCl, and 10 mM imidazole (pH 8.0). Cells were disrupted by sonication in the presence of 0.25 mg/mL lysozyme, 50 µg/mL DNAase I, 1 mL of 100 mM phenylmethanesulfonyl fluoride (PMSF) in isopropanol, and 5µg/mL leupeptin. The lysate was centrifuged (33,000xg, 1 hr.) and the supernatant fluid loaded onto 25 mL of Ni-nitrilotriacetic acid (NTA) agarose (Novagen), pre-equilibrated in lysis buffer. The column was washed sequentially with 2 column volumes each of lysis buffer, lysis buffer containing 20 mM imidazole, and lysis buffer containing 40 mM imidazole. eSS was subsequently eluted from the column with lysis buffer containing 250 mM imidazole. Immediately upon elution, dithio-threitol (DTT) and ethylenediaminetetraacetic acid (EDTA) were added to the fractions to final concentrations of 5 mM and 10 mM, respectively. Fractions were pooled and dialyzed overnight in buffer containing 15 mM Tris·HCl, 25 mM KCl, 5 mM $MgCl_2$, 5 mM dithiothreitol, and 5 mM EDTA (pH 8.0). Non-selenomethionine substituted protein was

prepared using an identical protocol, except cell growth and expression was done in LB media, and no amino acid supplements were added.

Protein concentration was determined by the method of Bradford (17) using bovine serum albumin as a standard. Protein purity was confirmed by sodium dodecylsulfate polyacryl-amide gel electrophoresis (SDS-PAGE) (18). Mass determinations of purified protein were done by the Iowa State University core facility using an Applied Biosystems Voyager System 6075 Matrix Assisted Laser Desorption/Ionization-Time-of-Flight Mass Spectrometer (MALDI-TOF MS). The specific activity of eSS was determined using previously described assay conditions (4) with substrate concentrations of 360 μM ATP-Mg^{2+}, 40 μM CAIR, and 5.6 mM L-aspartate. The dependence of velocity on the concentration of Mg^{2+} was investigated using the substrate concentrations of 300 μM ATP, 65 μM CAIR, and 7.5 mM L-aspartate, with concentrations of free-Mg^{2+} ranging from 90–7000 μM.

Crystallization— Crystals were grown by the method of hanging-drop vapor diffusion in VDX-plates (Hampton Research). Two μL of protein solution were mixed with 2 μL of well solution and allowed to equilibrate against 0.5 mL of well solution. For the ADP complex, a protein solution (15 mg/mL) was prepared in a buffer containing 15 mM Tris·HCl, 25 mM KCl, 55 mM $MgCl_2$, 50 mM ADP, 5 mM DTT, and 5 mM EDTA (pH 8.0). The protein solution for the CAIR•ADP complex was identical except for the addition of 1.5 mM CAIR and 10 mM L-aspartate and that the protein did not include selenomethione. Crystals used for this diffraction study grew from well solutions containing 3.4–3.8 M sodium formate and 50 mM Tris·HCl (pH 8.5).

Data Collection— For the ADP complex, crystals were transferred to a cryoprotectant solution containing 4 M sodium formate, 50 mM Tris·HCl pH 8.5, 25 mM $MgCl_2$, 25 mM ADP, and 10% (w/v) sucrose. This buffer was supplemented with 1 mM CAIR and 10 mM L-aspartate for the CAIR•ADP complex. After approximately 30 seconds of equilibration, crystals were plunged into liquid nitrogen.

For the ADP complex, MAD data were collected on Beamline 4.2.2 of the Advanced Light Source, Lawrence Berkley Laboratory. Complete anomalous sets were taken at wavelengths of peak absorbance, the inflection point, and remote from the absorption edge of Se. Data were indexed, integrated, scaled, and merged using d*trek (19). Intensities were converted to structure factors using the CCP4 (20) program TRUNCATE.

Data from the CAIR•ADP complex were collected at Iowa State University from a single crystal (temperature, 115 K) on a Rigaku R-AXIS IV++ rotating anode/image plate system using CuK_α radiation from an Osmic confocal optics system. Data were processed and reduced using the program package CrystalClear provided with the instrument. Intensities were converted to structure factors using the CCP4 program TRUNCATE.

Structure Determination and Refinement— Structure determination for the selenomethionine-replaced protein was accomplished using the SOLVE/RESOLVE software package (21,22). Electron density was modeled as polyalanine by RESOLVE, followed by manual fitting using Xtalview (23). Refinement was performed against the structure factors from the remote wavelength using CNS (24). Non-crystallographic restraints were not used during refinement. Refinement began with a cycle of simulated

annealing (starting temperature of 3500 K) with slow cooling in increments of 25 K to a final temperature of 300 K, followed by 100 steps of conjugate gradient energy minimization. Subsequent cycles had lower initial starting temperatures (as low as 500 K). Individual thermal parameters were refined after each cycle of simulated annealing and subject to the following restraints: bonded main-chain atoms, 1.5 $Å^2$; angle main-chain atoms, 2.0 $Å^2$; bonded side-chain atoms, 2.0 $Å^2$; and angle side-chain atoms, 2.5 $Å^2$. Water molecules were automatically added using CNS if a peak greater than 3.0σ was present in Fourier maps with coefficients $(F_{obs}–F_{calc})e^{i\alpha calc}$. Refined water sites were eliminated if they were further than 3.2 Å from a hydrogen-bonding partner or if their thermal parameters exceeded 50 $Å^2$. The contribution of the bulk solvent to structure factors was determined using the default parameters of CNS. Constants of force and geometry for the protein came from Engh and Huber (25) and those for ADP from CNS resource files with appropriate modification of dihedral angles of the ribosyl moiety to maintain a 2'-endo ring pucker.

For the native CAIR•ADP complex, molecular replacement was performed using AMORE with the ADP complex as the starting model. Refinement was performed using the methods employed for the ADP complex.

Routines in the CCP4 suite of programs were used in the calculation of surface areas and in the superposition of structures.

Results

Protein Preparation, Data Collection, and Structure Determination— Selenium-modified and native eSS were pure on the basis of sodium dodecylsulfate polyacrylamide

gel electrophoresis. The specific activity of the selenomethionine-substituted protein was 15±1 U/mg, comparable to that of the native protein (4). Mass spectrometry of native and selenomethionine-substituted proteins indicated 8.5 (relative to a maximum of 10) Se atoms per monomer. SOLVE initially located 17 Se sites, generating a phase set with a figure-of-merit of 0.37. Iterations of density modification by RESOLVE increased the figure-of-merit to 0.67. Statistics of data collection and refinement are in Tables I&II.

Overview of eSS Structure— An eSS homodimer occupies the crystallographic asymmetric unit. The subunits of the dimer are virtually identical with a superposition of all Cα atoms yielding a root-mean-squared deviation of 0.34 Å for both nucleotide complexes. No electron density is present for the polyhistidyl tag. Observable electron density begins with Met^{1} and continues to the C-terminus (Asp^{237}). Electron density is weak only for residues 35–39 of the ADP complex but strong for the same segment in the ADP•CAIR complex.

Domain 1 of the eSS fold (Fig. 1) consists of a β-sheet (strands β1−β3, β6, and β7) with its inter-strand connections (helix α1 and an anti-parallel loop β4–β5). Domain 2 consists of a β-sheet (strands β8–β13) and associated helices α2–α6. The beta sheet of Domain 1 curls (like the fingers of a right hand relative to its palm) over Domain 2, creating a cleft, half of which is filled by ADP-Mg^{2+} and the other half by CAIR. The subunits come together with two-fold symmetry forming a dimer that buries approximately 2400 $Å^2$ of surface in the interface.

The major structural difference between the ADP and ADP•CAIR complexes is the aforementioned levels of electron density associated with residues 35–39. Superposition of all Cα carbons of subunit A from the ADP and ADP•CAIR complexes

gives a root-mean-squared difference of 0.18 Å and a maximum displacement of 0.67 Å. The former value is comparable to the coordinate uncertainty of 0.25 Å determined by the CCP4 program SFCHECK. The high level of agreement occurs despite the difference in ligation, and infers selenomethionine substitution in the ADP complex causes little perturbation to the structure. The largest Cα displacements (0.7 Å) are in the loop (residues 124−130) that coordinates metal ions associated with CAIR and for residues in the vicinity of the 5'-phosphoryl group of CAIR. The conformation of the adenine nucleotide and its interactions with the protein are identical (within coordinate uncertainty) in the ADP and ADP•CAIR complexes.

Comparison of eSS to tSS— eSS (237 residues) and tSS (PDB identifier 1KUT, 230 residues) share 39% sequence identity. tSS, like eSS, is a dimer (Fig. 1). Cα atoms of the eSS and tSS subunits superimpose with a root-mean-squared deviation of approximately 1.2 Å, using the sequence alignment of Fig. 2; however, the polypeptide fold associated with segment 204–221 of eSS, which includes strand β13 and helix α5, differs strikingly from that of tSS (Figs. 1&3). The alternative fold of tSS exposes six hydrophobic residues and increases the solvent-accessible surface area of each subunit by approximately 1000 $Å^2$ (from 1220 $Å^2$ in eSS to 2200 $Å^2$ in tSS).

Unlike the alternative fold of tSS, the eSS fold has an extensive network of hydrogen bonds. Interacting residues fall in two clusters: Asp^{202}, Arg^{231}, and Thr^{205} and Arg^{39}, Asp^{175}, Arg^{199}, Asp^{210}, Lys^{211}, Asp^{212}, Arg^{213}, and Arg^{215}. The latter more extensive cluster apparently anchors helix α5 with respect to Domain 1 and Domain 2, while positioning hydrophilic side chains in the active site cleft of eSS. In contrast, helix α5 in tSS is displaced relative to that of eSS (Fig. 3), taking residues corresponding to

Arg^{199}, Lys^{211} and Arg^{215} away from the active site. Most of the residues in segment 204–221 of eSS are conserved among microbial SAICAR-synthetases; for instance, Asp^{175}, Arg^{199}, Asp^{210}, Lys^{211}, Asp^{212} and Arg^{215} are conserved and present in tSS.

Comparison of eSS to ySS— SAICAR synthetase from Sacharomyces cerivisae (ySS) has 69 more amino acids than eSS, appearing primarily as insertions before residues 1, 77, 105 and 221 of the E. coli synthetase (Figs. 1&2). Neglecting insertions, eSS and ySS are 27% identical in sequence, and superimpose with a root-mean-squared deviation of 3.3 Å. The first and second sequence insertions come together in ySS (PDB identifiers 1OBD, 1OBG, and 1A48), where they define a putative binding site for AMP. (AMP appears in good electron density only at a lattice contact in 1OBG. Hence, the functional significance of the first two insertions in the ySS sequence remains unclear). The third insertion occurs at the subunit interface of the eSS dimer and probably blocks the dimerization of ySS subunits. The fourth insertion extends the helix corresponding to α5 of eSS and the connecting segments at the N- and C-terminal ends of that helix. The fourth segment replaces residues 204–221 in eSS but nonetheless retains a functional active site.

Adenine nucleotide interactions— ADP-Mg^{2+} binds to eSS in an anti conformation (Fig. 4). Val^{15}, Leu^{24}, Leu^{26}, and Val^{81} are in contact with one side of the adenine base while Met^{86} packs against the other. Atom N1 of ADP binds to the backbone amide group of Leu^{84}, and the exocyclic amine, N6, binds to the backbone carbonyl group of Lys^{82} and the side chain of Gln^{69} (Table III). No side-chain interaction between atom N6 and the protein was reported for ySS (PDB identifiers 1OBG and 1OBD); however, His^{72} of ySS

structurally corresponds to Gln^{69} of eSS and is in a position to interact with the adenine nucleotide. This position is conserved as glutamine or histidine in microbial systems.

The ribosyl moiety is C2'-endo, as observed for the adenine nucleotides in ySS structures. Atom O2' of the ribose binds to Glu^{179}, corresponding to an equivalent interaction with Glu^{219} in ySS.

The polyphosphoryl group of the adenine nucleotide interacts with strands β1 and β2, which together constitute a P-loop motif (26,27). The α-phosphoryl group interacts with backbone amide groups of Lys^{11}, Ala^{12}, and Lys^{13}, with atom NZ of Lys^{13}, and with Mg^{2+} (hereafter, Mg^{2+} site-1). The β-phosphoryl group interacts with the backbone amide group and side-chain of Lys^{11}, the amino group of Lys^{123}, and Mg^{2+} site-1. Four water molecules complete the octahedral coordination sphere of the Mg^{2+} site-1 (Table IV). Lys^{13}, Glu^{179}, Lys^{177}, and Asp^{191} form additional hydrogen bonds with the hydrated magnesium.

Although adenine nucleotides in ySS and eSS are in proximity to corresponding residues, significant differences are evident. Structural superpositions using the β-sheet of Domain 2 reveal displacements in Domain 1 by as much as 4 Å, with the eSS structure being more tightly closed about its adenine nucleotide relative to the ySS structures. In 1OBD of ySS (ATP-Mg^{2+} introduced by soaking), a lattice neighbor hydrogen bonds with the P-loop and is in proximity to bound ATP-Mg^{2+}. In 1OBG (ATP-Mg^{2+} introduced by co-crystallization), the intrusive lattice contact is gone, but the active site has AMP and a sulfate anion. The α-phosphoryl group of ADP-Mg^{2+} in eSS, a sulfate anion in 1OBG, and a water molecule in 1OBD occupy corresponding sites; whereas, the

β-phosphoryl group of ADP-Mg^{2+} in eSS and the γ-phosphoryl group of ATP-Mg^{2+} in 1OBD occupy equivalent sites.

Interactions of CAIR— The CAIR molecule and its two associated Mg^{2+} atoms are covered by strong electron density (Fig. 5). The 5'-phosphoryl group of CAIR interacts with the side chains of Arg^{94}, Ser^{100} and Arg^{199} as well as backbone amide group of Ser^{100}. These interactions resemble those of the sulfate anion in ySS. The phosphoryl group is proximal to the N-terminal end of helix α2, a structural element often observed in the binding of phosphoryl groups (28). Hydrogen bonds between the 5'-phosphoryl group of CAIR and the protein involve only two of its terminal oxygen atoms; the third hydrogen bonds with a water molecule that in turn interacts with a hydrated Mg^{2+} associated with CAIR (hereafter, Mg^{2+} site-2).

The ribosyl moiety of CAIR is C2'-endo. Its 3'-hydroxyl group hydrogen bonds with Asp^{175} and its 2'-hydroxyl group interacts with Arg^{215} and the backbone carbonyl of Asp^{196}.

The base moiety of CAIR interacts extensively with the active site by way of octahedrally coordinated Mg^{2+} at site-2 and -3 (Fig. 6). The side chain of Glu^{90} bridges between the two metal sites, as do single oxygen atoms from the 4-carboxyl group of CAIR and the carboxyl side chain of Asp^{129}. Atom N3 of CAIR coordinates to Mg^{2+} site-2, while a formate molecule bridges Mg^{2+} site-1 and site-3. Water molecules occupy all other coordination positions of the metals, completing their octahedral coordination spheres.

Water molecules associated with metals at sites 2 and 3 hydrogen bond with Asp^{36} and Asp^{125}. In fact, the appearance of strong electron density for residues 35–39 in

the ADP•CAIR complex may be due to interactions of Asp^{36} with one water molecule in each of the inner coordination spheres of the metals (Fig. 7). Asp^{36} is in a loop that probably binds L-aspartate. The interactions of Asp^{36} appear in concert with several new hydrogen bonds between the backbone elements of Gly^{35}, Gly^{37}, Ala^{38}, and Arg^{39} and the side chain of Ser^{33}.

The high Mg^{2+} requirement for substrate recognition is consistent with findings from kinetics. Plots of reciprocal velocity vs. $1/[Mg^{2+}]$ and $1/[Mg^{2+}]^2$ are nonlinear; however, the plot of reciprocal velocity vs. $1/[Mg^{2+}]^3$ is linear with a regression r-value of 0.99 (data not shown).

Discussion

Nucleotide complexes presented here are probably the closest representations of a productive substrate-enzyme complex for a SAICAR synthetase to date. The number of direct hydrogen bonds between ADP-Mg^{2+} and protein in the eSS structure (a total of 12) exceeds that for the ySS structures (8 for 1OBD and 7 for 1OBG). Additional interactions may account for the more closed active sites in eSS relative to ySS complexes. Moreover, lattice contacts in 1OBD of ySS could prevent the relaxation of its P-loop in the presence of ATP-Mg^{2+}, and sulfate could well interfere with the recognition of the adenine nucleotide in all complexes of ySS. The recognition of the adenine nucleotide as observed in eSS may facilitate the binding of CAIR. The ADP•CAIR complex provides the first instance of an enzyme-bound CAIR molecule covered by strong electron density.

The reaction catalyzed by SAICAR synthetase could resemble that of adenylosuccinate synthetase, an enzyme involved in the first committed step in de novo AMP biosynthesis (29-31). Adenylosuccinate synthetase putatively transfers the γ-phosphoryl group of GTP to atom O6 of IMP. The α-amino group of L-aspartate then attacks the resulting phosphoryl intermediate (6-phosphoryl-IMP), forming adenylosuccinate. 6-Phosphoryl-IMP appears in crystal structures of adenylosuccinate synthetases from several sources (32-34). Kinetic experiments using positional isotope exchange (35) and isotope exchange at equilibrium (36) support this mechanism; however, no experiment has proven that 6-phosphoryl-IMP lies on the reaction pathway. Markham and Reed (37) have suggested an alternative mechanism in which L-aspartate first reacts with IMP. The resulting intermediate has a nucleophilic 6-oxyanion that attacks the γ-phosphoryl group of GTP, forming a tetrahedral intermediate identical to that created by the reaction of L-aspartate with 6-phosphoryl-IMP.

The two mechanisms as they pertain to the SAICAR synthetase reaction appear in Fig. 8. Unlike adenylosuccinate synthetase, no information is available regarding the intermediate generated in the active site of SAICAR synthetase. The electron-withdrawing effects of Mg^{2+} site-2 and site-3 should enhance the electrophilic properties of the carbon atom of the 4-carboxyl group. Conceivably then, L-aspartate could react with CAIR and form a dioxyanion intermediate, which in turn is phosphorylated by ATP. L-Aspartate, however, is present in the crystallization experiment, and yet no electron density appears for L-aspartate or the L-aspartate adduct of CAIR, suggesting the phosphorylation step precedes the nucleophilic attack of L-aspartate.

The ADP•CAIR structure is a reasonable starting point for modeling the transition state in the formation of a carbonyl phosphate intermediate (Fig. 9). The bridging oxygen atom between the β- and γ-phosphoryl groups of ATP coordinates the Mg^{2+} at site-1 and is in-line with the proximal oxygen atom of the 4-carboxyl group of CAIR. Terminal oxygen atoms of the γ-phosphoryl group of ATP hydrogen bond with Lys^{11}, Lys^{123}, and Lys^{177} and the metal ions at site-1 and site-3. The reaction coordinate is the movement of the γ-phosphorus atom of ATP through the plane defined by its terminal oxygen atoms.

Nelson et al. (4) suggested a catalytic abstraction of a proton from the 5-amino group of CAIR analogous to the abstraction of a proton from atom N1 of IMP by an aspartyl side chain in adenylosuccinate synthetase (31,38). No protein side chain of eSS, however, interacts or could be in a position to interact with the 5-amino group of CAIR. Furthermore, 4-carboxyimidazole ribonucleotide (CAIR without the 5-amino group) is a substrate for yeast SAICAR synthetase (14), again supporting the absence of any essential role for the 5-amino group of CAIR.

Other observations, however, caution against the complete dismissal of the 5-amino group of CAIR in the chemical mechanism. The 5-amino group of enzyme-bound CAIR is in a cluster of water molecules and probably has an environment similar to that of CAIR in solution. Even in solution, the 5-imino form of CAIR may be dominant. NMR resonances of atom H4 and atom C4 of AIR (CAIR without a carboxyl group) come at unusually high field strengths, consistent with the imino form (39). Slow chemical exchange of atom H4 of AIR with solvent deuterium further supports the imino form (39). Enhanced charge density at atom C4 would retard spontaneous decarboxylation of CAIR. Indeed, transition metals decrease decarboxylation rates

probably by stabilizing of the imino form of CAIR (40,41). Hence, Mg^{2+} site-2 and site-3 could stabilize the imino form as a means of protecting CAIR from spontaneous decarboxylation. The imino form of CAIR, as suggested by Nelson et al. (4), would also increase the dianionic form of the 4-carboxyl group and thereby enhance its nucleophilic properties.

Another mechanism by which the 5-amino group of CAIR could participate in the SAICAR synthetase reaction is by hydrogen bonding with L-aspartate. In this respect, differences in the active sites of the E. coli and yeast SAICAR synthetases are possible as malate is a substrate for the yeast (14) but not the E. coli enzyme (4).

The different folds for tSS and eSS present an intriguing issue: Does the solvent-exposed fold of tSS represent a functionally relevant state of microbial SAICAR-synthetases? Side-chain atoms in the eSS ADP complex move no further than 0.8 Å upon CAIR binding; whereas, in tSS they are up to 14 Å away from comparable positions. T. maritima is a thermophile, and elevated temperatures generally enhance hydrophobic and weaken electrostatic interactions. High temperatures, then, would increase the thermodynamic penalty associated with a fold that exposes hydrophobic residues (as observed in the tSS crystal structure) as well as reduce the importance of hydrogen bonds that evidently stabilize the eSS fold but are lacking in tSS. These factors might shift tSS toward an eSS-like fold at high temperatures but favor the observed tSS fold at low temperatures. Unfortunately, the specific activity for tSS at any temperature has not been reported (9).

The tSS structure could also represent a ligand-free conformation shared by most, if not all, microbial SAICAR synthetases. Adenine nucleotide binding could organize the

active site; but once organized, the enzyme would be meta-stable, returning to its less compact conformation on a time scale slow in comparison to catalytic events. The kinetic mechanism is rapid equilibrium random (4), but progress curves under specific conditions exhibit a significant lag phase[2]. The lag is consistent with a slow conformational transition from a catalytically nonfunctional to a functional state.

Vertebrate SAICAR synthetases differ fundamentally from their bacterial homologs in subunit organization (multimeric systems of perhaps eight subunits) and function (the vertebrate subunit combines SAICAR synthetase and AIR carboxylase activities). Hence, the alternative-folding phenomenon observed here for microbial systems may only be a remote possibility for vertebrate systems. Stabilization of this putative nonfunctional state of the bacterial system may be an effective strategy in the development of agents that selectively inhibit de novo purine biosynthesis in bacteria.

References

1. Lukens, L. N., and Buchanan, J. M. (1959) J Biol Chem 234, 1791-1798
2. Miller, R. W., and Buchanan, J. M. (1962) J Biol Chem 237, 485-490
3. Meyer, E., Leonard, N. J., Bhat, B., Stubbe, J., and Smith, J. M. (1992) Biochemistry 31, 5022-5032
4. Nelson, S. W., Binkowski, D. J., Honzatko, R. B., and Fromm, H. J. (2005) Biochemistry 44, 766-774
5. Levdikov, V. M., Grebenko, A. I., Barynin, V. V., Melik-Adamyan, W. R., Lamzin, V. S., and Wilson, K. S. (1996) Crystallography Reports 41, 275-286
6. Levdikov, V. M., Barynin, V. V., Grebenko, A. I., Melik-Adamyan, W. R., Lamzin, V. S., and Wilson, K. S. (1998) Structure 6, 363-376
7. Antonyuk, S. V., Grebenko, A. I., Levdikov, V. M., Urusova, D. V., Melik-Adamyan, V. R., Lamzin, V. S., and Wilson, K. S. (2001) Crystallography Reports 46, 687-691
8. Urusova, D. V., Antonyuk, S. V., Grebenko, A. I., Lamzin, V. S., and Melik-Adamyan, V. R. (2003) Crystallography Reports 48, 763-767
9. Zhang, R., Skarina, T., Evdokimova, E., Edwards, A., Savchenko, A., Laskowski, R., Cuff, M. E., and Joachimiak, A. (2006) Acta Crystallograph Sect F Struct Biol Cryst Commun 62, 335-339
10. Patey, C. A., and Shaw, G. (1973) Biochem J 135, 543-545

11. Firestine, S. M., and Davisson, V. J. (1994) Biochemistry 33, 11917-11926
12. Chen, Z. D., Dixon, J. E., and Zalkin, H. (1990) Proc Natl Acad Sci U S A 87, 3097-3101
13. Tyagi, A. K., and Cooney, D. A. (1980) Cancer Res 40, 4390-4397
14. Alenin, V. V., Ostanin, K. V., Kostikova, T. R., Domkin, V. D., Zubova, V. A., and Smirnov, M. N. (1992) Biokhimiia 57, 845-855
15. Batova, A., Diccianni, M. B., Omura-Minamisawa, M., Yu, J., Carrera, C. J., Bridgeman, L. J., Kung, F. H., Pullen, J., Amylon, M. D., and Yu, A. L. (1999) Cancer Res 59, 1492-1497
16. Van Duyne, G. D., Standaert, R. F., Karplus, P. A., Schreiber, S. L., and Clardy, J. (1993) J Mol Biol 229, 105-124
17. Bradford, M. M. (1976) Anal Biochem 72, 248-254
18. Laemmli, U. K. (1970) Nature 227, 680-685
19. Pflugrath, J. W. (1999) Acta Crystallogr D Biol Crystallogr 55, 1718-1725
20. 4, C. C. P. N. (1994) Acta Crystallogr D Biol Crystallogr 50, 760-763
21. Terwilliger, T. C., and Berendzen, J. (1999) Acta Crystallogr D50, 760-763
22. Terwilliger, T. C. (2000) Acta Crystallogr D Biol Crystallogr 56, 965-972
23. McRee, D. E. (1992) J Mol Graph 10
24. Brunger, A. T., Adams, P. D., Clore, G. M., DeLano, W. L., Gros, P., Grosse-Kunstleve, R. W., Jiang, J. S., Kuszewski, J., Nilges, M., Pannu, N. S., Read, R. J., Rice, L. M., Simonson, T., and Warren, G. L. (1998) Acta Crystallogr D Biol Crystallogr 54, 905-921
25. Engh, R. A., and Huber, R. (1991) Acta Crystallogr A47, 392-400
26. Dever, T. E., Glynias, M. J., and Merrick, W. C. (1987) Proc Natl Acad Sci U S A 84, 1814-1818
27. Saraste, M., Sibbald, P. R., and Wittinghofer, A. (1990) Trends Biochem Sci 15, 430-434
28. Hol, W. G., van Duijnen, P. T., and Berendsen, H. J. (1978) Nature 273, 443-446
29. Lieberman, I. (1956) J Biol Chem 223, 327-339
30. Fromm, H. J. (1958) Biochim Biophys Acta 29, 255-262
31. Honzatko, R. B., and Fromm, H. J. (1999) Arch Biochem Biophys 370, 1-8
32. Poland, B. W., Bruns, C., Fromm, H. J., and Honzatko, R. B. (1997) J Biol Chem 272, 15200-15205
33. Choe, J. Y., Poland, B. W., Fromm, H. J., and Honzatko, R. B. (1999) Biochemistry 38, 6953-6961
34. Iancu, C. V., Borza, T., Fromm, H. J., and Honzatko, R. B. (2002) J Biol Chem 277, 26779-26787
35. Bass, M. B., Fromm, H. J., and Rudolph, F. B. (1984) J Biol Chem 259, 12330-12333
36. Cooper, B. F., Fromm, H. J., and Rudolph, F. B. (1986) Biochemistry 25, 7323-7327
37. Markham, G. D., and Reed, G. H. (1978) J Biol Chem 253, 6184-6189
38. Honzatko, R. B., Stayton, M. M., and Fromm, H. J. (1999) Adv Enzymol Relat Areas Mol Biol 73, 57-102, ix-x
39. Groziak, M. P., Bhat, B., and Leonard, N. J. (1988) Proc Natl Acad Sci U S A 85, 7174-7176

40. Litchfield, G. J., and Shaw, G. (1971) J Chem Soc (B), 1474-1484
41. Groziak, M. P., Huan, Z. W., Ding, H., Meng, Z., Stevens, W. C., and Robinson, P. D. (1997) J Med Chem 40, 3336-3345
42. Kraulis, P. J. (1991) J Appl Crystallogr 24, 946-950

Table I. Statistics of data collection. Values for last shell are in parentheses.

	Inflection (E1)	Peak (E2)	Remote (E3)
Wavelength (Å)	0.97900	0.97884	0.98671
Resolution (Å)	46.4–2.00 (2.07–2.00)	46.4–2.20 (2.28–2.00)	46.4–2.00 (2.07–2.00)
Reflections measured	276309	215947	286076
Reflections unique	40967	31041	40775
Redundancy	6.74 (5.28)	6.96 (7.05)	7.02 (5.42)
% Completeness	99.7 (97.2)	100.0 (100.0)	99.6 (95.8)
R_{merge} [a]	0.133 (0.515)	0.107 (0.345)	0.067 (0.331)
I/σ(I)	7.9 (2.6)	10.3 (4.5)	16.3 (4.7)
f' (electrons)	-15.2	-9.45	-4.8
f" (electrons)	6.4	10.5	0.5

Table I. Footnotes.

[a] $R_{merge} = \Sigma_j\Sigma_i \mid I_{ij} - \langle I_j \rangle \mid / \Sigma_i\Sigma_j I_{ij}$, where i runs over multiple observations of the same intensity, and j runs over all crystallographically unique intensities.

Table II. Statistics of refinement.

	ADP complex	ADP•CAIR complex
Space Group	$P2_12_12_1$	$P2_12_12_1$
Unit Cell Parameters	a=59.42, b=67.13, c=148.5	a=59.43, b=67.12, c=149.3
Resolution	25–2.00 (2.07–2.00)	25–2.05 (2.12–2.05)
No. of Reflections	286076	205397
No. of Unique Reflections	40775	34593
% Completeness	99.6 (95.8)	90.4 (61.7)
R_{merge} [a]	0.067 (0.331)	0.059 (0.280)
No. of atoms	4207	4095
No of solvent sites	363	197
R_{factor} [b]	20.4	22.0
R_{free} [c]	24.0	26.3
Mean B for protein ($Å^2$)	25	31
Mean B for ligands ($Å^2$)	23	28
Mean B for waters ($Å^2$)	33	36
RMS deviations:		
Bond lengths (Å)	0.005	0.006
Bond angles (deg.)	1.3	1.3
Dihedral angles (deg.)	22.5	22.6
Improper angles (deg.)	1.98	1.86

Table II. Footnotes.

[a] $R_{merge} = \Sigma_j\Sigma_i \mid I_{ij} - \langle I_j \rangle \mid / \Sigma_i\Sigma_j I_{ij}$, where i runs over multiple observations of the same intensity, and j runs over all crystallographically unique intensities.

[b] $R_{factor} = \Sigma \parallel F_{obs} \mid - \mid F_{calc} \parallel / \Sigma \mid F_{obs} \mid$, where $\mid F_{obs} \mid > 0$.

[c] R_{free} based upon 10% of the data randomly culled and not used in the refinement.

Table III. Selected polar contacts involving ligands. Reported distances are for subunit A in the ADP•CAIR complex.

Ligand atom	Bonding partner	Distance (Å)
ADP:		
N1	Leu^{84} N	3.06
N6	Gln^{69} OE1	2.62
	Lys^{82} O	2.98
N7	Asp^{191} N	3.03
O2’	Glu^{179} OE2	2.92
O1A	Lys^{11} N	3.03
	Ala^{12} N	2.70
	Lys^{13} N	2.73
O2A	Lys^{13} NZ	2.78
O1B	Lys^{11} N	2.75
	Lys^{11} NZ	2.88
O2B	Lys^{123} NZ	2.91
CAIR:		
O3A	Ser^{100} OG	2.64
	Arg^{94} NH2	2.61
O2A	Arg^{94} NH1	3.15
	Ser^{100} N	2.93
	Arg^{199} NH1	2.96
O3'	Asp^{175} OD1	2.62
O2'	Arg^{215} NH2	2.77

Table IV. Coordination distances and coordinating atoms of Mg^{2+} at sites 1–3.

Mg^{2+} site-1		Mg^{2+} site-2		Mg^{2+} site-3	
ADP O2A	2.06	Asp^{129} OD2	2.12	Asp^{129} OD2	2.16
ADP O3B	2.11	Glu^{90} OE1	2.06	Glu^{90} OE1	2.17
Formate O1	2.05	CAIR O8	2.07	CAIR O8	2.12
Wat^{2}	2.12	CAIR N3	2.16	Wat^{11}	2.19
Wat^{3}	2.15	Wat^{9}	2.13	Wat^{12}	2.01
Wat^{4}	2.08	Wat^{10}	2.01	Formate O2	2.25

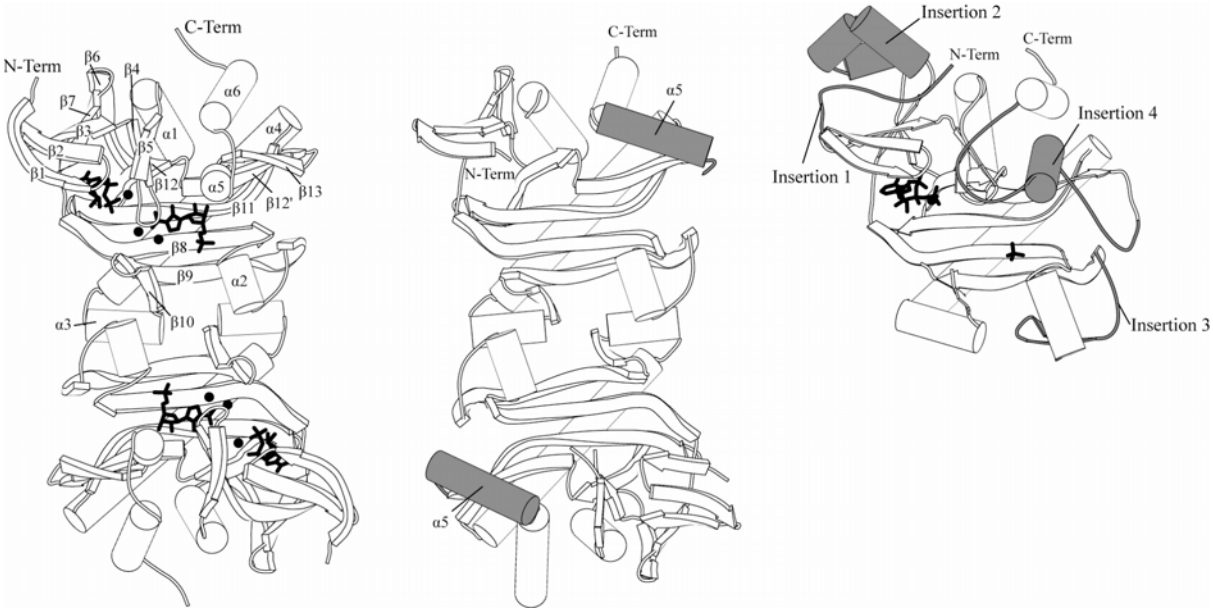

Figure 1. Structures of SAICAR synthetases. (left) The active site of eSS is a deep cleft that extends without interruption between subunits of the dimer. Bold lines and filled circles represent bound ADP-Mg^{2+} and CAIR-Mg^{2+}. (center) The schematic of tSS places the subdomain with the different fold (dark gray) in the context of the dimer. (right) The schematic of the ySS monomer reveals the structures of four sequence inserts (dark gray) described in the Results section. Parts of this figure were drawn with MOLSCRIPT (42)

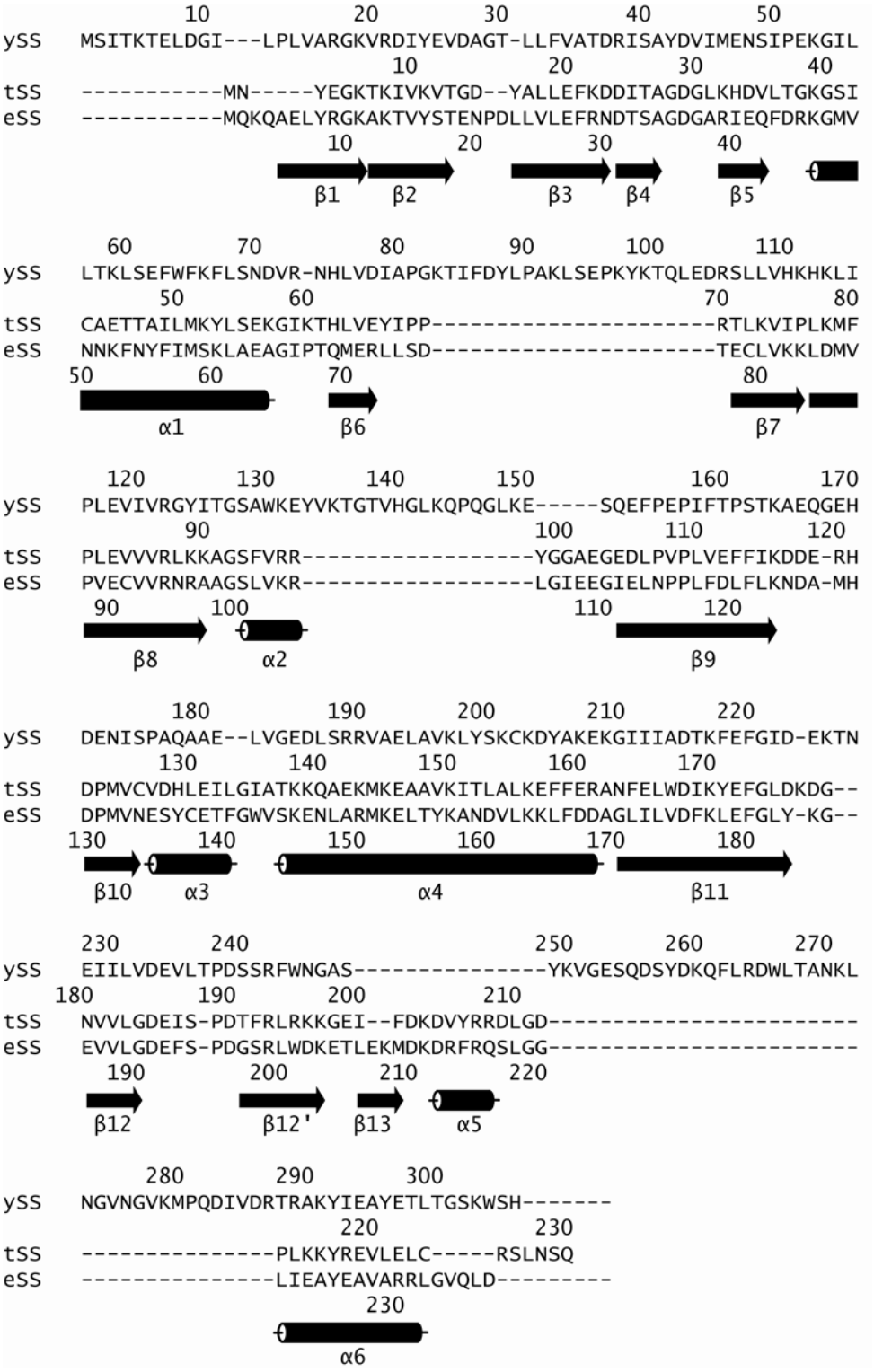

Figure 2. Sequence alignment based on structure. Superpositions of structures of SAICAR synthetase from yeast (ySS), T. maritima (tSS), and E. coli (eSS) determined corresponding residues. The relationship between elements of sequence and secondary structure (α-helices as cylinders and β-strands as arrows) of the E. coli synthetase appear immediately below its sequence.

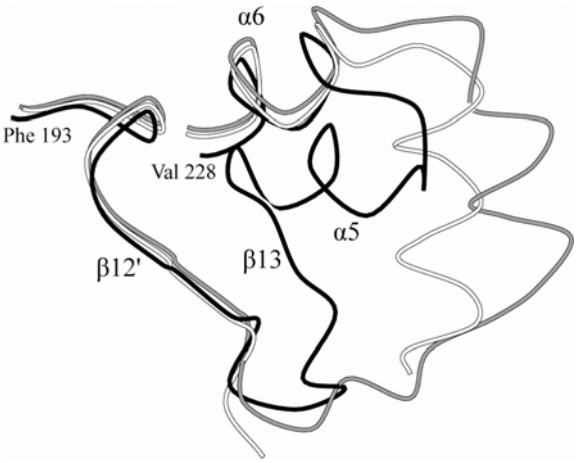

Figure 3. Variation in the folds of eSS and tSS. The superposition of subunits A and B of tSS onto eSS using the β-sheet of Domain 2 reveals significant variations between subunit A (white) and subunit B (gray) of tSS, as well as an even larger conformational difference between each of the tSS subunits and subunit A of eSS (black). Subunit B of eSS (not shown) is virtually identical in conformation to subunit A. Parts of this figure were drawn with MOLSCRIPT (42).

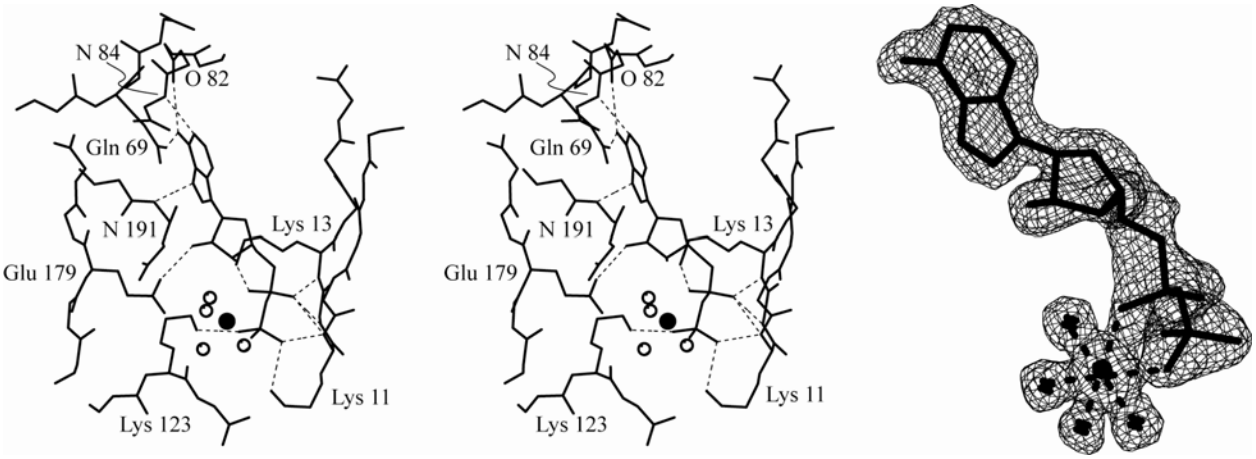

Figure 4. Enzyme-bound ADP. (left) Stereoview of ADP in which dotted lines represent donor-acceptor interactions. The filled circle represents Mg^{2+}, and open circles are water molecules coordinated to the metal. Parts of this figure were drawn with MOLSCRIPT (39). (right) Omit electron density covering the hydrated ADP-Mg^{2+} molecule bound at the active site of eSS. The contour level is at 1σ with a cutoff radius of 1 Å. Mg^{2+} is the filled circle and water molecules are crosses. Dotted lines indicate coordinate bonds to the metal. Parts of this figure were drawn with Xtalview (21).

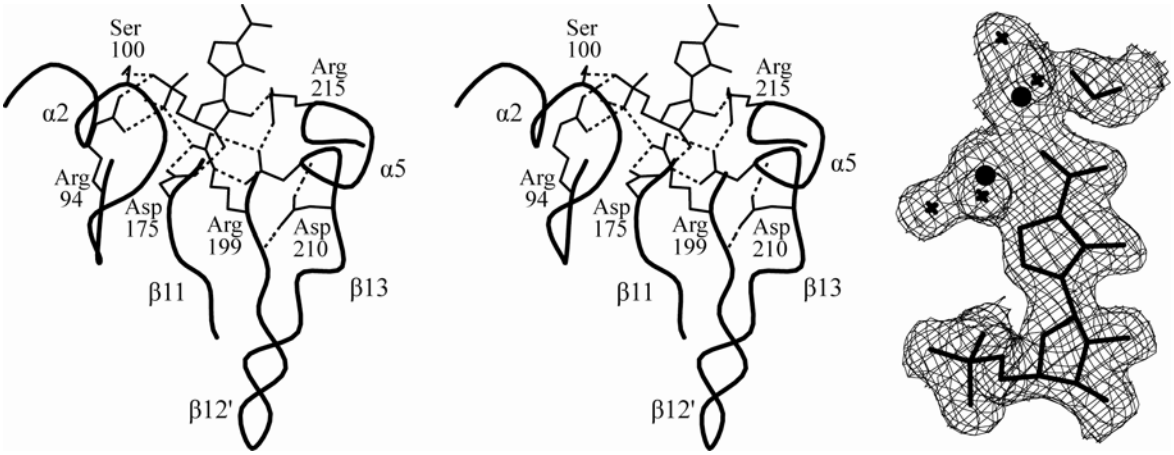

Figure 5. Enzyme-bound CAIR. (left) Stereoview of CAIR in which dotted lines represent donor-acceptor interactions. Asp^{212} is shown but not labeled. Parts of this figure were drawn with MOLSCRIPT (42). (right) Omit electron density (contour level of 1σ with a cutoff radius of 1 Å) covering formate, hydrated Mg^{2+} and CAIR. Filled circles are Mg^{2+}, and crosses are water molecules. Parts of this figure were drawn with Xtalview (23).

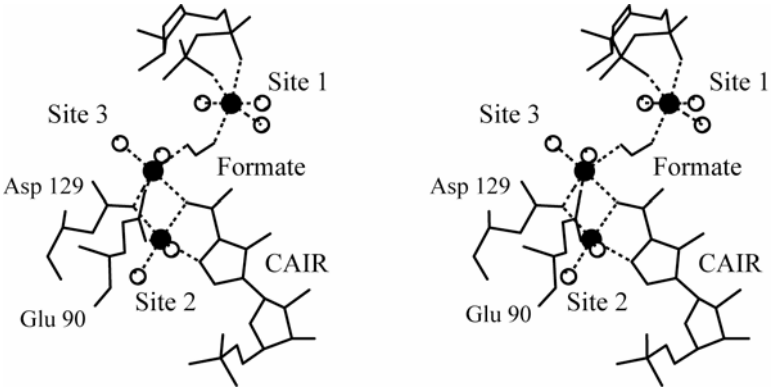

Figure 6. Stereoview of metal sites in the ADP•CAIR complex. Mg^{2+} and water molecules are filled and open circles, respectively. Coordination bonds are dashed lines. The adenine base is omitted for clarity. Parts of this figure were drawn with Molscript (42).

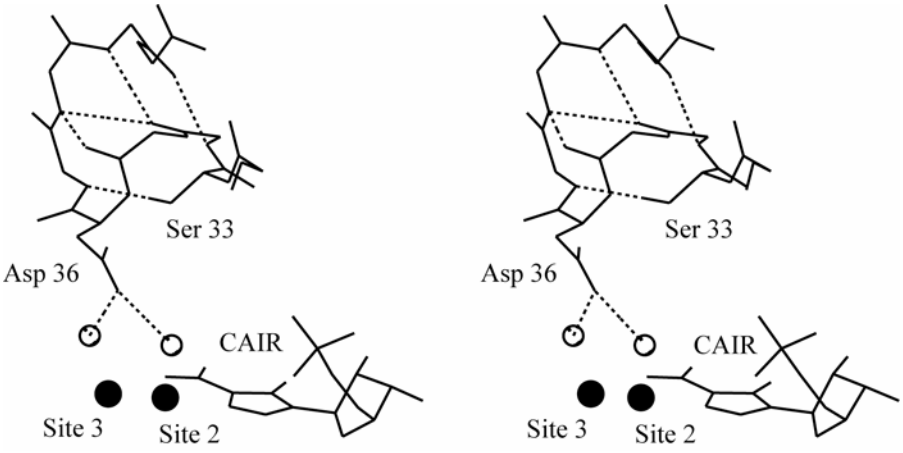

Figure 7. Stereoview of loop 32−40 of the ADP•CAIR complex. Side chains have been omitted except for Ser^{33} and Asp^{36}. Mg^{2+} are black spheres and water molecules are open spheres. Donor-acceptor are dotted lines. Parts of this figure were drawn with Molscript (42).

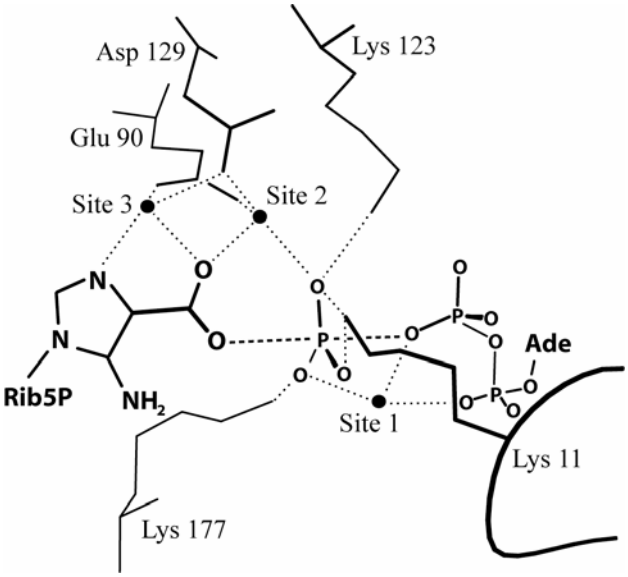

Figure 8. Model transition state for the phosphoryl transfer from ATP. See text for details.

Chapter III. Linkage of Function in Human AIR Carboxylase/SAICAR Synthetase[†]

Pending submission to Journal of Biological Chemistry

Daniel J. Binkowski, Nathaniel D. Ginder, Herbert J. Fromm and Richard B. Honzatko*

Abstract: In steps 6 and 7 of mammalian de novo nucleotide biosynthesis, a bifunctional enzyme converts 5-aminoimidazole ribonucleotide (AIR) to 4-carboxyl-5-aminoimidazole ribonucleotide (CAIR), and then CAIR to 5-aminoimidazole-4-(N-succinylcarboxamide) ribonucleotide (SAICAR). This, and other enzymes of purine nucleotide biosynthesis, are targets in the inhibition of growth in T-cell acute lymphoblastic lymphomas and of microorganisms injurious to human health. Data from initial velocity and inhibition kinetics shown here are consistent with a Steady State Ordered Sequential kinetic mechanism for human SAICAR synthetase activity with CAIR binding first, ATP second, and L-aspartate last. The kinetic mechanism for the human enzyme differs markedly from the Rapid Equilibrium Random Sequential mechanism reported for Escherichia coli SAICAR synthetase, and is consistent with a CAIR-induced conformational change that orders the active site of the human enzyme. Suppression of AIR carboxylase/CAIR decarboxylase activity in the human enzyme employed either a directed mutation (Lys^{304}→Ala) of the AIR carboxylase site or specific ligation of the AIR carboxylase pocket by NAIR, a slow, tight-binding inhibitor. The Michaelis constant for CAIR differs tenfold depending on whether the elimination of AIR

carboxylase activity is by inhibition or mutation. Ligation of the AIR carboxylase site by NAIR slows the rate of association of CAIR with the SAICAR synthetase pocket, indicating a functional linkage between the two active sites that maintains a constant flux through SAICAR synthetase.

---

[1]Abbreviations: 5-aminoimidazole-4-(N-succinylcarboxamide) ribonucleotide, SAICAR; 5-aminoimidazole-4-carboxy ribonucleotide, CAIR; 5-aminoimidazole-4-carboxamide-β-D-ribofuranoside, AICARs; 5-aminoimidazole ribonucleotide, AIR; 4-nitro-5-aminoimidazole ribonucleotide, NAIR; 5-(N-carboxy)-aminoimidazole-ribonucleotide, N^5-CAIR; ethylenediaminetetraacetic acid, EDTA. Escherichia coli SAICAR synthetase, eSS; Avian AIR carboxylase/SAICAR synthetase, avSS; Human SAICAR synthetase, hSSwt; Human SAICAR synthetase mutant Lys^{304}→Ala K304A, K304A, Ala304; Human SAICAR synthetase wild type with NAIR, hSSnair.

[2]Daniel J. Binkowski, Nathaniel D. Ginder, and Richard B. Honzatko, unpublished results.

Introduction

5-Aminoimidazole ribonucleotide 4-carboxylase/phosphoribosylaminoimidazole-succinocarboxamide synthetase (hereafter AIR[1] carboxylase/SAICAR synthetase), is a bifunctional enzyme that catalyzes steps 6 and 7 of mammalian de novo purine nucleotide biosynthesis (1-3):

$$AIR + CO_2 \rightarrow CAIR \qquad \text{AIR carboxylase}$$

$$CAIR + ATP + \text{L-aspartate} \rightarrow SAICAR + ADP + P_i \qquad \text{SAICAR synthetase}$$

In bacteria such as Escherichia coli, the conversion of AIR into SAICAR employs three single-function enzymes, PurK, PurE and PurC (4):

$$AIR + HCO_3^- + ATP \rightarrow N^5\text{-CAIR} + ADP + P_i \qquad N^5\text{-CAIR synthetase (PurK)}$$

N^5-CAIR → CAIR N^5-CAIR mutase (PurE)

CAIR + ATP + L-aspartate → SAICAR + ADP + P_i SAICAR synthetase (PurC)

Bacterial systems use ATP and bicarbonate in the generation of N^5-CAIR; whereas, vertebrate bifunctional enzymes use carbon dioxide and AIR directly without cofactors to make CAIR (5-8). Fungi such as Candida albicans and Cryptococcus neoformans combine the PurK and PurE activities in a single protein but retain a single-function enzyme for the synthesis of SAICAR from CAIR (9, 10).

Enzymes of de novo purine nucleotide biosynthesis are targets in the treatment of cancer and infectious disease. Many cancers, for instance, have damaged salvage pathways for purine nucleotides, and hence exhibit increased sensitivity to the inhibition of de novo purine nucleotide biosynthesis (11). L-Alanosine, an analog of L-aspartate, shows promise in treatments of leukemia and gliomas. SAICAR synthetase (in humans and bacteria) uses L-alanosine in forming 5-aminoimidazole-4-(N-alanosylcarboxamide) ribonucleotide, a potent inhibitor of adenylosuccinate synthetase and adenylosuccinate lyase (12-14). L-Alanosine toxicity is due to the blockage of de novo purine nucleotide biosynthesis, as supplemental doses of 2′-deoxyadenosine lessen toxicity. Treatments that employ L-alanosine and supplements of 2′-deoxyadenosine or methylthioadenosine analogs, however, selectively inhibit cancer cell lines deficient in methylthioadenosine phosphorylase (11).

Bacterial strains that are impaired in purine nucleotide biosynthesis can be effective inoculants against some strains of pathogenic bacteria. Blockage of purine

metabolism in Candida albicans and Crypotcoccus neoformans attenuates the virulence and invasiveness of the former (15) and moderates meningoenciphilitis infections in immune-compromised rodents caused by the latter (16). Virulence attenuation by removal of genes for purine nucleotide biosynthesis is also an attribute of Brucella species; vaccines against these infectious organisms are PurE knockouts (17-20).

Firestine and colleagues characterized avian AIR carboxylase/SAICAR synthetase and synthesized NAIR, a nitro analog of CAIR (7, 8, 21). Inhibition by NAIR and the source of carboxyl donor in the AIR carboxylase reactions differentiates vertebrate and bacterial AIR carboxylases. NAIR is a slow, tight-binding inhibitor of vertebrate AIR carboxylases, but a rapid-equilibrium inhibitor of bacterial enzymes (7, 21). Carbon dioxide is the carboxyl donor for vertebrate AIR carboxylases, but the bacterial enzyme uses bicarbonate (4, 8).

On the time scale of most laboratory experiments, NAIR binds irreversibly to the active site of AIR carboxylase, thereby eliminating the loss of CAIR due to the reverse (decarboxylation) reaction of the vertebrate bifunctional enzyme (7, 21). NAIR interferes with AIR carboxylase activity as an analog of AIR/CAIR, but does not inhibit the SAICAR synthetase activity of the Class-II bifunctional enzyme from chicken (7). Hence NAIR permits kinetic studies of the SAICAR synthetase reaction by inhibiting CAIR decarboxylation catalyzed by AIR carboxylase.

The structure of the human AIR carboxylase/SAICAR synthetase reveals a channel (9 Å minimum diameter, 70 Å length) between each AIR carboxylase/SAICAR synthetase active site of a homooctamer (23). CAIR produced in the AIR carboxylase site could travel directly to the SAICAR synthetase site without coming in contact with

the bulk solvent. Existing kinetics investigations, however, provide no support for channeling. With the AIR carboxylase site ligated by NAIR, CAIR from the bulk solvent still reaches the SAICAR synthetase active site (7). Herein we report the kinetic mechanism of the SAICAR synthetase reaction of the human enzyme with the AIR carboxylase pocket ligated by NAIR and with the same pocket impaired by the directed mutation of a conserved residue implicated in the binding of AIR and CAIR of the AIR carboxylase domain. The SAICAR synthetase activities of both forms of the enzyme are consistent with a Steady State Ordered Sequential kinetic mechanism, with CAIR first, followed by ATP and then L-aspartate; however, the K_m for CAIR is tenfold higher for the NAIR-ligated system relative to the mutant enzyme. This indicates that the SAICAR synthetase active site is sensitive to the functional status of the AIR carboxylase site. The increase in the K_m for CAIR in the presence of NAIR is not due to the binding of NAIR to the SAICAR synthetase pocket but most likely to a decrease in the rate of CAIR ligation of the SAICAR synthetase pocket.

Experimental

Materials—L-Aspartate, L-malate, maleate, ATP, NADH, phosphoenolpyruvate, pyruvate kinase and lactate dehydrogenase came from Sigma. L-Alanosine was obtained from the Drug Research and Development Branch, National Cancer Institute, Bethesda, MD. 5-Aminoimidazole-4-carboxamide-β-D-ribofuranoside (AICARs) was purchased from Toronto Research Chemicals. All other chemicals were reagent grade. The nucleoside precursor of NAIR and the human SAICAR synthetase gene (ADE2) were generous gifts from Dr. V. J. Davisson, Department of Medicinal Chemistry & Molecular

Pharmacology, Purdue University. Low-range molecular mass protein standards for SDS-PAGE came from Bio-Rad. Ampli-Taq DNA polymerase was purchased from Midwest Scientific. Restriction enzymes were purchased from New England Biolabs. Nickel-nitrilotriacetic acid-agarose resin and E. coli Rosetta (DE3) cells came from Novagen and Invitrogen, respectively. The Iowa State University DNA Sequencing and Synthesis Facility accomplished all primer synthesis and DNA sequencing for the confirmation of nucleic acid constructs.

Chemical Syntheses— NAIR was synthesized from its nucleoside precursor by the method of Yoshikawa (24). CAIR was synthesized by the methods of Firestine (7), which afford improved yields (>30%) relative to protocols published previously (4, 14). After lyophilization, CAIR was dissolved in 10 mM TAPS, pH 9.0, to prevent decarboxylation, and stored at –80 ºC. The concentration of CAIR was determined by the direct assay for organophosphate and by the coupling of ADP production to NADH conversion to NAD^+ by means of the pyruvate kinase/lactate dehydrogenase coupled enzyme assay (4, 14, 25). The concentration of NAIR was determined by the direct assay for organophosphate (14, 25). Multiple determinations of the concentrations of CAIR and NAIR are within 5% agreement for all studies reported here.

Subcloning and Directed Mutations— The original ADE2 gene was in a pET3a vector provided by V. J. Davisson. In order to facilitate rapid purification, the gene was transferred (using appropriate primers to incorporate cut sites NdeI and BamHI) to a pET24b vector bearing a C-terminal hexahistidyl tag. The resulting stop codon was removed by a point mutation affording an 8 amino acid linker between the last amino acid of the protein and the first histidine residue of the tag.

Construction of Lys304→Ala Enzyme— The mutation of Lys304 to alanine employed primers 5′-CTTCGAGTAACATCTGCGCATGCGGGACCAGATGAAACTCTGAGGATTAAAGC-3′ and 5′-GCTTTAATCCTCAGAGTTTCATCTGGTCCCGCATGCGCAGATGTTACTCGAAG-3′, where altered codons are in bold typeface. Protocols were used from the Stratagene Quick Change mutagenesis kit. Mutations were confirmed by DNA sequencing of the entire gene.

Purification of Recombinant Human AIR Carboxylase/SAICAR Synthetase— The tag-free form of the enzyme was isolated as a control to verify the properties of the C-terminal tagged protein. E. coli Rosetta cells were transformed with the pET3a vector containing the insert for untagged human SAICAR synthetase. Single colonies of each mutant were used to inoculate overnight cultures of Luria broth (LB) containing chloramphenicol (24 μg/mL) and ampicillin (100 μg/mL). Ten cultures of 800 mL LB in 2 L flasks were inoculated with the overnight culture and grown with shaking at 38 °C to an OD_{600} of 0.7, at which point the temperature was reduced to 16 ºC, followed by the induction of protein expression by the addition of 200 μL of 1 M isopropyl-β-D-thiogalactopyranoside (IPTG). Cells were collected 15 hrs post-induction, re-suspended in 50 mM Tris, pH 8.0, 2 mM EDTA, 5 μg/mL leupeptin, 1 mM phenylmethanesulfonyl fluoride (PMSF), and 0.25 mg/mL lysozyme, and then disrupted by French press at 4 ºC. After centrifugation (37000xg, 30 min.), streptomycin sulfate was added to the supernatant fraction with constant stirring to a final concentration of 1% (w/v). Precipitate was removed by centrifugation (37000xg, 15 min.), whereupon the supernatant fraction was subjected to

ammonium sulfate fractionation, retaining soluble protein between 22–32% saturation. Fractionated protein was dissolved in a minimal amount of 50 mM Tris, pH 8.0, 2 mM dithiothreitol (DTT), and 2 mM EDTA, and applied to a Sephacryl S-200 size exclusion column (2.5x80 cm) equilibrated with the same buffer. Fractions with substantial SAICAR synthetase and CAIR decarboxylase activities were pooled. Concentrated protein solution was applied to a DEAE cellulose column (2.5x50 cm.) equilibrated with 50 mM Tris, pH 8.0, 2 mM EDTA, and then eluted as pure enzyme by the same buffer. The enzyme was stored in this buffer without further dialysis. Protein purity was determined by sodium dodecylsulfate polyacrylamide gel electrophoresis (SDS-PAGE), and its concentration determined by method of Bradford using bovine serum albumin (BSA) as a standard (26).

Purification of C-terminal Polyhistidyl-tagged Wild-type and Mutant Human AIR Carboxylase/SAICAR Synthetase— C-terminal hexa-histidyl tagged clones (pET24b) were grown as above for the non-tagged protein using kanamycin (30 µg/mL) and no ampicillin. Cells were collected by centrifugation, re-suspended in lysis buffer (20 mM KP_i, 200 mM NaCl, 10 mM imidazole, pH 8.0, 5 µg/mL leupeptin, 1 mM phenylmethanesulfonyl fluoride (PMSF), 0.25 mg/mL lysozyme, and 50 µg/mL DNase I), and then disrupted by French press. After centrifugation (37000xg, 30 min) the supernatant fraction was loaded onto a column of nickel nitrilotriacetic acid (NTA)-agarose, equilibrated in 20 mM KP_i, 200 mM NaCl, and 10 mM imidazole, pH 8.0. The column was washed with 10 volumes of the equilibration buffer, and then the enzyme was eluted with 20 mM KP_i, 200 mM NaCl, and 250mM imidazole, pH 8.0. The protein was desalted by passage through a G-50 column (1.5x40 cm), equilibrated and run with

50 mM Taps, pH 8.5, 25 mM KCl, 2 mM EDTA, 2 mM dithiothreitol (DTT), and 20 mM sodium bicarbonate. Protein concentrations and purity were determined as above for the non-tagged enzyme.

Kinetics— Data were acquired by coupled and direct assays (4, 7, 14), using a Cary 100 Bio UV spectrophotometer. The coupled assay was verified over the pH range 5.5–11 by observing a linear relationship between enzyme concentration in the presence of saturating concentrations of substrates and the rate of disappearance of NADH, monitored at 340 nm. Analogs of ATP, CAIR, and L-aspartate were added individually at maximal concentrations with 100 μM ADP to verify the absence of inhibition of coupling enzymes. Assays performed on the wild-type enzyme in the presence of NAIR (done in triplicate) varied the concentration of one substrate while holding other substrates at $5xK_m$ (in studies involving inhibitors) or $10xK_m$ (in studies without inhibitors). Assays performed on the K304A mutant enzyme employed a fixed concentration of CAIR of 15 μM, which is at least a 20-fold excess over K_m. Details regarding the conditions of assay are in the legends of the figures. Assays of SAICAR synthetase activity (total volume of 1 mL) were performed in 50 mM Taps, pH 8.0, 10 mM $MgCl_2$, and 1 mM dithiothreitol (DTT) and initiated by the addition of enzyme to a final concentration of 4 μg/mL. Assays of CAIR decarboxylase activity were done in 50 mM Tris-HCl, pH 7.8, and 2 mM EDTA (prepared with water that had been boiled and degassed to remove dissolved CO_2) and initiated by the addition of enzyme to a final concentration 125 ng/mL. Direct and coupled assays were performed at 37 ºC with enzyme solutions stored on ice when not in use. Velocities for decarboxylase activity were based on an extinction coefficient of 11,500 $(cm\ M)^{-1}$, valid at pH 7.8, λ=250 nm.

For most assays, substrate concentrations change by less than 10% of their initial values. In such cases, data from linear progress curves provide measures of initial velocity, and such data were fit readily to the appropriate initial velocity models using software packages Grafit (27), Igorpro (Wavemetric, Inc.) and Dynafit (28). Initial concentrations of CAIR needed to determine its K_m for the Ala304 mutant enzyme were so low, however, that a 10% limiting depletion of substrate provided a signal too small for reliable detection. Progress curves for such assays were acquired to reaction endpoints (the equilibrium is far to the right due to the influence of the coupled assay), and the data fit to appropriate models by Dynafit (28, 29). In deciding the kinetic mechanism of inhibition, data were fit to models for competitive, uncompetitive, mixed and true noncompetitive inhibition. The best model was determined by Akaike weight (29) and lowest Chi-squared value, and when necessary, by the principle of Occam's Razor.

Dynamic Light Scattering— Protein samples were prepared by diluting recombinant wild type and K304A enzymes into filtered water to a final concentration of 1 mg/mL and a total volume of 1 mL. Centrifugation for 15 min removed insoluble debris from each sample. A sample of filtered and centrifuged water confirmed the cleanliness of the cuvette prior to its use in the determination of mass of the protein sample. A Protein Solutions Dynapro machine was used to collect and analyze light scattered from a 12 µL sample of dust-free mutant or wild type enzyme. Data were collected (approximately 400 scans) at 100% laser power at 25 ºC. Anomalous data were removed prior to the final mass calculations, using the Dynamics V6 software and an isotropic sphere model.

Results

Human SAICAR Synthetase Expression and Purification— Purification of non-tagged wild-type protein required 24 hours. The non-tagged recombinant enzyme had a k_{cat} one-third of that of the enzyme from chicken (7). The introduction of a C-terminal tag enabled rapid purification (3 hrs), improved yield by twofold, and increased k_{cat} by three-fold. The catalytic rate of the tagged human enzyme, then, is comparable to that of the native chicken enzyme (3.1–4 s^{-1}) (7). Eight liters of culture provided 250–300 mg of purified wild-type or K304A mutant enzyme with k_{cat} values of 3.6 ± 0.8 s^{-1} and 3.3 ± 0.3 s^{-1}, respectively (Table 1). Tagged and non-tagged systems were at least 95% pure by sodium dodecylsulfate-polyacrylamide gel electrophoresis (SDS-PAGE) (data not shown). The low specific activity of the non-tagged enzyme (not used in further investigations) was probably due to non-functional protein of identical or near-identical mass.

Elimination of CAIR Decarboxylation Activity— Decarboxylase activity in the chicken bifunctional enzyme is at least 50-fold faster than the consumption of CAIR in the synthesis of SAICAR (7). In order to avoid complications in determining the kinetic mechanism of human SAICAR synthetase, we eliminated CAIR decarboxylation by inhibition with NAIR and by directed mutation. The crystal structure of E. coli PurE (PDB accession identifier 1D7A) reveals Arg46 (corresponding to Lys304 of the human enzyme) in an interaction with the 5´-phosphoryl group of CAIR. Elimination of this interaction should lower the affinity of CAIR for the AIR carboxylase pocket in the bifunctional enzyme. Indeed, CAIR decarboxylase activity of the wild-type human enzyme exhibits a K_m for CAIR of 30 ± 3 μM and a k_{cat} of 130 ± 6 s^{-1}; whereas, the

K304A mutant enzyme exhibits decarboxylation rates of CAIR of ~0.002 s^{-1}, equivalent to the rate of decarboxylation of CAIR in the absence of enzyme. 10 μM NAIR reduces the rate of CAIR decarboxylation to baseline levels (~0.002 s^{-1}) as well. Concentrations of NAIR up to 250 μM have no observable effect on the rate of SAICAR synthesis of either the wild-type or K304A mutant enzyme. Hence the K304A mutant enzyme and the NAIR-ligated wild-type enzyme are distinct systems that allow the investigation of the SAICAR synthetase reaction in the context of a nonfunctional AIR carboxylase active site.

General Kinetic Properties of the Human Enzyme— Although a crystal structure of the human enzyme is available (23), the kinetic properties of human AIR carboxylase/SAICAR synthetase are not in the literature. The native masses of the polyhistidyl-tagged wild-type and K304A mutant enzyme as determined by dynamic light scattering are 380 ± 10 kDa for each protein. Native masses (and the specific activities) of the wild-type and mutant enzymes decrease during storage at 4 °C, a process accelerated at 25 °C. Hence, all work reported here uses enzyme aged not more than 36 hrs post-purification, and stored on ice before use in assays. As the calculated mass for the tagged subunit is 50 kDa, the values observed here are consistent with the 400 kDa expected mass for an octamer, which agrees with the oligomeric state observed in the crystal structure (23). Wild-type and K304A constructs showed optimum activity between pH 7.9–8.1.

Plausible Kinetic Mechanisms from Initial Velocity Studies— Initial velocity data with one substrate at saturation (10xK_m) and the systematic variation of the concentrations of the other two substrates about their K_m values appear in Figure 1. Two of three families

of Lineweaver-Burk plots clearly have a common point of intersection in quadrants 2 or 3. The third plot favors a family of parallel lines, but the alternate interpretation of a set of intersecting lines with the point of intersection deep into quadrant 3 is a possibility. The Lineweaver-Burk plots of Figure 1 excludes a Ping-Pong kinetic mechanism, as at least two and perhaps all three of the plots would be sets of parallel lines. Moreover, equations for Rapid Equilibrium Sequential mechanisms with ordered substrate binding or with any pair of substrates binding randomly (Random AB, Random BC, and Random AC) lack one or more terms necessary to account for the qualitative appearance of the plots in Figure 1. The Steady State Ordered Sequential mechanism (A first, B second, C last) is the simplest that accounts for the data of Figure 1:

$$\frac{V_{max}}{v} = 1 + \frac{K_a}{A} + \frac{K_b}{B} + \frac{K_c}{C} + \frac{K_{ia}K_b}{AB} + \frac{K_{ib}K_c}{BC} + \frac{K_{ia}K_{ib}K_c}{ABC} \qquad (1)$$

where v is the observed initial velocity, V_{max}, the maximal velocity, A, B, and C the concentrations of CAIR, ATP, and L-aspartate, respectively, and the kinetic parameters are combinations of elementary rate constants defined in Table 1 and by Scheme 1. The Rapid Equilibrium Random Sequential mechanism, however, is also consistent with the data of Figure 2, and results in a slightly more complex relationship:

$$\frac{V_{max}}{v} = 1 + \frac{K_a}{A} + \frac{K_b}{B} + \frac{K_c}{C} + \frac{K_aK_{bc}}{AB} + \frac{K_cK_{ab}}{AC} + \frac{K_bK_{ca}}{BC} + \frac{K_aK_{bc}K_{ic}}{ABC} \qquad (2)$$

Where v, V_{max}, A, B, and C are defined as in Equation 1, and the definition of kinetic parameters are given by Nelson et al. (14) and Fromm (30, 31). For the Rapid Equilibrium Random Sequential mechanism to account for the data of Figure 2c, parameter K_{ab} associated with the 1/AC term of Equation 2 must be near zero. K_{ab} near zero corresponds to virtually no dissociation of CAIR from the E•CAIR•ATP complex, a

distinct possibility if the enzyme stabilizes the carbonyl phosphate intermediate of CAIR to form a complex of E•CAIR-phosphoryl•ADP.

We choose the Steady State Ordered Sequential mechanism (Equation 1) to interpret the data of Figure 2 (the experimental justification for excluding the Rapid Equilibrium Random Sequential mechanism (Equation 2) comes in the next section.) A global fit of Equation 1 requires V_{max} from each plot of Figure 1 to be the same. As data sets were collected on different days and from different preparations of enzyme, the data of Figures 2a,b,&c were fit by Equations 3, 4 and 5, respectively.

$$\frac{V_{max}}{v} = 1 + \frac{K_a}{A} + \frac{K_b}{B} + \frac{K_{ia}K_b}{AB} \tag{3}$$

$$\frac{V_{max}}{v} = 1 + \frac{K_b}{B} + \frac{K_c}{C} + \frac{K_{ib}K_c}{BC} \tag{4}$$

$$\frac{V_{max}}{v} = 1 + \frac{K_a}{A} + \frac{K_c}{C} \tag{5}$$

Equations 3, 4 and 5 come from Equation 1 by eliminating the terms associated with the substrate at a saturating concentration. Parameters K_a, K_b, and K_c are the Michaelis constants for CAIR, ATP and L-aspartate, respectively. For a steady state mechanism, the Michaelis constants are not dissociation constants but depend, as shown in Table 1, on the off-rates of products as well as the on-rates of the substrates. Equations 3–5 provide two independent determinations of K_a, K_b, and K_c, and three determinations of k_{cat}, all of which are in reasonable agreement (Table 1).

The data in Figure 1 come from the NAIR-ligated enzyme. The low K_m for CAIR of the K304A mutant enzyme requires initial concentrations of CAIR too small for the accurate determination of product levels. (An alternative protocol presented in the next section, however, allows the determination of K_a, the K_m for CAIR). Nonetheless values

for K_b, K_c, and k_{cat} are available from experiments in which CAIR is at a saturating concentration ($10xK_m$). Assays which varied the concentration of CAIR place an upper limit of 1 μM on K_a (Table 1).

Inhibition Kinetics— The response of NAIR-ligated and K304A SAICAR synthetases to competitive inhibitors with respect to CAIR, ATP and L-aspartate can distinguish between the Steady State Ordered and the Rapid Equilibrium Random kinetic mechanisms. Moreover, the coupled assay pulls the reaction to completion, converting low initial concentrations of CAIR completely to product. The time dependence of product formation over the entire progress curve at different inhibitor concentrations also has the necessary information to make a determination of the kinetic mechanism of inhibition.

ADP cannot be used as a competitive inhibitor of ATP in these studies, as the assay couples to ADP production by SAICAR synthetase. Moreover, ADP at nonzero concentrations invalidates simplified steady-state initial velocity equations, which rest on the assumption of a product concentration of zero. AMP circumvents the forgoing problems, being a competitive inhibitor with respect to ATP (Figures 2e and 3e) and an uncompetitive inhibitor with respect to CAIR (Figures 2d & 3d). (Uncompetitive inhibition with respect to CAIR precludes an interaction of AMP at the CAIR pocket). IMP, a competitive inhibitor with respect to CAIR for E. coli SAICAR synthetase (14), has no effect on the wild-type or K304A enzymes. AICAR inhibition of the human systems is weak but competitive with respect to CAIR (Figures 2a & 3a). Maleate, a competitive inhibitor with respect to L-aspartate for the Ala304 mutant enzyme (Figure 3i), is a mixed inhibitor with respect to L-aspartate of the NAIR-ligated wild-type

enzyme. L-Malate, however, exhibits competitive inhibition with respect to L-aspartate of the NAIR-ligated wild-type enzyme (Figure 2i).

Analysis of data from Figure 3 and Figures 3b,c,e,f,h&i employs Equations 6–8, which together represent inhibition of the Steady State Ordered Sequential kinetic mechanism by competitive inhibitors of A, B or C from Scheme I:

$$\frac{V_{max}}{v} = 1 + \frac{K_a}{A}\left(1 + \frac{I_a}{K_{Ia}}\right) + \frac{K_b}{B} + \frac{K_c}{C} + \frac{K_{ia}K_b}{AB}\left(1 + \frac{I_a}{K_{Ia}}\right) + \frac{K_{ib}K_c}{BC} + \frac{K_{ia}K_{ib}K_c}{ABC}\left(1 + \frac{I_a}{K_{Ia}}\right) \quad (6)$$

$$\frac{V_{max}}{v} = 1 + \frac{K_a}{A} + \frac{K_b}{B}\left(1 + \frac{I_b}{K_{Ib}}\right) + \frac{K_c}{C} + \frac{K_{ia}K_b}{AB} + \frac{K_{ib}K_c}{BC}\left(1 + \frac{I_b}{K_{Ib}}\right) + \frac{K_{ia}K_{ib}K_c}{ABC} \quad (7)$$

$$\frac{V_{max}}{v} = 1 + \frac{K_a}{A} + \frac{K_b}{B} + \frac{K_c}{C}\left(1 + \frac{I_c}{K_{Ic}}\right) + \frac{K_{ia}K_b}{AB} + \frac{K_{ib}K_c}{BC} + \frac{K_{ia}K_{ib}K_c}{ABC} \quad (8)$$

In Equations 6–8, I_a, I_b, and I_c are the concentrations of competitive inhibitors of A (CAIR), B (ATP), and C (L-aspartate), respectively, and K_{Ia}, K_{Ib}, and K_{Ic} are dissociation constants for the competitive inhibitors of A, B, and C, respectively. All other terms are defined as in Equation 1. Fixing the concentrations of any two of three substrates simplifies Equations 6–8 to familiar relationships for inhibition of a one-substrate system: competitive, uncompetitive and non-competitive inhibition. For instance, fixing B and C in Equation 6 leads to Equation 9:

$$\frac{V_{max}}{v} = 1 + \frac{K_b}{B} + \frac{K_c}{C} + \frac{K_{ia}K_c}{BC} + \left(K_a + \frac{K_{ia}K_b}{B} + \frac{K_{ia}K_{ib}}{BC}\right)\left(1 + \frac{I_a}{K_{ia}}\right)\left(\frac{1}{A}\right) \quad (10)$$

Equation 9 is mathematically identical to competitive inhibition of a single substrate enzyme, except that the slope in a 1/v vs. 1/A plot depends on the fixed concentrations of B and C. Analysis of the data here employs standard models of inhibition for a single substrate system and hence inhibitor dissociation constants are apparent constants. To distinguish between Steady State Ordered and Rapid Equilibrium Random mechanisms,

the particular values of K_{Ia}, K_{Ib}, and K_{Ic} are unimportant; rather, the mechanism of inhibition for each of 9 sets of data (3 inhibitors x 3 pairs of fixed substrates) reveals the mechanism (30, 31). Using Dynafit (28), the data of each panel of Figure 2 and Figure 3b,c,e,f,h,&i were fit to models of competitive, uncompetitive, noncompetitive, and mixed inhibition of a single substrate system. The best-fitting models appear in Table 2. The occurrence of uncompetitive inhibition is inconsistent with the Rapid Equilibrium Random mechanism, but all patterns of inhibition are consistent with the Steady State Ordered mechanism.

In conducting initial velocity investigations of the K304A enzyme, however, all concentrations of CAIR were well above the determined value of K_c (Michaelis constant for CAIR). The extinction coefficient for NADH→NAD^+ precludes lower concentrations of CAIR, and fluorescence detection of NADH is not an option due to the self-quenching properties of NADH at high initial concentrations in the coupled assay. On the other hand, the high initial concentrations of NADH and PEP insure that the SAICAR synthetase assays run to completion in the presence of limiting concentrations of CAIR. Hence, Figure 4a,d&g represent data taken at fixed concentrations of CAIR and ($5xK_m$) for ATP and L-aspartate, while the concentrations of each of the three different inhibitors are varied. Fitting data to models of inhibition for a single-substrate enzyme allowed the determination of mechanism (Table 3). The K304A mutant enzyme likewise demonstrates the Steady State Ordered mechanism determined for the NAIR-ligated, wild-type enzyme.

Substrate Specificity and Inhibition by Dicarboxylic Acids— In searching for competitive inhibitors of L-aspartate, data were compiled that indicated significant differences in the

human systems (both NAIR-ligated wild-type and K304A enzyme) and E. coli SAICAR synthetase (Table 3). The human enzyme discriminates against L-alanosine (12–15-fold higher K_m than that of L-aspartate); whereas, the E. coli synthetase uses L-aspartate and L-alanosine with equal facility. L-Cysteine sulfinic acid is a substrate but exhibits substrate inhibition only for the NAIR-ligated wild-type human enzyme. Fumarate did not inhibit the three enzymes. Maleate and succinate are competitive inhibitors with respect to L-aspartate for the E. coli and K304A enzymes, but non-competitive inhibitors of the NAIR-ligated wild-type human enzyme. Non-competitive mechanisms are not due to the chelation of Mg^{2+} at high concentrations of ligand, as the mechanism remains competitive for the E. coli enzyme at comparable concentrations of ligand. L-Malate is a competitive inhibitor with respect to L-aspartate for all three systems.

Discussion

The study here is the first determination of a kinetic mechanism for a bi-functional SAICAR synthetase. The mechanism, Steady State Ordered Sequential with CAIR binding first, ATP second and L-aspartate last, differs from that of E. coli SAICAR synthetase which is Rapid Equilibrium Random Sequential. There is a precedent for enzymes from different organisms that catalyze identical chemical mechanisms having different kinetic mechanisms. Adenylosuccinate synthetases from human placenta and E. coli have Rapid Equilibrium Random mechanisms; whereas, the mechanism of the enzyme from Plasmodia falciparum is Ordered (32-34). Other examples include adenine phosphoribosyltransferases from Leishmania donovoni and Giardia lamblia, the former having an Ordered kinetic mechanism and the latter Random (35, 36).

Ordered and Random kinetic mechanisms fit well with the observed structures of E. coli SAICAR synthetase and human AIR carboxylase/SAICAR synthetase (23, 37). ADP and CAIR•ADP complexes of the E. coli enzyme are well ordered, with only a small region of disorder in the ADP complex associated with an element (residues 34–38) that may be critical in the recognition of L-aspartate (37). A Rapid Equilibrium Random kinetic mechanism does not exclude the possibility of a preferred pathway for the binding of substrates, and recent evidence from directed mutations of the active site suggest a dependence of L-aspartate association on the presence of CAIR, and perhaps even ATP[2].

The human enzyme, in contrast, is highly disordered in the SAICAR synthetase active site (23). Residues corresponding to 34–56 and 199–220 of the E. coli enzyme are without electron density in the human bifunctional enzyme, and many of these absent residues correspond to those that interact with CAIR. Figure 4 illustrates these portions of the protein. Additionally the average B-factor for residues 1-265 (corresponding to the SAICAR synthetase domain) is 63.4 $Å^2$; while the B-factor for residues 266-425 (corresponding to the AIR carboxylase domain) is 35.6 $Å^2$. This indicates an average B-factor that is nearly 2-fold larger for the SAICAR synthetase domain. It is unclear what the source of this disorder is. The SAICAR synthetase active site of the bifunctional human enzyme may require bound CAIR to induce order. The binding of ATP may be an obligatory second substrate, because its presence could lead to the formation of the carbonyl phosphate of CAIR. For the human enzyme, the carbonyl phosphate intermediate may be a prerequisite for the binding of L-aspartate. Indeed, L-aspartate is present in crystallization conditions in the CAIR•ADP complex of the E. coli enzyme but not bound to the active site (37). Hence, even for the E. coli enzyme, which has the

Random mechanism, L-aspartate may bind productively only after the phosphorylation of CAIR.

As the kinetic mechanism of SAICAR synthetase reaction catalyzed by the human bifunctional enzyme is steady state, the Michaelis constants (K_a, K_b, and K_c) listed in Table I are not dissociation constants of the respective substrates from the fully ligated enzyme complex. As indicated in Table I, K_a, K_b, and K_c depend on elementary rate constants for the association of substrates, and the release of products. One cannot simply ascribe a change in a Michaelis constant to an equilibrium-binding phenomenon as would be the case for a rapid equilibrium kinetic mechanism. The 10-fold increase in K_a (the Michaelis constant for CAIR) could arise from a complex variation in rate constants k_1, k_7, k_9, and k_{11} (Scheme I defines these elementary rate constant); but k_7, k_9, and k_{11} also appear in the definitions of k_{cat}, K_b and K_c. Hence, if k_7, k_9, and/or k_{11} change, then k_{cat}, K_a, K_b and K_c are all likely to change. A 10-fold change in K_a (Table 1) with no significant change in k_{cat} then is likely due to a change in k_1, the "on" rate for CAIR. In other words, the 10-fold increase in K_a for the NAIR-ligated AIR carboxylase/SAICAR synthetase relative to that of the K304A enzyme likely stems from a 10-fold decrease in k_1 of the NAIR-ligated system relative to that of the K304A system. Evidently, the SAICAR synthetase active site can sense the status of the AIR carboxylase active site. Differences in the kinetics of the two forms of the human enzyme studied here also extend to the recognition of dicarboxylic acid analogs of L-aspartate (Table 3): maleate is a competitive inhibitor with respect to L-aspartate in the K304A mutant but a noncompetitive inhibitor of the NAIR-ligated wild-type enzyme. Cysteine sulfinate is a

substrate for both human forms, but only the NAIR-ligated wild-type enzyme exhibits substrate inhibition.

Two mechanisms could account for the NAIR-dependent on rate for CAIR. On the basis of the recent crystal structure of the human enzyme, NAIR probably cannot directly impede the flow of CAIR to the SAICAR synthetase pocket. The AIR carboxylase/SAICAR synthetase octamer, however, has a set of channels that interconnect active sites (23). The ligation of the AIR carboxylase pocket by NAIR could impair mechanisms that facilitate the transport CAIR to the SAICAR synthetase pocket through these channels. If the rate of diffusion of CAIR from the bulk solvent to the SAICAR synthetase active site is less than the rate of transport through these channels, the presence of NAIR would increase the on rate for CAIR. Alternatively, NAIR ligation to the AIR carboxylase site may promote conformational disorder in the SAICAR synthetase active site. The decrease in the rate constant k_1 (the on-rate for CAIR) could reflect a NAIR-impeded reorganization of the SAICAR synthetase active site in response to the binding of CAIR. In fact, the linking element between the AIR carboxylase and SAICAR synthetase domains directly connects the NAIR and CAIR binding pockets (Fig 5).

The change in the Michaelis constant for CAIR at the SAICAR synthetase pocket may be a metering mechanism by which the bifunctional enzyme outputs a steady flow of SAICAR even as concentrations of CAIR fluctuate. This could be important if any of the metabolites downstream of CAIR in de novo purine nucleotide biosynthesis are toxic or if upstream metabolites participate in regulatory functions. In principle, AIR carboxylase activity overwhelms SAICAR synthetase activity when AIR and CO_2 levels are

sufficient. The AIR carboxylase activity of the bifunctional chicken enzyme, for instance, is 10-fold higher than its SAICAR synthetase activity when CAIR is removed from solution by exogenous E. coli SAICAR synthetase (8). Moreover, AIR carboxylase catalyzes its reverse reaction 4-fold faster than its forward reaction. Under circumstances of high concentrations of AIR and CO_2, then, either CAIR or AIR saturates the AIR carboxylase pocket, a condition perhaps mimicking the NAIR-ligated system. If flux through AIR carboxylase falls below that of SAICAR synthetase, however, the production of SAICAR will not diminish immediately. As local concentrations of CAIR fall, the association rate for CAIR (k_1 in the SAICAR synthetase reaction) increases and the K_m for CAIR falls. Consequently, the concentration of CAIR remains above its Michaelis constant, allowing the enzyme to operate at V_{max} over at least a 10-fold decline in the local concentration of CAIR. The Steady State Ordered mechanism may have evolved from a Rapid Equilibrium Random mechanism as a way to maintain even flux through the de novo pathway for purine nucleotide biosynthesis.

References

1. Miller, R. W., and Buchanan, J. M. (1962) Biosynthesis of the purines. 27. N-(5-Amino-1-ribosyl-4-imidazolylcarbonyl)-L-aspartic acid 5'-phosphate kinosynthetase. J Biol Chem 237, 485-90.
2. Lukens, L. N., and Buchanan, J. M. (1959) Biosynthesis of the purines. XXIII. The enzymatic synthesis of N-(5-amino-1-ribosyl-4-imidazolylcarbonyl)-L-aspartic acid 5'-phosphate. J Biol Chem 234, 1791-8.
3. Lukens, L. N., and Buchanan, J. M. (1959) Biosynthesis of the purines. XXIV. The enzymatic synthesis of 5-amino-1-ribosyl-4-imidazolecarboxylic acid 5'-phosphate from 5-amino-1-ribosylimidazole 5'-phosphate and carbon dioxide. J Biol Chem 234, 1799-805.
4. Meyer, E., Leonard, N. J., Bhat, B., Stubbe, J., and Smith, J. M. (1992) Purification and characterization of the purE, purK, and purC gene products: identification of a previously unrecognized energy requirement in the purine biosynthetic pathway. Biochemistry 31, 5022-32.

5. Patey, C. A., and Shaw, G. (1973) Purification and properties of an enzyme duet, phosphoribosylaminoimidazole carboxylase and phosphoribosylaminoimidazolesuccinocarboxamide synthetase, involved in the biosynthesis of purine nucleotides de novo. Biochem J 135, 543-5.
6. Chen, Z. D., Dixon, J. E., and Zalkin, H. (1990) Cloning of a chicken liver cDNA encoding 5-aminoimidazole ribonucleotide carboxylase and 5-aminoimidazole-4-N-succinocarboxamide ribonucleotide synthetase by functional complementation of Escherichia coli pur mutants. Proc Natl Acad Sci U S A 87, 3097-101.
7. Firestine, S. M., and Davisson, V. J. (1994) Carboxylases in de novo purine biosynthesis. Characterization of the Gallus gallus bifunctional enzyme. Biochemistry 33, 11917-26.
8. Firestine, S. M., Poon, S. W., Mueller, E. J., Stubbe, J., and Davisson, V. J. (1994) Reactions catalyzed by 5-aminoimidazole ribonucleotide carboxylases from Escherichia coli and Gallus gallus: a case for divergent catalytic mechanisms. Biochemistry 33, 11927-34.
9. Firestine, S. M., Misialek, S., Toffaletti, D. L., Klem, T. J., Perfect, J. R., and Davisson, V. J. (1998) Biochemical role of the Cryptococcus neoformans ADE2 protein in fungal de novo purine biosynthesis. Arch Biochem Biophys 351, 123-34.
10. Schmuke, J. J., Davisson, V. J., Bonar, S. L., Gheesling Mullis, K., and Dotson, S. B. (1997) Sequence analysis of the Candida albicans ADE2 gene and physical separation of the two functionally distinct domains of the phosphoribosylaminoimidazole carboxylase. Yeast 13, 769-76.
11. Batova, A., Diccianni, M. B., Omura-Minamisawa, M., Yu, J., Carrera, C. J., Bridgeman, L. J., Kung, F. H., Pullen, J., Amylon, M. D., and Yu, A. L. (1999) Use of alanosine as a methylthioadenosine phosphorylase-selective therapy for T-cell acute lymphoblastic leukemia in vitro. Cancer Res 59, 1492-7.
12. Tyagi, A. K., and Cooney, D. A. (1980) Identification of the antimetabolite of L-alanosine, L-alanosyl-5-amino-4-imidazolecarboxylic acid ribonucleotide, in tumors and assessment of its inhibition of adenylosuccinate synthetase. Cancer Res 40, 4390-7.
13. Casey, P. J., and Lowenstein, J. M. (1987) Inhibition of adenylosuccinate lyase by L-alanosyl-5-aminoimidazole-4-carboxylic acid ribonucleotide (alanosyl-AICOR). Biochem Pharmacol 36, 705-9.
14. Nelson, S. W., Binkowski, D. J., Honzatko, R. B., and Fromm, H. J. (2005) Mechanism of action of Escherichia coli phosphoribosylaminoimidazolesuccinocarboxamide synthetase. Biochemistry 44, 766-74.
15. Donovan, M., Schumuke, J. J., Fonzi, W. A., Bonar, S. L., Gheesling-Mullis, K., Jacob, G. S., Davisson, V. J., and Dotson, S. B. (2001) Virulence of a phosphoribosylaminoimidazole carboxylase-deficient Candida albicans strain in an immunosuppressed murine model of systemic candidiasis. Infect Immun 69, 2542-8.
16. Perfect, J. R., Toffaletti, D. L., and Rude, T. H. (1993) The gene encoding phosphoribosylaminoimidazole carboxylase (ADE2) is essential for growth of Cryptococcus neoformans in cerebrospinal fluid. Infect Immun 61, 4446-51.

17. Cheville, N. F., Olsen, S. C., Jensen, A. E., Stevens, M. G., Florance, A. M., Houng, H. S., Drazek, E. S., Warren, R. L., Hadfield, T. L., and Hoover, D. L. (1996) Bacterial persistence and immunity in goats vaccinated with a purE deletion mutant or the parental 16M strain of Brucella melitensis. Infect Immun 64, 2431-9.
18. Drazek, E. S., Houng, H. S., Crawford, R. M., Hadfield, T. L., Hoover, D. L., and Warren, R. L. (1995) Deletion of purE attenuates Brucella melitensis 16M for growth in human monocyte-derived macrophages. Infect Immun 63, 3297-301.
19. Crawford, R. M., Van De Verg, L., Yuan, L., Hadfield, T. L., Warren, R. L., Drazek, E. S., Houng, H. H., Hammack, C., Sasala, K., Polsinelli, T., Thompson, J., and Hoover, D. L. (1996) Deletion of purE attenuates Brucella melitensis infection in mice. Infect Immun 64, 2188-92.
20. Alcantara, R. B., Read, R. D., Valderas, M. W., Brown, T. D., and Roop, R. M., 2nd. (2004) Intact purine biosynthesis pathways are required for wild-type virulence of Brucella abortus 2308 in the BALB/c mouse model. Infect Immun 72, 4911-7.
21. Firestine, S. M., and Davisson, V. J. (1993) A tight binding inhibitor of 5-aminoimidazole ribonucleotide carboxylase. J Med Chem 36, 3484-6.
22. Youn, H. (1997) in Medicinal Chemistry pp 141, Purdue University, West Lafayette, IN.
23. Li, S. X., Tong, Y. P., Xie, X. C., Wang, Q. H., Zhou, H. N., Han, Y., Zhang, Z. Y., Gao, W., Li, S. G., Zhang, X. C., and Bi, R. C. (2007) Octameric structure of the human bifunctional enzyme PAICS in purine biosynthesis. J Mol Biol 366, 1603-14.
24. Yoshikawa, M., Kato, T., and Takenishi, T. (1967) A novel method for phosphorylation of nucleosides to 5'-nucleotides. Tetrahedron Lett 50, 5065-8.
25. Ames, B. N., and Dubin, D. T. (1960) The role of polyamines in the neutralization of bacteriophage deoxyribonucleic acid. J Biol Chem 235, 769-75.
26. Bradford, M. M. (1976) Anal Biochem 72, 248-254.
27. Leatherbarrow, R. J. (2001), Erithacus Software Ltd.
28. Kuzmic, P. (1996) Program DYNAFIT for the analysis of enzyme kinetic data: application to HIV proteinase. Anal Biochem 237, 260-73.
29. Burnham, K. P., and Anderson, D. R. (2002) Model selection and multimodel inference : a practical information-theoretic approach, 2nd ed., Springer, New York.
30. Fromm, H. J. (1975) Initial rate enzyme kinetics, Springer-Verlag, Berlin ; New York.
31. Purich, D. L., and Schramm, V. L. (1979) Enzyme kinetics and mechanism, Academic Press, New York.
32. Raman, J., Mehrotra, S., Anand, R. P., and Balaram, H. (2004) Unique kinetic mechanism of Plasmodium falciparum adenylosuccinate synthetase. Mol Biochem Parasitol 138, 1-8.
33. Van der Weyden, M. B., and Kelly, W. N. (1974) Human adenylosuccinate synthetase. Partial purification, kinetic and regulatory properties of the enzyme from placenta. J Biol Chem 249, 7282-9.

34. Rudolph, F. B., and Fromm, H. J. (1969) Initial rate studies of adenylosuccinate synthetase with product and competitive inhibitors. J Biol Chem 244, 3832-9.
35. Sarver, A. E., and Wang, C. C. (2002) The adenine phosphoribosyltransferase from Giardia lamblia has a unique reaction mechanism and unusual substrate binding properties. J Biol Chem 277, 39973-80.
36. Bashor, C., Denu, J. M., Brennan, R. G., and Ullman, B. (2002) Kinetic mechanism of adenine phosphoribosyltransferase from Leishmania donovani. Biochemistry 41, 4020-31.
37. Ginder, N. D., Binkowski, D. J., Fromm, H. J., and Honzatko, R. B. (2006) Nucleotide complexes of Escherichia coli phosphoribosylaminoimidazole succinocarboxamide synthetase. J Biol Chem 281, 20680-8.

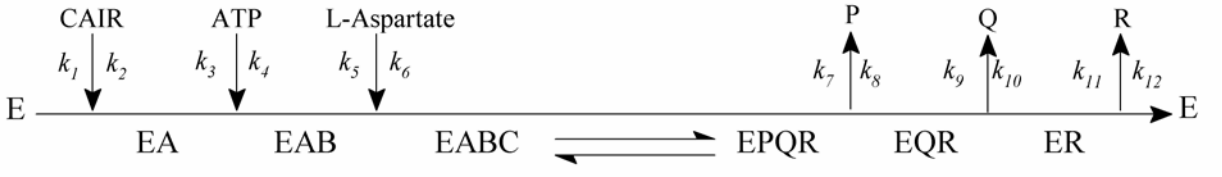
CAIR
ATP
L-Aspartate
P
Q
R
k_1 k_2
k_3 k_4
k_5 k_6
k_7 k_8
k_9 k_{10}
k_{11} k_{12}
E
E
EA
EAB
EABC
EPQR
EQR
ER

Scheme I

Table 1. Steady state Ordered Sequential model for human SAICAR synthetase.

Parameter	Fitted values and weighted mean
$k_{cat} = k_7k_9k_{11}/(k_7k_9+k_7k_{11}+k_9k_{11})$	3.6 ± 0.1 (Figure 1a) 3.5 ± 2 (Figure 1b) 3.6 ± 0.3 (Figure 1c) 3.6 ± 0.8 (mean) (3.3 ± 0.3)
$K_a = k_7k_9k_{11}/[k_1(k_7k_9+k_7k_{11}+k_9k_{11})]$	8.6 ± 0.7 (Figure 1a) 11 ± 2 (Figure 1b) 9.8 ± 1.4 (mean) (<1)
$K_b = k_7k_9k_{11}/[k_3(k_7k_9+k_7k_{11}+k_9k_{11})]$	23 ± 3 (Figure 1a) 24 ± 3 (Figure 1c) 24 ± 3 (mean) (34 ± 3)
$K_c = k_9k_{11}(k_6+k_7)/[k_5(k_7k_9+k_7k_{11}+k_9k_{11})]$	430 ± 50 (Figure 1b) 620 ± 90 (Figure 1c) 530 ± 70 (mean) (500 ± 40)
$K_{ia} = k_2/k_1$	4 ± 1 (Figure 1a)
$K_{ib} = k_4/k_3$	29 ± 5 (Figure 1b)

The symbol E represents polyhistidyl-tagged SAICAR synthetase in the presence of 10 μM NAIR, and substrates A, B and C represent CAIR, ATP and ASP, respectively. Indicated parenthetically are the data used in determining the fitted value for a parameter. The weighted mean is $\Sigma(1/\sigma_j)^2P_j/\Sigma(1/\sigma_j)^2$, where the summations run over independent determinations of a specific parameter P_j and its standard deviation σ_j. Values for k_{cat} are in s^{-1}, and all other parameters in μM. E_0 is the total enzyme concentration in all of its forms. All calculations employed six-digit values, the final entry being rounded to its first significant digit. Values in parenthesis are for the Lys^{304}→Ala enzyme determined at saturating concentrations of CAIR.

Table 2. Inhibition mechanisms of NAIR-ligated wild-type and Lys^{304}→Ala AIR carboxylase/SAICAR synthetases.

Inhibitor	Varied substrate		
	CAIR[a]	ATP	L-Aspartate
AICAR	Competitive 0.37 ± 0.05/0.12 ± 0.06	Non-competitive 4.6 ± 0.3/1.6 ± 0.7	Non-competitive 5.6 ± 0.4/2.16 ± 0.09
AMP	Uncompetitive 7.6 ± 0.2/8.8 ± 7	Competitive 2.3 ± 0.1/6.9 ± 0.6	Non-competitive 10.6 ± 0.6/9.2 ± 0.4
L-Malate	Uncompetitive 108 ± 5/ –	Uncompetitive 77 ± 3/ –	Competitive 16.8 ± 0.7/ –
Maleate	Uncompetitive – /4.3 ± 0.9	Uncompetitive – /9.4 ± 0.3	Competitive – /2.2 ± 0.1

Table 2. Footnote.
Dissociation constants are apparent (dependent upon fixed concentrations of substrates at which they were determined). Values for dissociation constants (in mM) are paired, the first corresponding to inhibition of the NAIR-ligated wild-type enzyme and the second to the Lys^{304}→Ala enzyme. Models of inhibition define parameters K_i, the constant of disoociation for the inhibitor from the enzyme•inhibitor complex, and K_{is} the dissociation of the inhibitor from the enzyme•substrate•inhibtior complex. Competitve inhibition uses only K_i, uncompetitive inhibition only K_{is}, and non-competitive inhibition both K_i and K_{is} with K_i=K_{is}.

[a]For the Lys^{304}→Ala enzyme, the data from experiments which systematically varied CAIR provided a value for K_c, the Michaelis constant for CAIR, of 0.??±0.?? μM, substantially lower than K_c for the NAIR-ligated wild-type enzyme reported in Table 1.

Table 3. Kinetic parameters for analogs of L-aspartate in SAICAR synthetase reactions.

Substrate/Inhibitor	Enzyme source		
	Human recombinant, NAIR-ligated	Human recombinant Lys^{304}→Ala	E. coli recombinant
L-Aspartate[a]	K_m=0.5±0.1 k_{cat}=3.3±0.7	K_m=0.67±0.05 k_{cat}=3.4±0.1	K_m=0.77±0.08 k_{cat}=6.2±0.2
L-Alanosine[a]	K_m=15±2 k_{cat}=3.0±0.6	K_m=5.5±0.5 k_{cat}=3.3±0.1	K_m=0.83±0.05 k_{cat}=6.0 ± 0.7
L-Cysteine sulfinate[a]	K_m=50±20 k_{cat}=3±1 K_{ss}=40±20[b]	K_m=40±4 k_{cat}=3.4±0.1	K_m=5.6±0.3 k_{cat}=6.0 ± 0.1
L-Malate[c]	K_i=16.8±0.7	K_i=12.7±0.9	K_i=20±1
Maleate[c]	K_i=3.5±0.4, K_{is}=10±3[d]	K_i=2.2±0.1	K_i=1.6±0.3
Succinate[c]	K_i=68±8, K_{is}=260±40[d]	K_i=44±2	K_i=64±5

Table 3. Footnotes.
Assays employs saturating concentrations (5xK_m) of CAIR and ATP, in 50 mM Taps, pH 8.0, 10 mM $MgCl_2$, and 1 mM dithiothreitol (DTT) at a temperature of 37º C. Michaelis and inhibition parameters have units of mM, and k_{cat} is in units of s^{-1}.

[a]Data are fit to a Michaelis-Menten equation using Grafit (27).
[b]K_m, K_{ss}, and k_{cat} come from a model of substrate inhibition in which the binding of a second substrate molecule (governed by the parameter K_{ss}) to the enzyme-substrate complex prevents catalysis.
[c]Data are fir to a model of competitive inhibition with respect to L-aspartate using Dynafit (28) in which K_i governs the dissociation of inhibition from the enzyme•CAIR•ATP•inhibitor complex.
[b]Data are fit to a model of noncompetitive inhibition with respect to L-aspartate using Dynafit (28) in which K_i governs the dissociation of inhibition from the enzyme•CAIR•ATP•inhibitor complex and Kis governs the dissociation of inhibitor from the enzyme•CAIR•ATP•L-aspartate•inhibitor complex.

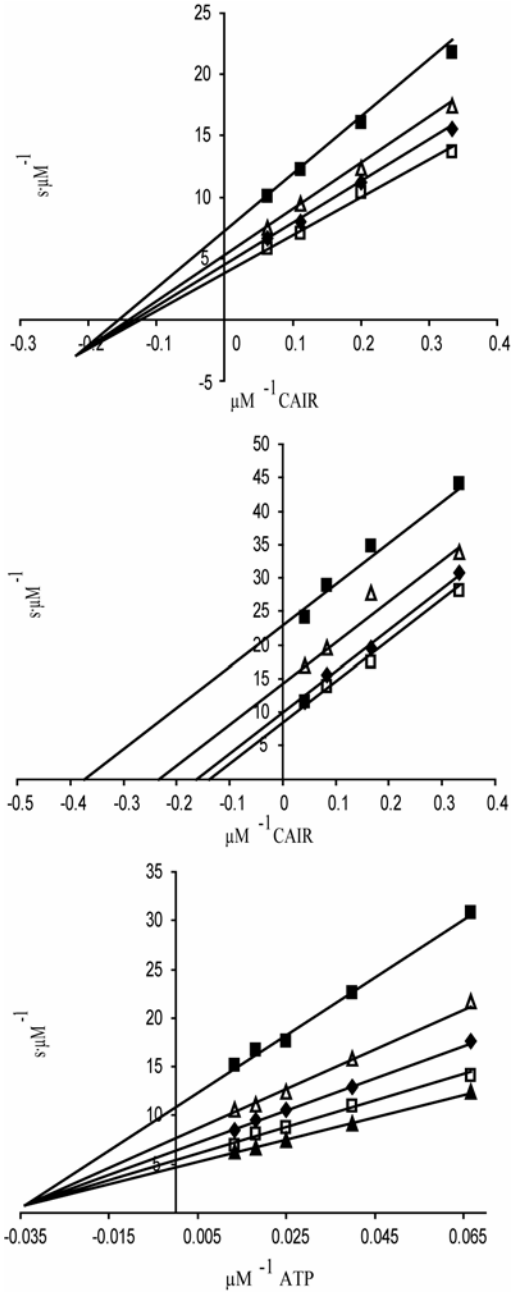

Figure 1. Reciprocal velocity versus reciprocal substrate concentration. Solid lines are Equations 3, 4 and 5 for panels A, B and C, respectively, using the parameters of Table 1. (A) Concentrations of CAIR vary from 3–16 μM, and those of ATP are (■) 20, (Δ) 40, (♦) 65, and (□) 160 μM. (B) Concentrations of ATP vary from 15–75 μM, and those of L-aspartate are (■) 200, (Δ) 350, (♦) 500, (□) 750, and (▲) 1200 μM. (C) Concentrations of CAIR vary from 3–24 μM, and those of L-aspartate are (■)200, (Δ) 400, (♦) 800, and (□) 1200 μM.

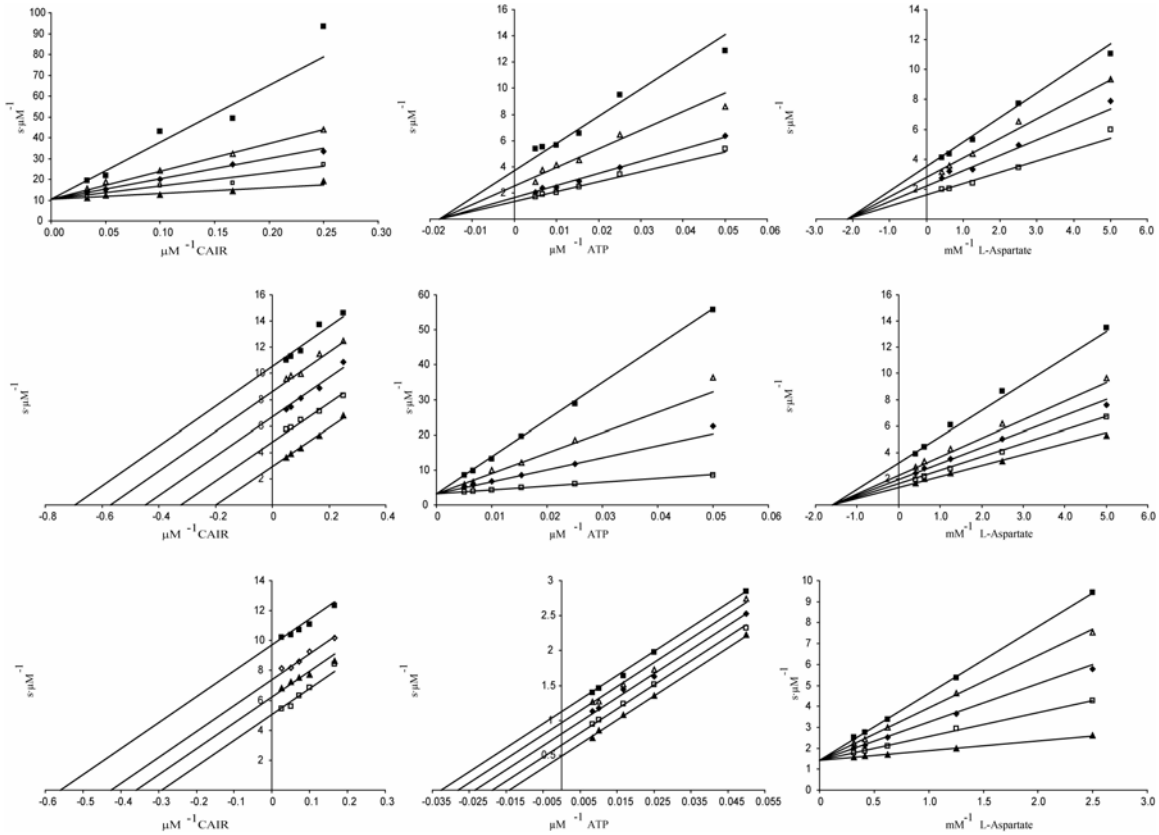

Figure 2. Response of NAIR-ligated wild-type AIR carboxylase/SAICAR synthetase to inhibitors. Lines come from fits of data to competitive, uncompetitive and non-competitive models of inhibition of a single-substrate enzyme as described in the text. Fixed substrate concentrations are: ATP and L-aspartate at 200μM and 3mM, respectively, for panels A, D, and G, CAIR and L-aspartate at 32μM and 3mM, respectively, for panels B, E and H, and CAIR and ATP at 35 μM and 200μM, respectively, for panels C, F, and I. (A) Concentrations of CAIR vary from 4–30μM, and those of AICAR are (▲) 0, (□) 0.5, (♦) 1, (Δ) 1.5, (■) 3.5 mM. (B) Concentrations of ATP vary from 20–200μM, and those of AICAR are (□) 0, (♦) 1, (Δ) 4, and (■) 8mM. (C) Concentrations of L-aspartate vary from 0.2–2.4 mM, and those of AICAR are (□) 0, (♦) 2, (Δ) 4, and (■) 6.5 mM. (D) Concentrations of CAIR vary from 4–20 μM, and those of AMP are (▲) 0, (□) 5, (♦) 10, (Δ) 15, (■) 20 mM. (E) Concentrations of ATP vary from 20–200 μM, those of AMP are (□) 0, (♦) 5, (Δ) 10, and (■) 10 mM. (F) Concentrations of L-aspartate vary from 0.2–2.4 mM, and those of AMP are (▲) 0, (□) 2.5, (♦) 5, (Δ) 7.5, and (■) 15 mM. (G) Concentrations of CAIR vary from 6–40 μM, and those of L-malate are (□) 0, (▲) 25, (◊) 50, and (■) 100mM. (H) Concentrations of ATP vary from 20–120 μM, and those of L-malate are (▲) 0, (□) 25, (♦) 50, (Δ) 75, and (■) 100 mM. (I) Concenrations of L-aspartate vary from 0.4–3.2 mM, and those of L-malate are (▲) 0, (□) 25, (♦) 50, (Δ) 75, and (■) 100 mM.

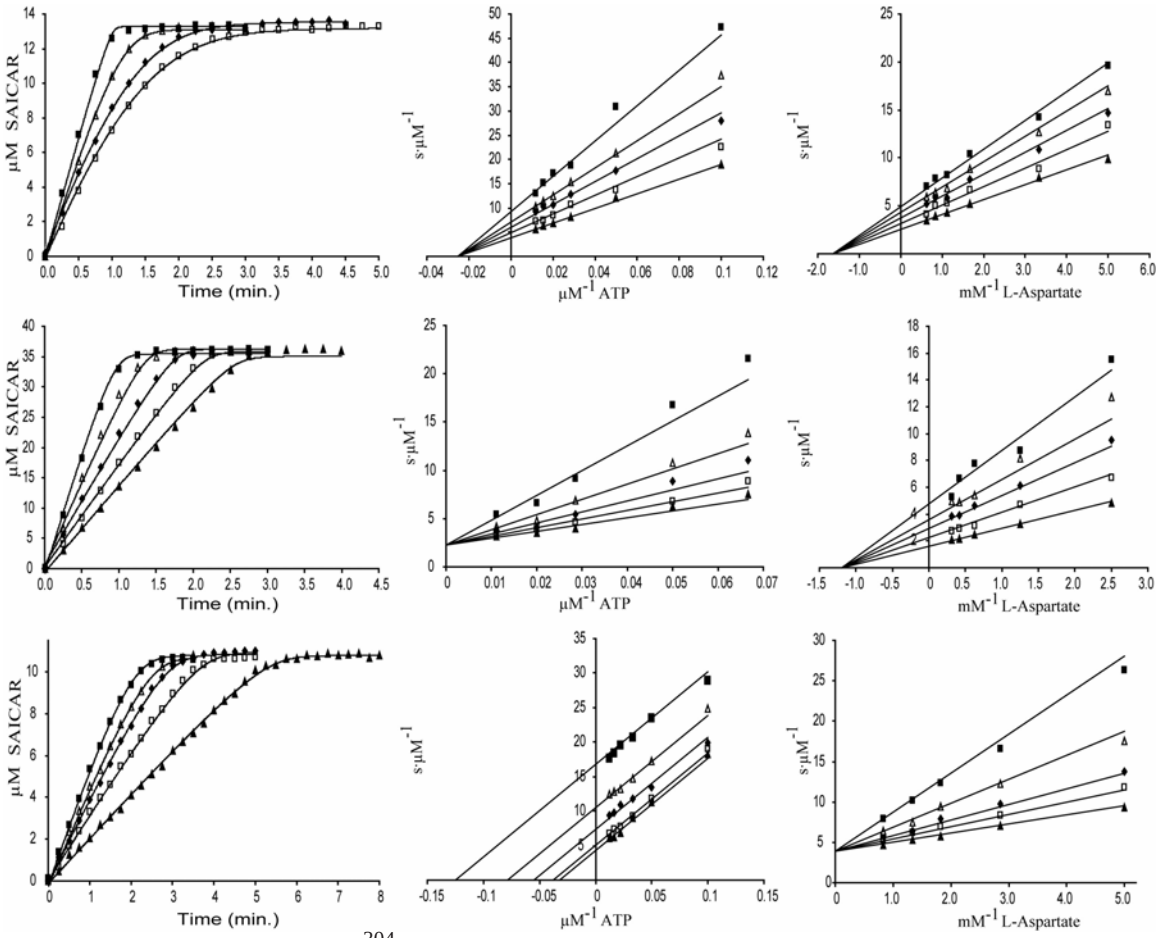

Figure 3. Response of Lys^{304}→Ala AIR carboxylase/SAICAR synthetase to inhibitors. Lines come from fits of data to competitive, uncompetitive and non-competitive models of inhibition of a single-substrate enzyme as described in the text. Fixed substrate concentrations are: ATP and L-aspartate at 200μM and 2.5mM, respectively, for panels A, D, and G, CAIR and L-aspartate at 15μM and 3mM, respectively, for panels B, E and H, and CAIR and ATP at 18μM and 200μM, respectively, for panels C, F, and I. Panels A, D and G are plots of product formation vs. time, whereas panels B, C, E, F, H, and I are plots of reciprocal velocity vs. reciprocal substrate concentration. (A) Concentration of CAIR is 13.3 μM, and those of AICAR are (■) 0, (Δ) 0.5, (♦) 1.5, and (□) 2 mM. (B) Concentrations of ATP vary from 10–85 μM, and those of AICAR are (▲) 0, (□) 0.5, (♦) 1, (Δ) 1.5, and (■) 2.5 mM. (C) Concentrations of L-aspartate vary from 0.2–1.6 mM, and those of AICAR are (▲) 0, (□) 0.5, (♦) 1, (Δ) 1.5, and (■) 2 mM. (D) Concentration of CAIR is 36 μM, and those of AMP are (■) 0, (Δ) 3.75, (♦) 7.5, (□) 11.25, and (▲) 15 mM. (E) Concentrations of ATP vary from 30–240 μM, and those of AMP are (■) 0, (Δ) 5, (♦) 10, and (□) 20 mM. (F) Concentrations of L-aspartate vary from 0.4–3.2 mM, and those of AMP are (▲) 0, (□) 3.75, (♦) 7.5, (Δ) 11.25, and (■) 18 mM (G) Concentration of CAIR is 11 μM and those of maleate are (■) 0, (Δ) 1, (♦) 2, (□) 4, and (▲) 8 mM. (H) Concentrations of ATP vary from 10–80 μM, and those of maleate are (▲) 0, (□) 1, (♦) 2, (Δ) 4, and (■) 8 mM. (I) Concentrations of L-aspartate vary from 0.2–1.2 mM, and those of maleate are (▲) 0, (□) 0.9, (♦) 1.8, (Δ) 3.6, and (■) 7.2 mM.

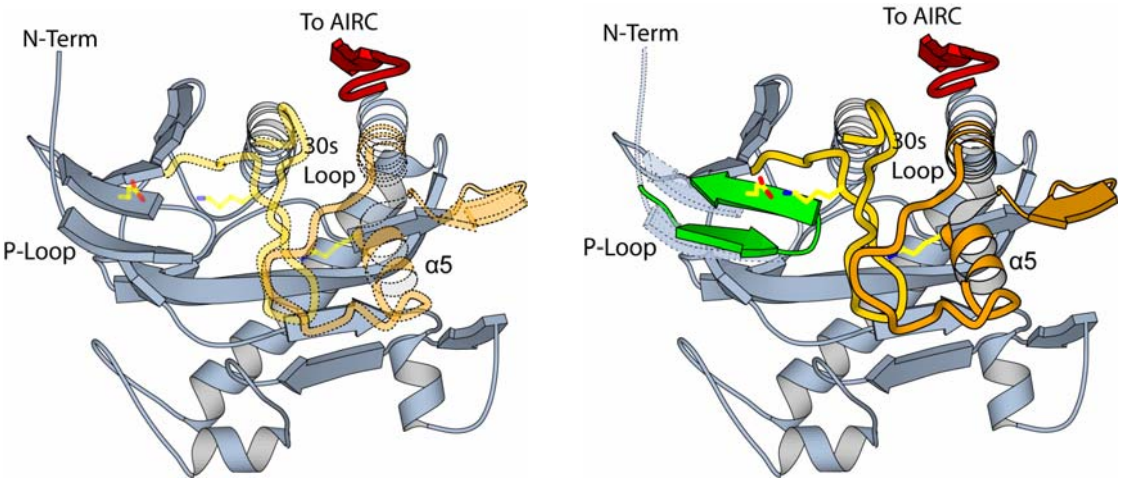

Figure 4: Human SAICAR synthetase domain with missing elements modeled from ***E. coli*** and ***S. cerevisiae*** SAICAR synthetase. Elements in light blue were generated from the coordinates of the human enzyme (2H31). The orange beta strand is modeled from E. coli structure 2GQS. The 30s loop in gold, the rest of the orange domain, and the green P-loop was modeled from S. cerevisiae structure 2CNQ. (left) the SAICAR synthetase domain from humans. The 30s loop and elements close to α5 that had no density are modeled using structures from other organisms. These are shown as transparent. (right) a model of what human SAICAR synthetase might look like when ordered. The P-loop, from yeast, is raised relative to that of the human structure. This lifting might be caused by the ordering of the gold and orange elements when CAIR is bound.

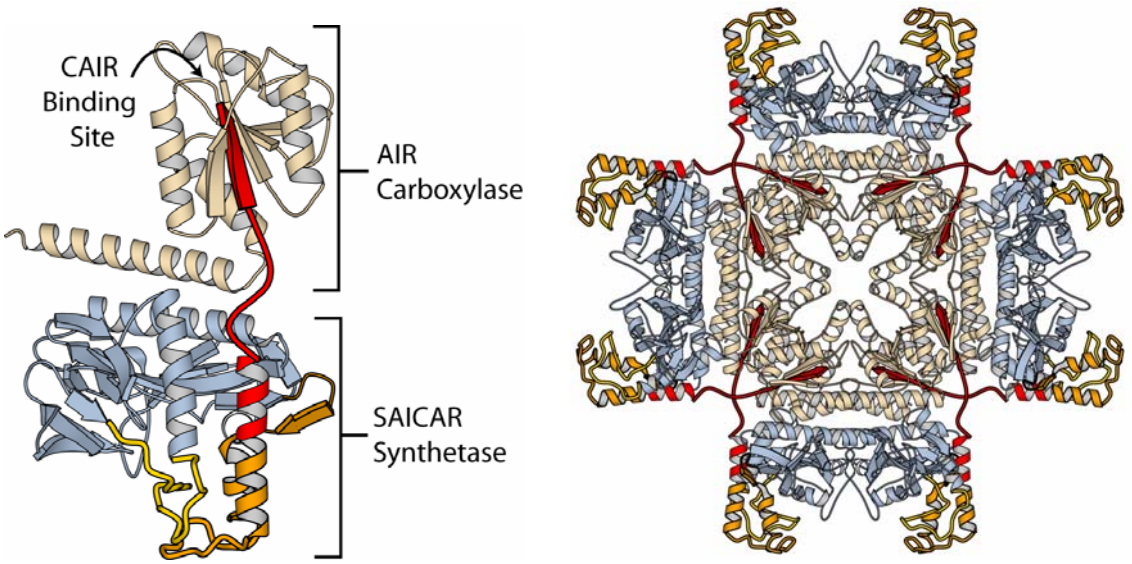

Figure 5. A proposed mechanism for linking the NAIR binding site of the AIR Carboxylase Domain to the CAIR binding site of SAICAR synthetase of the human bi-functional enzyme. The SAICAR synthetase domain is in light blue, the AIR carboxylase is in tan, and the interconnecting element is in red. Parts of the SAICAR synthetase active site not present in the human model are gold and orange and modeled from S. cerevisiae SAICAR synthetase (2CNQ). (left) View of a single bi-functional subunit. (right) View of the entire octamer.

Chapter IV Entrapment of Phosphoryl Intermediates by SAICAR Synthetase[*,†]

Pending submission to The Journal of Biological Chemistry

Nathaniel D. Ginder[1], Daniel J. Binkowski[1], Xiaoming Chen, Jay C. Nix, Herbert J. Fromm, and Richard B. Honzatko[‡]

Abstract

Phosphoribosyl-aminoimidazole-succinocarboxamide synthetase (SAICAR synthetase) catalyzes the eighth step in bacterial de novo purine nucleotide biosynthesis and is a target in the development of antimicrobial and chemotherapeutic agents. The proposed enzyme-mediated reaction proceeds by the transfer of the γ-phosphoryl group of ATP to the carboxyl group of 4-carboxy-5-aminoimidazole ribonucleotide (CAIR), followed by the nucleophilic attack of the α-amino group of L-aspartate on the carbonyl phosphate intermediate. No evidence exists to support this or any other mechanism of SAICAR synthetase action. Presented here are data from structure determinations and positional isotope exchange that are consistent with the formation of the carbonyl phosphate of CAIR as a reaction intermediate. Enzyme from Escherichia coli crystallized with IMP, ATP and Mg^{2+} has 1-N-phosphoryl IMP in its active site, as evidenced by X-ray diffraction data to 1.5 Å resolution. Moreover under similar conditions, 4-carboxamide-5-aminoimidazole ribonucleotide (AICAR) is N-phosphorylated in crystal structures. In positional isotope exchange kinetics using E. coli and human enzymes, ^{18}O in the β,γ-

bridging position of ^{18}O-γ ATP moves to a terminal position of the β-phosphoryl group only in the presence of enzyme and CAIR. The positional exchange of ^{18}O is consistent with the reversible formation of a stable phosphoryl intermediate and combined with crystallographic data is fully consistent with the formation of the carbonyl phosphate of CAIR. The N-phosphorylated derivatives of IMP and AICAR may represent tight-binding analogues of the carbonyl phosphate of CAIR.

---

[1]These authors contributed equally to this work

*This work was supported in part by National Institutes of Health Research Grant NS 10546.

[†]Coordinates and structure factors (accession label 3BSI, 3BSJ, 3BSK, 3BSL) for the structure described in this paper have been deposited in the Protein Data Bank, Research Collaboratory for Structural Bioinformatics (RCSB).

[‡]Corresponding author. Telephone: (515) 294-6116. Fax: (515) 294-0453. E-mail: honzatko@iastate.edu.

Abbreviations: SAICAR, 4(N-succinylcarboxamide)-5-aminoimidazole ribonucleotide; CAIR, 4-carboxy-5-aminoimidazole ribonucleotide; CAIRs, 5-aminoimidazole-4-carboxy ribonucleoside; AICARs, 5-aminoimidazole-4-carboxamide ribonucleoside; eSS, Escherichia coli SAICAR synthetase; tSS, Thermatoga maritime SAICAR synthetase; ySS, Saccharomyces cerevisiae SAICAR synthetase.

Introduction

Phosphoribosyl-aminoimidazole-succinocarboxamide synthetase [EC.6.3.2.6, 5'-phosphoribosyl-4-carboxy-5-aminoimidazole:L-aspartate ligase (ADP)] (SAICAR[1] synthetase) catalyzes the eighth step in bacterial de novo purine nucleotide biosynthesis:

ATP + L-aspartate + CAIR → ADP + P_i + SAICAR

Lukens and Buchanan (1) first described the enzyme in 1959. Miller and Buchanan (2) then demonstrated its presence in a variety of life forms, and reported the purification and

properties of the synthetase from chicken liver. More recently, the Stubbe laboratory purified SAICAR synthetase from Escherichia coli (3). The E. coli enzyme (hereafter eSS) is a homodimer of 27 kDa subunits, and adopts a Rapid Equilibrium Random Sequential kinetic mechanism (4,5). Comparable enzymes from vertebrates are homo-octamers and bifunctional, combining 5-aminoimidazole ribonucleotide carboxylase (AIR carboxylase) and SAICAR synthetase activities in subunits of 47 kDa (6-9). The kinetic mechanism of SAICAR synthetase of the human bifunctional enzyme, unlike the E. coli enzyme, is Steady State Ordered Sequential with CAIR binding first, then ATP and last L-aspartate (10). Hence, bacterial and vertebrate SAICAR synthetases exhibit substantial differences in subunit size, subunit organization and kinetic mechanism. The ultimate goal here is to exploit differences in microbial and vertebrate enzymes in the development of antibiotic or antifungal agents.

SAICAR synthetase is already a target in the treatment of cancer. L-Alanosine is a natural product of Streptomyces alanosinicus with antiviral and antitumor activities. L-Alanosine is a substrate analogue of L-aspartate in vitro and in vivo for SAICAR synthetase (4,11). The product of the L-alanosine reaction is L-alanosyl-5-amino-4-imidazolecarboxylic acid ribonucleotide, a compound responsible for L-alanosine toxicity and a potent inhibitor of adenylosuccinate synthetase and adenylosuccinate lyase (enzymes participating in de novo purine nucleotide biosynthesis) (11-13).

A complication of L-alanosine therapy is its comparable toxicity toward healthy and cancerous cells; however, specific cancers show enhanced susceptibility toward the toxic effects of L-alanosine. Methylthioadenosine phosphorylase (MTAP) is an important salvage enzyme for adenine nucleotides. The gene for MTAP in humans is

proximal to tumor suppressor genes p15 and p16, and as a consequence, many tumor cells that lack one or more suppressor genes also have no gene for MTAP. Approximately 30% of T-cell acute lymphocytic leukemia lack the MTAP salvage pathway and rely entirely on de novo purine nucleotide biosynthesis for adenine nucleotides (14-18). L-Alanosine is toxic to cell lines of such cancers at concentrations well below those that poison cells with intact salvage pathways. Hence, L-alanosine in combination with salvage pathway precursors of adenine nucleotides offers an effective therapy for these cancers (15-19).

Although several structures of microbial SAICAR synthetases (9,20-24) are available, as well as one structure of human AIR carboxylase/SAICAR synthetase (9), most of what is known about enzyme-bound CAIR and essential metal cofactors comes from investigations of the synthetase from E. coli (PDB identifier 2GQS) (5). The eSS subunit folds into two domains, each consisting of a central β-sheets (strands β1─β3, β6, and β7 in Domain 1 and strands β8–β13 in Domain 2) with inter-strand connections that contribute important structural elements to the active site (anti-parallel beta-loop β4–β5 and helix α5). The two domains define a cleft, half of which is filled by ADP and the other half by CAIR (5). Three magnesium cations are in the active site, one associated with the α- and β-phosphoryl groups of ADP, and the other two with the 4-carboxyl group of CAIR. Nelson et al. (4) suggest a mechanism involving the initial formation of the carbonyl phosphate of CAIR, which is attacked subsequently by the α-amino group of L-aspartate. The CAIR•ADP•Mg^{2+} structure is the basis for a model of the transition state for the phosphoryl transfer step of the reaction (5).

The putative chemical mechanism for SAICAR synthetase is similar to the reaction catalyzed by adenylosuccinate synthetase:

GTP + L-aspartate + IMP → GDP + P_i + SAMP

The widely accepted mechanism of adenylosuccinate synthetase first proposed by Lieberman (25) and more fully explored by others (26-31), also involves the formation of a phosphorylated intermediate, 6-phosphoryl IMP, with subsequent nucleophilic substitution by L-aspartate. In this regard, adenylosuccinate synthetase and SAICAR synthetase catalyze similar chemistry, even though the respective enzymes from E. coli bear little structural similarity.

Provided here is the first evidence for the existence of a phosphoryl intermediate in the SAICAR synthetase reaction. AICAR and IMP are analogues of CAIR and intermediates of de novo purine nucleotide biosynthesis; SAICAR synthetase phosphorylates each on a nitrogen atom corresponding in position to an oxygen atom of the 4-carboxyl group of CAIR. The phosphoramidates of AICAR and IMP are present in the active sites of crystal structures of eSS. Additionally, ^{18}O-labeled ATP undergoes positional isotope exchange (PIX) in the presence of enzyme, CAIR and Mg^{2+}, but not in the presence of the enzyme alone. Positional isotope exchange influences chemical shifts of ^{31}P resonances in NMR due to the redistribution of ^{18}O and ^{16}O atoms covalently attached to the β- and γ-phosphoryl groups of ATP. A chemical shift difference of 0.012 ppm occurs as a result of the migration of ^{18}O from the β-γ bridging position of ATP to a non-bridging position of the β-phosphoryl group (32). The structures of phosphoryl intermediates reported here support efforts to develop specific inhibitors of microbial SAICAR synthetases.

Experimental Procedures

Materials— ATP, L-aspartate, NADH, phosphoenolpyruvate, pyruvate kinase, and lactate dehydrogenase were purchased from Sigma. CAIR was synthesized as described previously (4). E. coli strain BL21(DE3) came from Invitrogen. NAIR was synthesized as previously described (10,33). Other materials and their sources are provided in the procedures that follow.

Enzyme Preparation— N-terminal hexa-histidyl tagged eSS and C-terminal hexa-histidyl tagged hSS were prepared by Ni-NTA affinity chromatography as described previously(5,10). Protein concentration was determined by the method of Bradford (34) using bovine serum albumin as a standard. Protein purity was confirmed by sodium dodecylsulfate polyacrylamide gel electrophoresis (SDS-PAGE) (35).

Synthesis of $P^{18}O_4^{2-}$— Synthesis and isolation of $P^{18}O_4^{2-}$ followed Boyer et al. (36). 0.45 g of PCl_5 was added to 1 g of frozen 97% ^{18}O enriched water (Stable Isotope Laboratories) in a 50 mL round bottom flask, sealed with a one way vent to relieve pressure. The flask was equilibrated slowly to room temperature, then allowed to stand for 15 min before the addition of 1.25 g of imidazole. The reaction mixture was diluted with water to 1 L, adjusted to pH 9.0 with KOH, and loaded onto a 2x20 cm column of AG1X4 (Dowex-2, Biorad). The column was washed with distilled/deionized water and eluted with 30 mM HCl. Phosphate content was determined by the acid molybdate assay (37). Product was dried to a brownish syrup.

Synthesis of the bis(4-Morpholine N,N′-dicylcohexylcarboxamidine) Salt of ADP-Morpholidate— The synthesis of ADP-morpholidate followed Moffatt et al (38).

Dicyclohexylcabodiimide (1 g, 4.8 mmoles) was dissolved in 35 mL of t-butyl alcohol (Fisher Scientific). The dicyclohexylcabodiimide solution was added dropwise over 3 hours to a 16 mL refluxing mixture of 50 mM ADP (MP Biochemicals) and 31 mM morpholine (Sigma) in 50% aqueous t-butyl alcohol. The mixture refluxed for an additional 3 hrs., then cooled to room temperature. The volume of the mixture was reduced in vacuo to 25 mL, then added to 50 mL of diethyl ether. Solid dicyclohexyl urea was removed by filtration, and the filtrate applied to a 2x25 cm. column of Dowex-2 (HCO_3^-), equilibrated with 1 mM triethyl ammonium bicarbonate (TEAB). After thoroughly washing the column with water, a 6 L gradient of triethyl ammonium bicarbonate (5–500 mM) eluted AMP-morpholidate first and ADP-morpholidate second (at about 0.3 M triethyl ammonium bicarbonate). Fractions from the second peak were pooled and lyophilized. The resulting powder was dissolved in methanol, and 3 equivalents of 4-morpholine N,N′-dicyclohexylcarboxamidine were added. (Wehrli and Moffatt (39) describe the preparation of dicyclohexylcarboxamidine). This mixture was dried in vacuo, dissolved in 3 mL of methanol, and precipitated with 30 mL diethyl ether. Triturating the resulting syrup with fresh diethyl ether gave 0.1 mmole of the bis(4-morpholine N,N′-dicyclohexylcarboxamidine) salt of ADP-morpholidate.

Synthesis of γ-^{18}O-ATP— The bis(4-morpholone N,N′-dicyclohexylcarboxamidine) salt of ADP-morpholidate (0.1 mmole) was dissolved in 3 mL dry pyridine, evaporated to dryness, and rendered anhydrous by three more evaporations with 2-mL portions of pyridine. Residual pyridine was removed by two evaporations with 2-mL portions of anhydrous benzene.

Distilled tri-n-butylamine (0.072 mL, 0.3 mmole, Sigma) was added to $H_3P^{18}O_4$, evaporated to dryness, and then made anhydrous by evaporations of three 2-mL portions of distilled pyridine. Residual pyridine was removed by evaporations with two 2-mL portions of benzene. Anhydrous $H_3P^{18}O_4$ was dissolved in distilled anhydrous dimethyl sulfoxide (2 mL) and added to the anhydrous bis(4-morpholine N,N′-dicyclohexlcarboxamidine) salt of ADP-morpholidate. The solution was sealed and stored at 35 °C for 45 hr. The mixture was diluted with 40 mL of distilled/deionized water, and applied to a 2 x33 cm. column of DEAE-cellulose (HCO_3^-). After thorough washing with water, a 3-L linear gradient of 0.005–0.35 M triethylamine-bicarbonate eluted purified γ-^{18}O ATP. The product was twice lyophilized and analyzed by electrospray ionization mass spectroscopy (ESI-MS). γ-^{18}O-ATP was quantified by the action of yeast hexokinase (Roche) coupled to glucose-6-phosphate dehydrogenase. Positional Isotope Exchange—Three 1 mL samples containing 3μg eSS, 5 mM γ-^{18}O-ATP, 11 mM $MgCl_2$, 1 mM DTT, 100 mM Hepes, pH 7.8, and 10 mM KCl were prepared. One sample had additionally 2.5 mM L-aspartate, and another 100 μM CAIR. After 8 hrs of incubation, the addition of 20 mM EDTA stopped the reactions. Experiments involving hSS employed similar conditions, using 50 mM Taps, pH 8.1, supplemented with 10 μM NAIR, instead of 100 mM Hepes, pH7.8. NAIR extinguishes the conversion of CAIR to AIR by hSS (10),

Fifty μL of chloroform was added to each sample, followed by centrifugation to remove precipitated protein. The aqueous fraction was diluted by half with water and injected onto a 2x8 cm 650M DEAE (TosoHaus) HPLC column. The column was washed with 50 mM Hepes, pH 7.0, 4 mM KP_i (Buffer A) for 10min at a flow-rate of 1

mL/min. A gradient from 0–150 mM in NaCl (15 min.) followed by a wash with 150 mM NaCl (10 min.) eluted AMP, ADP, L-aspartate, and CAIR, and then a gradient from 150–500 mM NaCl (45 min.) eluted ATP. ATP fractions containing the highest absorbance at 259 nm were used for NMR. Samples were prepared by adding 100 μL of 500 mM CDTA (pH 7.0) and 20 μL of 50 mM 2,2-dimethyl-2-silapentane-5-sulfonic acid (pH 7.0) to make a final volume of 1 mL.

NMR experiments— All NMR experiments were performed on a Bruker DRX-400 NMR spectrometer operating at 121.5 MHz. Data was collected over 1320–1972 scans with a pulse-width and -angle of 12 μs and a 75˚, respectively. Data were transformed using 0.2 Hz line broadening constant. An indirect shift reference was applied to all samples using an ^{1}H NMR spectra of the internal 2,2-dimethyl-2-silapentane-5-sulfonic acid standard (40) (SR_{calc} = 671.3 Hz, –1.091 ppm).

Crystallization— Crystals were grown by the method of hanging-drop vapor diffusion in VDX-plates (Hampton Research). Two μL of a protein solution were mixed with 2 μL of a well solution and then equilibrated against 0.5 mL of well solution. All protein solutions contained 15 mg/mL eSS, 15 mM Tris-HCl, 25 mM KCl, 5 mM dithiothreitol, 40 mM $MgCl_2$, and 5mM EDTA (pH 8.0). The protein solutions for the 1-PIMP•ADP•Mg^{2+}, IMP•ADP•Mg^{2+}, and AICAR•ADP•Mg^{2+} complexes were supplemented with 15 mM IMP/25 mM ATP, 15 mM IMP/25 mM ADP, and 15 mM AICAR/25 mM ADP, respectively. The well solutions contained 50 mM Tris-HCl and 3.4–3.8 M sodium formate (pH 8.5). The protein solution for the PAICAR•ADP•Mg^{2+} complex contained 15 mM AICAR, 25 mM ADP, 40 mM $MgCl_2$, and the well solution contained 0.5–0.7 M L-aspartate, 50 mM Tris-HCl (pH 8.5) and 27–30% PEG 8000.

Crystallization conditions for the AICAR•ADP•Mg^{2+} and PAICAR•ADP•Mg^{2+} complexes differed only in the choice of precipitant (3.4-3.8 M formate as opposed to PEG 8000) and the time for crystals to grow sufficiently for data collection (48 hrs. as opposed to more than 1 week).

Data Collection— The crystals grown from formate were transferred to a cryoprotectant solution containing 4 M sodium formate, 50 mM Tris·HCl, pH 8.5, 10% w/v sucrose, and ligands at the same concentrations as their respective protein solutions. For the PEG 8000 condition, 10% w/v sucrose was added to the well solution, and it was supplemented with the ligands present in the protein solution. After approximately 30 seconds of equilibration, crystals were plunged into liquid nitrogen.

Data from the complexes other than 1-PIMP•ADP•Mg^{2+} were collected at Iowa State University from a single crystal (temperature, 115 K) on a Rigaku R-AXIS IV++ rotating anode/image plate system using CuK_{α} radiation from an Osmic confocal optics system. Data were processed and reduced using the program package CrystalClear provided with the instrument. For the 1-PIMP•ADP•Mg^{2+} complex, data were collected on Beamline 4.2.2 of the Advanced Light Source, Lawrence Berkley Laboratory (wavelength of 1 Å). Data were indexed, integrated, scaled, and merged using d*trek (41). Intensities were converted to structure factors using the CCP4 (42) program TRUNCATE.

Structure Determination and Refinement— Structures were solved by molecular replacement with the program AMoRE (42) and 2GQS (less ligands and water molecules) as the starting model. Refinement was performed using CNS 1.1 (43), beginning with a cycle of simulated annealing (starting temperature of 3500 K) with slow

cooling in increments of 25 K to a final temperature of 300 K, followed by 100 steps of conjugate gradient energy minimization. Subsequent cycles had lower initial starting temperatures (as low as 500 K). Individual B-factors were refined after each cycle of simulated annealing and subject to the following restraints: bonded main-chain atoms, 1.5 $Å^2$; angle main-chain atoms, 2.0 $Å^2$; bonded side-chain atoms, 2.0 $Å^2$; and angle side-chain atoms, 2.5 $Å^2$. Water molecules were automatically added using CNS if a peak greater than 3.0σ was present in Fourier maps with coefficients $(F_{obs}–F_{calc})e^{i\alpha calc}$. Refined water sites were eliminated if they were further than 3.2 Å from a hydrogen-bonding partner or if their thermal parameters exceeded 50 $Å^2$. The contribution of the bulk solvent to structure factors was determined using the default parameters of CNS. Non-crystallographic restraints/constraints were not used during refinement. Constants of force and geometry for the protein came from Engh and Huber (44) and those for ADP, IMP, 1-PIMP, PAICAR, AICAR, and formate from CNS resource files, with appropriate modification of dihedral angles of the ribosyl moiety to maintain a 2'-endo ring pucker.

Results

Protein Preparation, Data Collection, and Structure Determination—eSS and hSS were pure on the basis of sodium dodecylsulfate polyacrylamide gel electrophoresis. eSS and hSS had specific activities of 15 ± 1 and 3.7 ± 0.1 U/mg, respectively, comparable to values previously reported (4,10).

General Features of Ligand Complexes of eSS— An eSS homodimer occupies the crystallographic asymmetric unit in the IMP•ADP•Mg^{2+}, AICAR•ADP•Mg^{2+}, 1-PIMP•ADP•Mg^{2+}, and PAICAR•ADP•Mg^{2+}complexes reported here (Fig. 1). The

subunits are identical to within the coordinate uncertainty. Electron density is not present for the polyhistidyl tag; however, observable electron density begins with Met^{1} and continues to the C-terminal Asp^{237}. The protein component of the four different complexes is nearly identical to that of the CAIR•ADP•Mg^{2+} structure (2GQS) (5). Differences in protein structure appear in the 30s loop (anti-parallel loop defined by β-strands 4 and 5 of Domain 1). Electron density for the IMP•ADP•Mg^{2+} complex is weak for residues 35–39, but represented well by a single conformation with reasonable stereochemistry and contacts. The 30s-loops in the 1-PIMP•ADP•Mg^{2+}, AICAR•ADP•Mg^{2+}, and PAICAR•ADP•Mg^{2+}complexes are identical to that of the CAIR•ADP•Mg^{2+} complex (5). Superposition of all C_{α} positions of the A subunit of each complex against the CAIR•ADP•Mg^{2+} structure gave root-mean-squared deviations from 0.3–0.4 Å.

Phosphoryl Intermediates— Phosphoryl groups form phosphoramidate bonds with the amide nitrogen of AICAR and the N1 atom of IMP, resulting in PAICAR and 1-PIMP (Fig. 2). The phosphorylated nitrogen atoms correspond to the oxygen atom of the 4-carboxyl group of CAIR (position O7 in PDB 2GQS) that accepts the γ-phosphoryl of ATP in the proposed mechanism (4). The distances between N and P atoms in the phosphoramidate linkages are 1.76 and 1.79 Å for PAICAR and 1-PIMP, respectively, close to the observed N-P bond distance of 1.77 Å, taken from the crystal structure of $NaHPO_3NH_2$ (45).

The observed electron density in the 1-PIMP•ADP•Mg^{2+} complex cannot represent an average of IMP•ADP and ADP•P_i complexes, bound with mutual exclusivity. Crystallization of the enzyme in the presence of IMP, ADP, Mg^{2+} and P_i

(data not shown) results in electron density identical to that reported here for the IMP•ADP•Mg^{2+} complex. Hence, the presence of P_i is not responsible for the appearance of density associated with atom N1 of IMP. Moreover, thermal parameters of atoms for ligands and protein are comparable throughout the active site indicating full occupancy of the ligands. Finally, the relative positions of the ribosyl and base moieties of IMP and 1-PIMP (and an associated Mg^{2+}) in the IMP•ADP•Mg^{2+} and 1-PIMP•ADP•Mg^{2+} complexes differ, consistent with substantially different modes of ligand recognition by the enzyme. Similar arguments leave but one reasonable interpretation of the electron density extending from the amide group of AICAR, that being a covalently linked phosphoryl group.

Ligand-protein interactions in the 1-PIMP•ADP•Mg^{2+} and PAICAR•ADP•Mg^{2+} complexes correspond to those of the CAIR•ADP•Mg^{2+} complex as presented by Ginder et al. (5). Described here are only the new interactions involving the additional phosphoryl group of each intermediate. The phosphoryl group (whether it be part of 1-PIMP or PAICAR) coordinates magnesium ions at sites 1 and 3, and hydrogen bonds with the side chains of Lys^{11} and Lys^{177} (Fig. 3). Protein and metal ions recognize only two of three oxygen atoms of the phosphoryl group; the remaining oxygen atom projects toward the putatively binding locus of L-aspartate, and interacts with the Mg^{2+} at site 1 through a bridging water molecule. The following atoms of PAICAR and 1-PIMP define trigonal bipyramidal geometries: the nitrogen atom of the phosphoamidate bond, three oxygen atoms of the N-phosphoryl group, and one oxygen atom of the β-phosphoryl group of ADP. Such geometry is consistent with the transition state proposed by Ginder et al. (5) for the phosphotransfer reaction. Distances (averaged over both subunits) from

the N- and P-atoms of the phosphoramidate bond to the nearest β-oxygen atom of ADP are 4.8 and 3.1 Å, respectively, for the PAICAR complex and 4.9 and 3.2 Å for the 1-PIMP complex. The N-P-O bond angle (averaged over both subunits) is 164° and 170° for the PAICAR and 1-PIMP complexes, respectively.

Although, not involved in a direct interaction with the phosphoryl intermediates, the χ^1 angle of Ser^{33} differs by ~120° relative to its value in the CAIR•ADP•Mg^{2+}, AICAR•ADP•Mg^{2+}, and IMP•ADP•Mg^{2+} complexes. The change in χ^1 breaks a hydrogen bond between Ser^{33} and the amide nitrogen of Gly^{37}. The significance of the conformational change in Ser^{33} is weighed in the discussion section.

Binding Variations of Nucleotides— The relative positions and conformations of the adenine nucleotide in the four complexes reported here and the two reported previously (5) are identical. The positions and interactions of AICAR and CAIR define a first binding mode, 1-PIMP and PAICAR together define a second binding mode, and IMP a third mode.

AICAR binds so that its carbonyl oxygen coordinates Mg^{2+} at sites 2 and 3 (mode 1). The 5′-phosphoribosyl group of PAICAR takes up the same position as that of AICAR, but the dihedral angle defined by atoms C2′-C1′-N1-C2 differs by ~30° (Fig 4). The ~30° rotation of the carbonyl of PAICAR relative to that of AICAR and CAIR distorts the octahedral symmetry of the inner coordination spheres of Mg^{2+} at sites 2 and 3, and perhaps weakens interactions between atoms N3 and the carbonyl oxygen of PAICAR, while enhancing interactions of the N-linked phosphoryl group. Comparable distortions in the octahedral symmetry of Mg^{2+} at sites 2 and 3, and a ~30° rotation in the dihedral angle C2′-C1′-N9-C8 of 1-PIMP, occur in the 1-PIMP•ADP•Mg^{2+} complex.

Differences in the interactions of IMP in the IMP•ADP•Mg^{2+} complex (binding mode 3) and CAIR in the CAIR•ADP•Mg^{2+} complex (binding mode 1) are more pronounced than those between binding modes 1 and 2 (Fig. 5). Although the 5′-phosphoryl groups are nearly identical in position and orientation, the ribosyl and base moieties take up different positions, largely due to changes in dihedral angles O3A-PA-O5′-C5′ (~18°) and C2′-C1′-N9-C8 (~40°). In the superposition of the two protein complexes, the positions of atoms C4′ and C1′ differ by 1.0 and 0.9 Å, respectively, and the positions of atoms of CAIR corresponding to atoms N7 and O6 of IMP differ by 1.8 and 3.5 Å, respectively. Mg^{2+} is absent from site 2 in the IMP•ADP•Mg^{2+} complex, but remains coordinated to atom N7 of IMP. Four water molecules coordinate this Mg^{2+} (hereafter, site 2′), defining a square pyramidal inner coordination complex. An oxygen atom of the 5′ phosphoryl group and the O6 atom of IMP hydrogen bond with water molecules coordinated to the Mg^{2+} at site 2′. A formate ion bridges metal sites 1 and 3 as in the CAIR•ADP•Mg^{2+} and AICAR•ADP•Mg^{2+} complexes; however, a second formate ion spans the Mg^{2+} at metal site 1 and atom N1 of IMP (Figure 4).

Positional Isotope Exchange— A principle peak of 514 appears in the electrospray ionization mass spectrum consistent with the calculated mass (515.2) of the γ-^{18}O-ATP (data not shown). The ^{31}P NMR spectrum of a 1:1 mixture of γ-^{16}O-ATP (Sigma) and γ-^{18}O-ATP (Fig. 6) reveals differences in chemical shift of 0.098 and 0.017 ppm in the γ- and β-P resonances, consistent with the reported value of 0.085 and 0.017 ppm, respectively (46). No positional isotope exchange occurs in γ-^{18}O-ATP in the presence of enzyme alone (either eSS or hSS) or enzyme and L-aspartate; however, exchange does occur in the presence of enzyme and CAIR (Fig. 7). The appearance of a new triplet

associated with the β-phosphoryl resonance is due to the migration of ^{18}O from the β-γ bridging position to a terminal oxygen position of the β-P atom.

Discussion

In the case of adenylosuccinate synthetase, the results of positional isotope exchange and the entrapment of 6-PIMP in crystals structures offer persuasive evidence in favor of 6-PIMP as an intermediate in the enzyme mediated reaction (26,27,47,48). The proposed mechanism for SAICAR synthetase is analogous to that of adenylosuccinate synthetase in that PCAIR is the putative intermediate formed prior to the nucleophilic attack of L-aspartate (4,5). The results here are consistent with the formation of PCAIR in the active site of SAICAR synthetase, and for the first time, demonstrate the capacity of a SAICAR synthetase to transfer the γ-phosphoryl group of ATP to form intermediates (1-PIMP and PAICAR) structurally similar to PCAIR.

The combination of AICAR, ADP and Mg^{2+} with SAICAR synthetase results in different crystalline complexes, depending on the choice of precipitant, PEG 8000 or formate. The results are reproducible. In an initial preliminary structure of the AICAR•ADP•Mg^{2+} complex, grown in the presence of formate and ATP, weak electron density was present at the N-phosphoryl locus. Such density could arise from a slow enzyme-mediated reaction between AICAR and ATP. Repeating the experiment using formate and ADP, and minimizing the time of crystal growth (2-days), the weak electron density disappeared, resulting in the AICAR•ADP•Mg^{2+} complex reported here. A complex with PAICAR at full occupancy in the active site, however, resulted fortuitously under conditions of crystallization in which PEG 8000 replaced formate as a precipitant.

Evidently, sufficient ATP was present to phosphorylate AICAR under conditions of crystallization. ATP exists as a minor impurity in the ADP, and could form over time by the slow disproportionation of ADP into ATP and AMP. The absence of formate may enhance the rate of phosphorylation of AICAR by ATP; the formate anion binds at the N-phosphoryl site and may synergistically enhance ADP inhibition of SAICAR synthetase just as the nitrate anion enhances GDP inhibition of adenylosuccinate synthetase (49,50)

A preliminary structure of the 1-PIMP complex (data not shown) indicated that the initial choice of crystallization conditions (using ATP and formate) were near optimal. Data complete to 1.5 Å were taken resulting in the structure reported here. In order to demonstrate the role of ATP in the formation of 1-PIMP, crystals were grown for an equal length of time in the presence of ADP. The resulting complex had IMP and ADP in the active site. Efforts to trap phosphoryl intermediates of GMP and XMP resulted in ADP complexes only with no evidence for additional ligand binding beyond the presence of some electron density at the 5′-phosphoryl binding locus.

Efforts to trap a phosphoryl intermediate of CAIR in a crystalline complex have yet to succeed. The phosphate ester linkage of PCAIR is presumably less stable than the corresponding phosphoramidate linkages of PAICAR and 1-PIMP. At pH 8.5, the hydroxide anion is in relative abundance, and the net rate of ATP hydrolysis through PCAIR probably depletes the reservoir of ATP. Experimental conditions of PIX differ from those of crystallography primarily in the concentration of enzyme subunits (0.1 μM vs. 500 μM) and pH (7.0 vs. 8.5). If the hydrolysis of enzyme bound PCAIR by the hydroxide anion is first-order in the concentrations of the enzyme-PCAIR complex and the hydroxide anion, then the rate of ATP hydrolysis during the PIX experiment 160,000-

fold lower than under the conditions of crystallization. In fact, little, if any, hydrolysis of ATP occurred during the PIX experiment.

The IMP•ADP•Mg^{2+} complex may represent an initial binding step of CAIR with the active site. Mg^{2+} is absent from site 2, but remains associated with the N-7 and O-6 atoms of IMP (Figure 4). These atoms correspond to atom N-3 and an oxygen atom of the 4-carboxyl group of CAIR, suggesting a comparable enzyme-bound CAIR•Mg^{2+} as a possibility. The preferred substrate for SAICAR synthetase then could be CAIR•Mg^{2+}, hence accounting for the requirement of 8 mM Mg^{2+} in order to achieve maximum velocity (4). Litchfield and Shaw have shown that transition metals reduce the rate of decarboxylation of CAIR, suggesting that a metal-nucleotide complex in solution involving the 4-carboxyl group would protect the substrate outside of the active site of the enzyme (51).

The ~30° rotation about the C1′-N1 bond of PAICAR relative to AICAR (Figure 4) may explain the failure of L-aspartate to bind to the CAIR•ADP•Mg^{2+} complex reported in previous work and for the absence of a functional group in the active site that recognizes the 5-amino group of CAIR (5) The altered tilt angle in the base moiety due presumably to the N-phosphoryl adduct, would change the optimal direction of approach for the α-amino group of L-aspartate. Furthermore if the active site were to hydrogen bond with the 5-amino group of CAIR, then the altered tilt angle of PCAIR would likely disrupt that hydrogen bond. (The 5-amino group differs in position by 1.1 Å in superpositions of the AICAR and PAICAR complexes). Hence by not recognizing the 5-amino group, the active site enhances the stability of the carbonyl phosphate intermediate relative to that of CAIR. L-Aspartate could bind in the absence of CAIR, as is consistent

with a Random kinetic mechanism, but the binding is nonproductive until after the formation of the carbonyl phosphate. The failure of L-aspartate to bind to the PAICAR complex (L-aspartate is present during crystallization) is unclear. Differences in hydrogen-bonding interactions between PAICAR and PCAIR are the likely cause, suggesting a critical role in the recognition of L-aspartate by the phosphoester oxygen atom of the carbonyl phosphate of PCAIR. The observed conformational change in Ser^{33} is also consistent with a cause-and-effect relationship between the binding pocket for L-aspartate and the functional moiety occupying the N-phosphoryl locus.

AICAR and IMP are downstream intermediates in de novo purine biosynthesis, but they are usually not at concentrations high relative to CAIR. Hence the formation of PAICAR and 1-PIMP in vivo is unlikely under most circumstances. IMP levels in muscle, however, rise 200-fold during ischemia and anoxia (52-56), reaching 3.8 μmol/g wet weight in skeletal muscle after 20 minutes of induced ischemia (60% of the concentration of ATP under control conditions) (55). The soreness in muscle following severe exercise is linked to ischemia (55,57) and the break-down of ATP to ADP, AMP, IMP, adenosine, inosine, adenine, and hypoxanthine (54,58-61). The effects of ischemia on heart muscle are similar though not as extreme (62-68). Injury to heart muscle during reperfusion after ischemia is a matter of concern in heart surgery and transplantation (62). Formation of 1-PIMP could exacerbate the effects of purine nucleotide loss due to ischemia by diminishing de novo purine nucleotide biosynthesis through the inhibition of SAICAR synthetase.

One of the long-term goals of research is the development of new antibiotics that target bacterial SAICAR synthetases, but not the multifunctional enzyme (AIR

carboxylase/SAICAR synthetase) present in vertebrates. Not surprisingly, the PIX data for the E. coli and human enzymes are consistent with the formation of a carbonyl phosphate intermediate of CAIR. Nonetheless, both the subunit organization and amino acid sequence of the human enzyme differs substantially from that of the E. coli enzyme (5,6,9), holding out the possibility for substantial differences in ligand binding for the E. coli and human enzymes. Given that SAICAR synthetase can transfer the γ-phosphoryl group of ATP to an amide nitrogen, the enzyme itself has the capacity to synthesize its own potent inhibitor.

References

1. Lukens, L. N., and Buchanan, J. M. (1959) J Biol Chem 234(7), 1791-1798
2. Miller, R. W., and Buchanan, J. M. (1962) J Biol Chem 237, 485-490
3. Meyer, E., Leonard, N. J., Bhat, B., Stubbe, J., and Smith, J. M. (1992) Biochemistry 31(21), 5022-5032
4. Nelson, S. W., Binkowski, D. J., Honzatko, R. B., and Fromm, H. J. (2005) Biochemistry 44(2), 766-774
5. Ginder, N. D., Binkowski, D. J., Fromm, H. J., and Honzatko, R. B. (2006) J Biol Chem 281(30), 20680-20688
6. Patey, C. A., and Shaw, G. (1973) Biochem J 135(3), 543-545
7. Firestine, S. M., and Davisson, V. J. (1994) Biochemistry 33(39), 11917-11926
8. Chen, Z. D., Dixon, J. E., and Zalkin, H. (1990) Proc Natl Acad Sci U S A 87(8), 3097-3101
9. Li, S. X., Tong, Y. P., Xie, X. C., Wang, Q. H., Zhou, H. N., Han, Y., Zhang, Z. Y., Gao, W., Li, S. G., Zhang, X. C., and Bi, R. C. (2007) J Mol Biol 366(5), 1603-1614
10. Binkowski, D. J., Ginder, N. D., Fromm, H. J., and Honzatko, R. B. (2008) Biochemistry Submitted for publication
11. Tyagi, A. K., and Cooney, D. A. (1980) Cancer Res 40(12), 4390-4397
12. Anandaraj, S. J., Jayaram, H. N., Cooney, D. A., Tyagi, A. K., Han, N., Thomas, J. H., Chitnis, M., and Montgomery, J. A. (1980) Biochem Pharmacol 29(2), 227-245
13. Casey, P. J., and Lowenstein, J. M. (1987) Biochem Pharmacol 36(5), 705-709
14. Illei, P. B., Rusch, V. W., Zakowski, M. F., and Ladanyi, M. (2003) Clin Cancer Res 9(6), 2108-2113

15. Batova, A., Diccianni, M. B., Omura-Minamisawa, M., Yu, J., Carrera, C. J., Bridgeman, L. J., Kung, F. H., Pullen, J., Amylon, M. D., and Yu, A. L. (1999) Cancer Res 59(7), 1492-1497
16. Batova, A., Diccianni, M. B., Nobori, T., Vu, T., Yu, J., Bridgeman, L., and Yu, A. L. (1996) Blood 88(8), 3083-3090
17. Efferth, T., Gebhart, E., Ross, D. D., and Sauerbrey, A. (2003) Biochem Pharmacol 66(4), 613-621
18. Li, W., Su, D., Mizobuchi, H., Martin, D. S., Gu, B., Gorlick, R., Cole, P., and Bertino, J. R. (2004) Oncol Res 14(7-8), 373-379
19. Efferth, T., Miyachi, H., Drexler, H. G., and Gebhart, E. (2002) Blood Cells Mol Dis 28(1), 47-56
20. Zhang, R., Skarina, T., Evdokimova, E., Edwards, A., Savchenko, A., Laskowski, R., Cuff, M. E., and Joachimiak, A. (2006) Acta Crystallograph Sect F Struct Biol Cryst Commun 62(Pt 4), 335-339
21. Levdikov, V. M., Grebenko, A. I., Barynin, V. V., Melik-Adamyan, W. R., Lamzin, V. S., and Wilson, K. S. (1996) Crystallography Reports 41(2), 275-286
22. Antonyuk, S. V., Grebenko, A. I., Levdikov, V. M., Urusova, D. V., Melik-Adamyan, V. R., Lamzin, V. S., and Wilson, K. S. (2001) Crystallography Reports 46(4), 687-691
23. Levdikov, V. M., Barynin, V. V., Grebenko, A. I., Melik-Adamyan, W. R., Lamzin, V. S., and Wilson, K. S. (1998) Structure 6(3), 363-376
24. Urusova, D. V., Antonyuk, S. V., Grebenko, A. I., Lamzin, V. S., and Melik-Adamyan, V. R. (2003) Crystallography Reports 48(5), 763-767
25. Lieberman, I. (1956) J Biol Chem 223(1), 327-339
26. Bass, M. B., Fromm, H. J., and Rudolph, F. B. (1984) J Biol Chem 259(20), 12330-12333
27. Choe, J. Y., Poland, B. W., Fromm, H. J., and Honzatko, R. B. (1999) Biochemistry 38(21), 6953-6961
28. Cooper, B. F., Fromm, H. J., and Rudolph, F. B. (1986) Biochemistry 25(23), 7323-7327
29. Fromm, H. J. (1958) Biochim Biophys Acta 29(2), 255-262
30. Honzatko, R. B., and Fromm, H. J. (1999) Arch Biochem Biophys 370(1), 1-8
31. Rudolph, F. B., and Fromm, H. J. (1969) J Biol Chem 244(14), 3832-3839
32. Cohn, M., and Rao, B. D. N. (1979) Magn. Reson. Imaging 1, 38-60
33. Firestine, S. M., and Davisson, V. J. (1993) J Med Chem 36(22), 3484-3486
34. Bradford, M. M. (1976) Anal Biochem 72, 248-254
35. Laemmli, U. K. (1970) Nature 227, 680-685
36. Hackney, D. D., Stempel, K. E., and Boyer, P. D. (1980) Methods Enzymol 64, 60-83
37. Ames, B. N., Dubin, D.T. (1960) J. Biol. Chem. 235, 764
38. Wehrli, W. E., Verheyden, D. L., and Moffatt, J. G. (1965) J Am Chem Soc 87, 2265-2277
39. Wehrli, W. E., and Moffatt, J. G. (1965) J Am Chem Soc 87, 3760-3766
40. Maurer, T., and Kalbitzer, H. R. (1996) J Magn Reson B 113(2), 177-178
41. Pflugrath, J. W. (1999) Acta Crystallogr D Biol Crystallogr 55, 1718-1725
42. 4, C. C. P. N. (1994) Acta Crystallogr D Biol Crystallogr 50, 760-763

43. Brunger, A. T., Adams, P. D., Clore, G. M., DeLano, W. L., Gros, P., Grosse-Kunstleve, R. W., Jiang, J. S., Kuszewski, J., Nilges, M., Pannu, N. S., Read, R. J., Rice, L. M., Simonson, T., and Warren, G. L. (1998) Acta Crystallogr D Biol Crystallogr 54, 905-921
44. Engh, R. A., and Huber, R. (1991) Acta Crystallogr A47, 392-400
45. Corbridge, D. E. C. (1974) The Structural Chemistry of Phosphorous, Elsevier Scientific Publishing Company, Amsterdam
46. Cohn M, N. R. B. (1979) Bulletin of Magnetic Resonance 1, 38-60
47. Poland, B. W., Bruns, C., Fromm, H. J., and Honzatko, R. B. (1997) J Biol Chem 272(24), 15200-15205
48. Iancu, C. V., Borza, T., Fromm, H. J., and Honzatko, R. B. (2002) J Biol Chem 277(30), 26779-26787
49. Poland, B. W., Fromm, H. J., and Honzatko, R. B. (1996) J Mol Biol 264(5), 1013-1027
50. Markham, G. D., and Reed, G. H. (1977) Arch Biochem Biophys 184(1), 24-35
51. Litchfield, G. J., and Shaw, G. (1971) J Chem Soc (B), 1474-1484
52. Idstrom, J. P., Soussi, B., Elander, A., and Bylund-Fellenius, A. C. (1990) Am J Physiol 258(6 Pt 2), H1668-1673
53. Dudley, G. A., and Terjung, R. L. (1985) Am J Physiol 248(1 Pt 1), C43-50
54. Tullson, P. C., Whitlock, D. M., and Terjung, R. L. (1990) Am J Physiol 258(2 Pt 1), C258-265
55. Arabadjis, P. G., Tullson, P. C., and Terjung, R. L. (1993) Am J Physiol 264(5 Pt 1), C1246-1251
56. Boffi, F. M., Ozaki, J., Matsuki, N., Inaba, M., Desmaras, E., and Ono, K. (2002) J Vet Med Sci 64(6), 483-488
57. Davies, K. J., Quintanilha, A. T., Brooks, G. A., and Packer, L. (1982) Biochem Biophys Res Commun 107(4), 1198-1205
58. Dobson, J. G., Jr., Rubio, R., and Berne, R. M. (1971) Circ Res 29(4), 375-384
59. Phair, R. D., and Sparks, H. V. (1979) Am J Physiol 237(1), H1-9
60. Rubio, R., Berne, R. M., and Dobson, J. G., Jr. (1973) Am J Physiol 225(4), 938-953
61. Tullson, P. C., and Terjung, R. L. (1990) Int J Sports Med 11 Suppl 2, S47-55
62. Carlucci, F., Biagioli, B., Maccherini, M., Sani, G., Simeone, F., Bizzarri, F., Perrett, D., Marinello, E., Pagani, R., and Tabucchi, A. (1998) Clin Biochem 31(4), 235-239
63. Hohl, C. M. (1999) Am J Physiol 276(5 Pt 2), H1502-1510
64. Imai, S., Riley, A. L., and Berne, R. M. (1964) Circ Res 15, 443-450
65. Gustafson, L. A., Zuurbier, C. J., Bassett, J. E., Barends, J. P., van Beek, J. H., Bassingthwaighte, J. B., and Kroll, K. (1999) Cardiovasc Res 44(2), 333-343
66. Reibel, D. K., and Rovetto, M. J. (1978) Am J Physiol 234(5), H620-624
67. Reibel, D. K., and Rovetto, M. J. (1979) Am J Physiol 237(2), H247-252
68. Jacob, M. I., and Berne, R. M. (1960) Am J Physiol 198, 322-326
69. Kraulis, P. J. (1991) J Appl Crystallogr 24, 946-950

Table 1: Statistics of X-Ray Data Collection and Refinement

Ligand Complex	AICAR, Mg^{2+}, ADP	PAICAR, Mg^{2+}, ADP	IMP, Mg^{2+}, ADP	N1-PIMP, Mg^{2+}, ADP
Space Group	$P2_12_12_1$	$P2_12_12_1$	$P2_12_12_1$	$P2_12_12_1$
Unit Cell Parameters	a=59.43, b=66.83, c=153.72	a=59.20, b=68.21, c=149.14	a=59.32, b=67.75, c=146.53	a=59.18, b=67.34, c=148.81
Resolution	61.3 – 1.95 (2.02 – 1.95)	62.0 – 2.29 (2.47 – 2.29)	61.5 – 2.00 (2.07 – 2.00)	44.5 – 1.50 (1.55 – 1.50)
Reflections	221756	148,200	234,413	429897
Unique Reflections	42798	27,893	37,051	93,711
% Completeness	94.1 (62.9)	99.8 (100)	91.0 (55.2)	97.7 (97.0)
R_{merge}[a]	0.066 (0.186)	0.091 (0.236)	0.055 (0.194)	0.066 (0.490)
No. of atoms	4,154	4,148	4,161	4,354
No of solvent sites	256	248	255	452
R_{factor}[b]	21.5	20.7	21.3	23.2
R_{free}[c]	24.5	25.2	24.2	24.8
Mean B for protein ($Å^2$)	24.1	28.3	27.5	24.6
Mean B for ligands ($Å^2$)	19.6	24.7	25.4	20.4
Mean B for waters ($Å^2$)	28.6	29.9	31.2	34.5
Bond lengths (Å)	0.006	0.006	0.006	0.005
Bond angles (deg.)	1.2	1.2	1.3	1.2
Dihedral angles (deg.)	22.6	22.6	22.8	22.6
Improper angles (deg.)	0.72	0.73	0.73	0.72

Table II. Footnotes.

[a] $R_{merge} = \Sigma_j\Sigma_i \mid I_{ij} - \langle I_j \rangle \mid / \Sigma_i\Sigma_j I_{ij}$, where i runs over multiple observations of the same intensity, and j runs over all crystallographically unique intensities.

[b] $R_{factor} = \Sigma \mid\mid F_{obs} \mid - \mid F_{calc} \mid\mid / \Sigma \mid F_{obs} \mid$, where $\mid F_{obs} \mid > 0$.

[c] R_{free} based upon 10% of the data randomly culled and not used in the refinement.

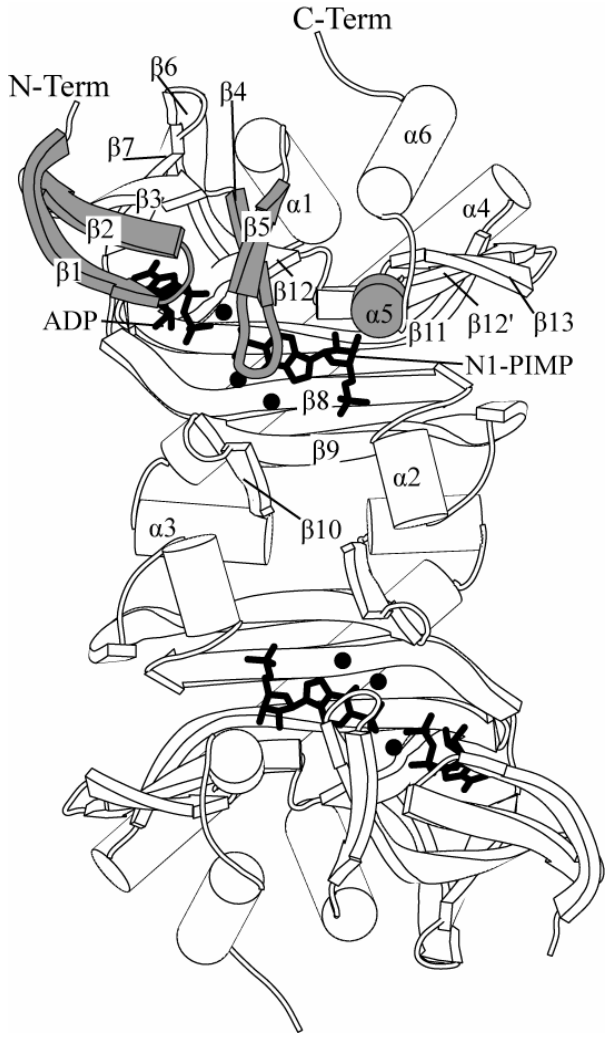

Figure 1. Structure of SAICAR synthetase. The active site of eSS is a deep cleft that extends without interruption between subunits of the dimer. Bold lines and filled circles represent bound 1-PIMP, ADP, and Mg^{2+}. Secondary elements are labeled and the P-loop (β1,β2), the 30s loop (β4, β5), and helix 5 (α5) are shaded in grey. Parts of this figure were drawn with MOLSCRIPT (69).

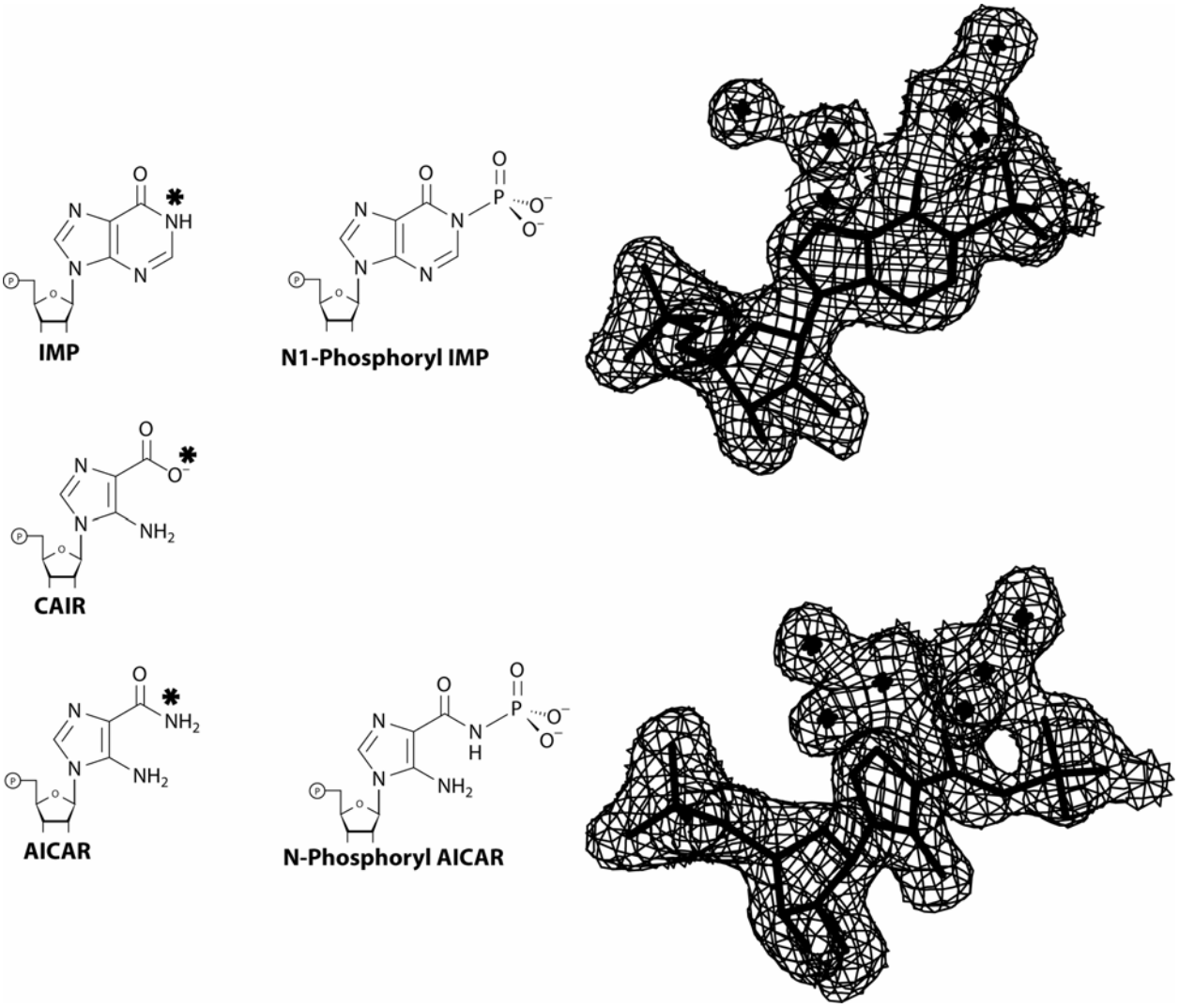

Figure 2. CAIR Analogues and demonstration of their electron density. (left) Chemical structures of AICAR, CAIR, and IMP with an asterisk marking the corresponding nucleophilic atoms. (center) Chemical structures of 1-PIMP and N-phosphoryl AICAR. (right) Omit electron density covering the hydrated 1-PIMP-Mg^{2+} molecule and N-phosphoryl AICAR bound at the active site of eSS. The contour level is at 1σ with a cutoff radius of 1 Å. Parts of this figure were drawn with Xtalview (21).

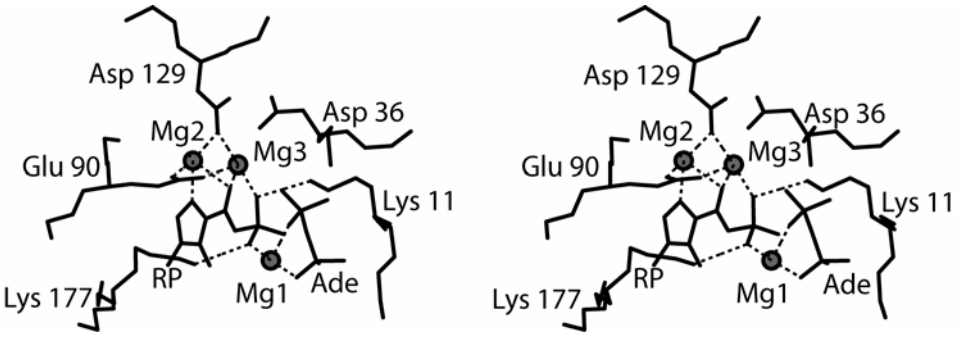

Figure 3. Stereoview of the active site of the PAICAR•ADP•Mg^{2+} complex. Mg^{2+} at sites 1, 2 and 3 are filled circles. Coordination bonds are dashed lines. Adenosine is omitted for clarity and labeled as Ade. The 5'-ribose moiety of PAICAR is labeled as RP. Parts of this figure were drawn with Molscript (69).

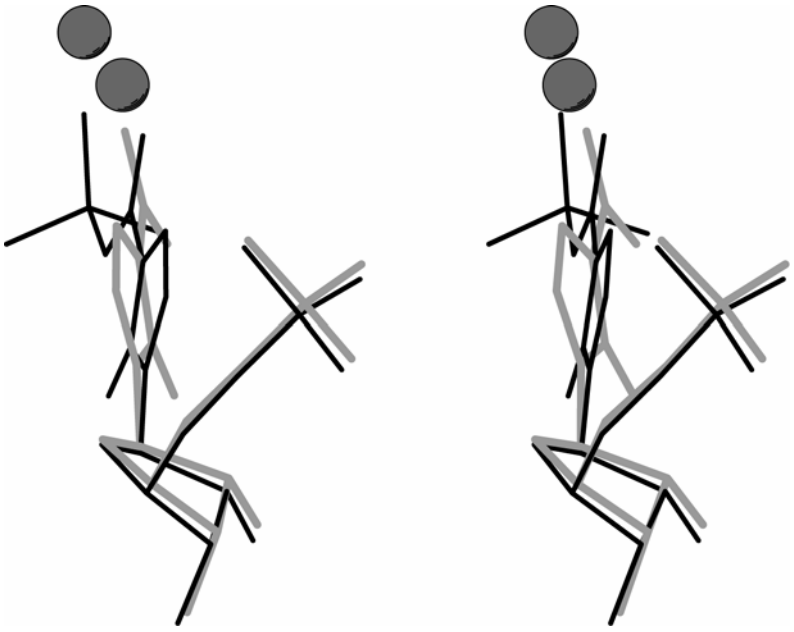

Figure 4. Stereoview of the superposition of AICAR•Mg^{2+} and PAICAR•Mg^{2+}. Mg^{2+} at sites 2 and 3 in the two structures are nearly identical, so they are drawn as a single set of filled circles. PAICAR is drawn in black lines and AICAR in grey lines. The rotation around the C2'-C1'-N1-C2 torsion angle is evident by looking at how well the 5'-ribose moieties overlay. Parts of this figure were drawn with Molscript (69).

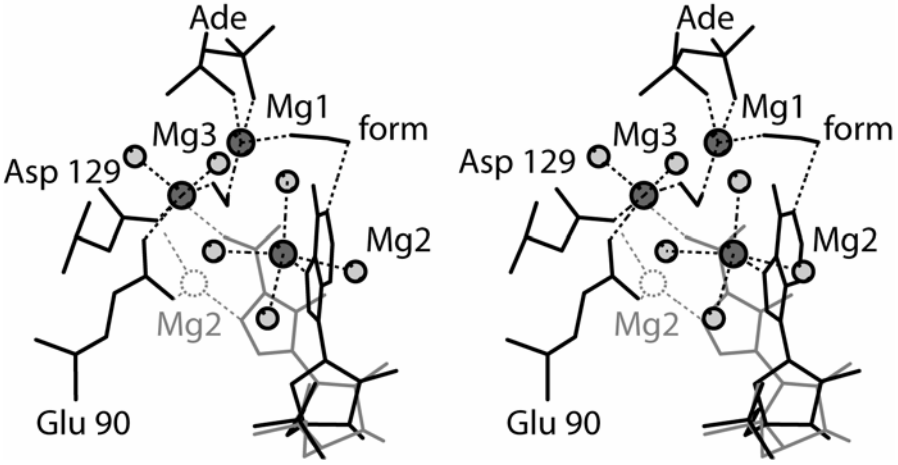

Figure 5. Stereoview of the IMP•ADP•Mg^{2+} Complex. Mg^{2+} at sites 1, 2 and 3 are filled circles. Coordination bonds are dashed lines. Adenosine is omitted for clarity and labeled as Ade. IMP is drawn in black lines. The CAIR•ADP•Mg^{2+} structure of 2GQS is superimposed and CAIR is drawn in grey and magnesium site 2 in dashed grey lines. The formate ion that bridges sites 1 and 2 is not labeled for clarity, and the other binding site is abbreviated as "form." Parts of this figure were drawn with Molscript (69).

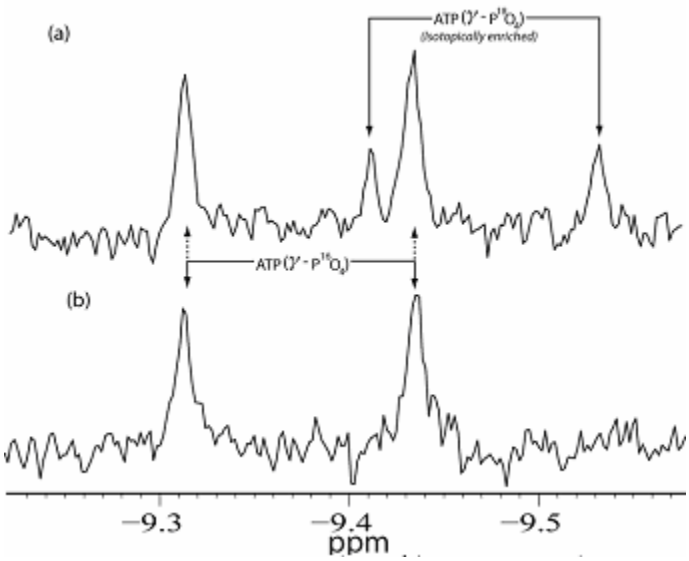

Fig. 6. ^{31}P NMR spectrum of the γ-phosphorus of a 1:1 mixture of γ-^{16}O/ γ-^{18}O ATP each at 5mM (a), and 5mM γ-^{16}O ATP (unlabeled) (b). Both samples contained 50mM HEPES (pH 7.0), 10% D_2O, 4mM KP_i, and NaCl from HPLC isolation (see experimental procedures). 1mM DSS (2,2-dimethyl-2-silapentane-5-sulfonic acid) was also added for indirect chemical shift referencing by use of 1D ^{1}H NMR (parameters for calculation of a new SR value are listed in results).

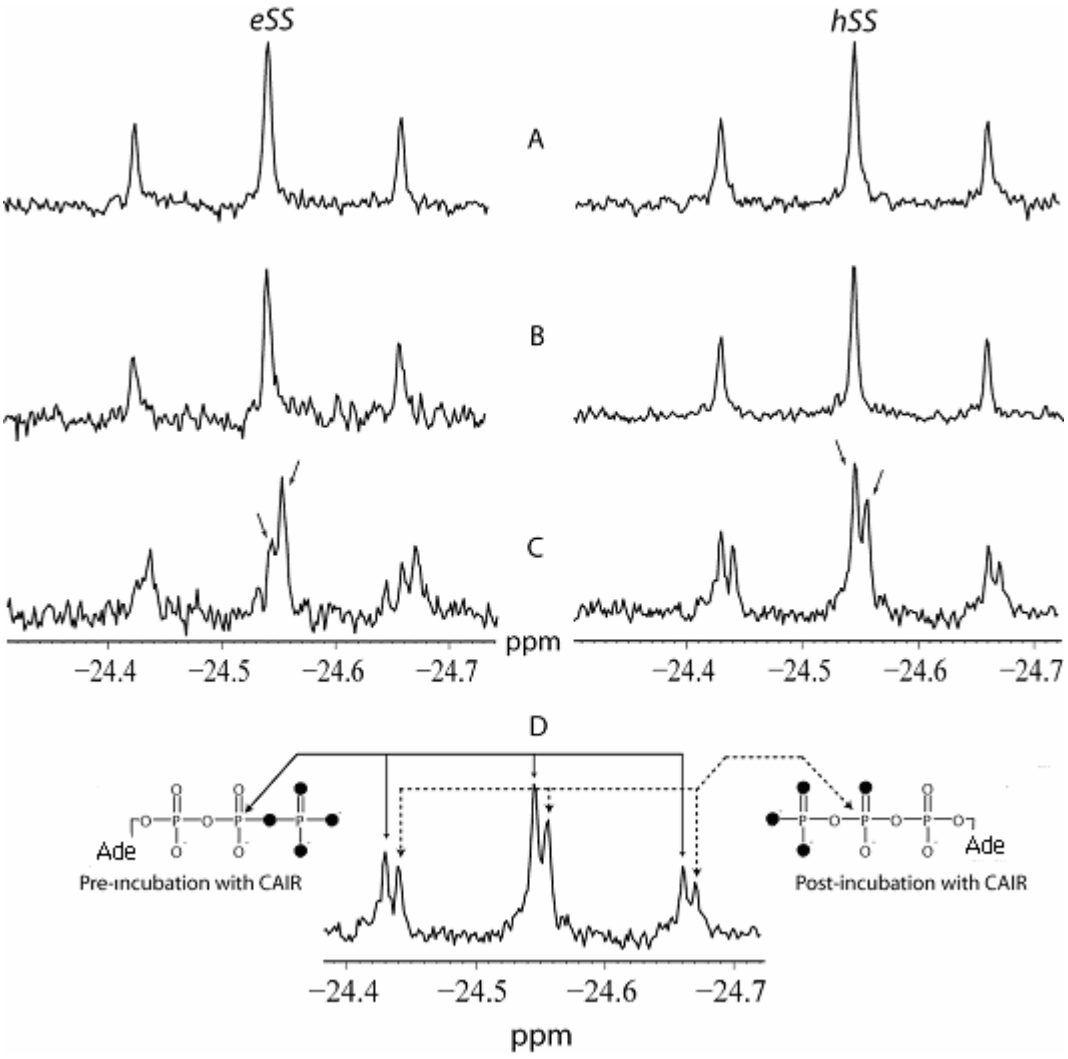

Figure 7. ^{31}P-NMR spectrums of the **β**-P^{18}O$_4$ peaks of purified **γ**-^{18}O ATP from three different incubation conditions using eSS (***left***) and hSS (***right***). (A) 5mM γ-^{18}O ATP only, (B) 5mM γ-^{18}O ATP, 5 mM L-aspartate; (C) 5mM γ-^{18}O ATP, 1mM CAIR[2,3]; (D) depiction of the chemical shift of the β-phosphate peaks associated with movement of the β-γ bridging ^{18}Oxygen to a terminal β-phosphate position. γ-^{18}O ATP incubation utilizing CAIR for hSS incorporated 10μM NAIR to prevent decarboxylation of CAIR by the AIRC half of the enzyme. Arrows denote the original and chemical shifted peaks for (C).

Chapter V: Determinants of L-Aspartate Recognition in Phosphoribosyl-Aminoimidazole-Succinocarboxamide Synthetase[†]

A paper pending submission to Biochemistry

Nathaniel D. Ginder[1], Daniel J. Binkoski[1], Lu Shen, Muneaki Watanabe, Herbert J. Fromm, and Richard B. Honzatko[*]

Abstract

Phosphoribosyl-aminoimidazole-succinocarboxamide synthetase [EC 6.3.2.6, 5′-phosphoribosyl-4-carboxy-5-aminoimidazole: L-aspartate ligase (ADP)] (hereafter, SAICAR synthetase) is a target in the treatment of cancer. Conformational differences in SAICAR synthetases suggest significant conformational change attends the binding of the substrate 4-carboxy-5-aminoimidazole ribonucleotide (CAIR). The radius of gyration of the enzyme from Escherichia coli, as measured by dynamic light scattering, decreases in response to CAIR binding. Alanine mutations of Asp36??, Arg94, Ser100, Asp175, Arg199, Lys211 and Arg215 (all in proximity to CAIR) cause up to a 95-fold increase in the K_m for CAIR, but some (alanine mutations of Asp36, Lys211, and Arg215) cause more than 100-fold increases in the K_m for L-aspartate with no effect on the K_m of CAIR or ATP. Additional mutations, which probe the interaction of Asp36 with hydrated Mg^{2+} associated with the 4-carboxyl group of CAIR, further implicate the 30s loop (residues 31–43) as an important determinant in L-aspartate recognition. Structural data presented

here reveal interactions involving Arg215 and the 30s loop with L-aspartate, and that maleate, a competitive inhibitor with respect to L-aspartate, binds to the β-carboxyl locus of the amino acid substrate. These data support a mechanism in which CAIR organizes the active site for the productive binding of L-aspartate through its interactions with Arg215 and the 30s loop.

---

[1]These authors contributed equally to this work.

[†]This work was supported in part by National Institutes of Health Research Grant NS 10546.

[*]Corresponding author. Telephone: (515) 294-7103. Fax: (515) 294-0453. E-mail: honzatko@iastate.edu.

[2]Abbreviations are as follows: 5-aminoimidazole-4(N-succinylcarboxamide) ribonucleotide, SAICAR; 4-carboxy-5-aminoimidazole ribonucleotide, CAIR; 5-aminoimidazole-4-carboxamide-β-D-ribofuranoside, AICARs; 5-aminoimidazole-5-(N-carboxy) ribonucleotide, N^5-CAIR; Escherichia coli SAICAR synthetase, eSS, Thermatoga maritima SAICAR synthetase, tSS; Saccharomyces cerevisiae SAICAR synthetase, ySS.

[3]Nathaniel D. Ginder and Richard B. Honzatko, unpublished results.

Introduction

Phosphoribosyl-aminoimidazole-succinocarboxamide synthetase (SAICAR[2] synthetase), an enzyme in de novo purine biosynthesis, catalyzes the conversion of ATP, 4-carboxy-5-aminoimidazole ribonucleotide (CAIR) and L-aspartate into 5-aminoimidazole-4-(N-succinylcarboxamide) ribonucleotide (SAICAR), ADP, and P_i. In bacteria such as Escherichia coli, the conversion of 5-aminoimidazole ribonucleotide (AIR) into SAICAR employs three single-function enzymes, PurK (AIR to N^5-CAIR), PurE (N^5-CAIR to CAIR), and PurC (CAIR to SAICAR) (5); whereas in vertebrates, a single enzyme catalyzes the transformation of AIR to SAICAR (1,2,4,62). The chemistry of the AIR to

SAICAR transformation differs for vertebrate and bacterial systems, the latter using ATP and bicarbonate in the generation of N^5-CAIR (3,41,62); whereas, the vertebrate enzyme uses carbon dioxide and AIR directly to make CAIR. Fungi such as Candida albicans and Cryptococcus neoformans combine the PurK and PurE functions into a single protein but retain a single-function enzyme similar to that of the E. coli system for the synthesis of SAICAR from CAIR (38,39).

Enzymes of de novo purine nucleotide biosynthesis are targets in the treatment of cancer and infectious disease. Many cancers, for instance, have damaged salvage pathways for purine nucleotides and, hence, are more sensitive to the inhibition of de novo purine nucleotide biosynthesis than non-cancerous cells (13). Blockage of purine metabolism in Candida albicans and Crypotcoccus neoformans attenuates meningoencephilitis infections in immune compromised rodents, even though these organisms are capable of salvaging purines from the host (63,64). Similarly, mutant Brucella with a PurE gene knockout, but intact salvage pathways, exhibit diminished virulence. Such mutants have been used in vaccines for humans and animals (65).

L-Alanosine therapy shows promise as a treatment for certain types of leukemia and gliomas (13). SAICAR synthetase in humans uses L-alanosine in place of L-aspartate, forming the SAICAR analog, 5-aminoimidazole-4-(N-alanosylcarboxamide) ribonucleotide, a potent inhibitor of adenylosuccinate synthetase and adenylosuccinate lyase (25,27). L-Alanosine is toxic to both cancerous and normal cells, but supplemental doses of deoxyadenosine ameliorates L-alanosine toxicity toward normal cells (25), allowing for the selective inhibition of cancer cell lines with homozygous deficiencies in methylthioadenosine phosphorylase (13).

L-Alanosine has potential as a drug because SAICAR synthetase is unable to distinguish it from L-aspartate (6). In contrast, L-alanosine is a poor substrate for adenylosuccinate synthetase and aspartate carbamoyltransferase (66,67). Hence, the recognition of L-aspartate in SAICAR synthetase must differ in some fundamental way from its recognition in these other systems. Recent structures of E. coli SAICAR synthetase in complexes with ADP•Mg^{2+} and CAIR•ADP•Mg^{2+} infer a role for CAIR in the recognition of L-aspartate (35). Reported here is a crystal structure of an L-aspartate•sulfate•ADP•Mg^{2+} complex that confirms the interaction of Arg215 and residues 31–43 (30s loop) with the amino acid substrate. The properties of mutant SAICAR synthetases are consistent with a mechanism in which the binding of CAIR brings Arg215 and the 30s loop into the active site. The CAIR-induced conformational changes enable the productive binding of L-aspartate. The enzyme interacts directly with only one of two oxygen atoms of the β-carboxyl group of L-aspartate, as opposed to more extensive recognition of the same moiety by adenylosuccinate synthetase and aspartate carbamoyltransferase. The weak recognition of the β-carboxyl group by SAICAR synthetase may explain its inability to distinguish the true substrate from L-alanosine.

Experimental Procedures

Materials— L-Aspartate, L-malate, L-cysteine sulfinate, succinate, maleate, ATP, NADH, phosphoenolpyruvate, pyruvate kinase and lactate dehydrogenase came from Sigma, 5-aminoimidazole-4-carboxamide-β-D-ribofuranoside (AICARs) from Toronto Research Chemicals, alkaline phosphatase from Roche, kanamycin sulfate from Gibco, E. coli strains BL21(DE3) and chemically competent DH5α from Invitrogen, isopropyl-β-D-

thiogalactopyranoside (IPTG) from Anatrace, 2′-deoxyribonucleoside triphosphates and restriction endonuclease DpnI from New England Biolabs, PfuTurbo DNA polymerase from Stratagene, QIAprep Spin Miniprep kit for plasmid isolation from Qiagen, and Ni-nitrilotriacetic acid (NTA)-agarose from Novagen. L-Alanosine was obtained from the Drug Research and Development Branch, National Cancer Institute, Bethesda MD. All other chemicals were of reagent grade. The pET 28b vector containing the insert coding for eSS with an N-terminal hexahistidyl tag came from previous work (6). Integrated DNA Technologies and the Iowa State University DNA Synthesis and Sequencing Facility generated oligonucleotide primers.

Synthesis of CAIRs— AICARs (250 mg) was saponified for 4 hours in 6 M NaOH (4 mL) as described by Srivastava et al. (68) subject to modifications (6). 4 mL of pure ethanol was added (via syringe to avoid the introduction of O_2) to the reaction mixture (under N_2 at 0 °C), then mixed vigorously. The syrupy bottom phase was transferred by pipette to 10 mL of pure ethanol in a dry 250 mL lyophilizer flask, and mixed with a magnetic stir-bar. The ethanol layer was discarded, and the remaining syrup triturated with 10 mL ethanol three times. The resulting hard, light purple, glassy residue was triturated with 1–2 mL of methanol, yielding a whitish-purple colloid. Lyophilization provided a light purple hygroscopic substance, which was purified by DEAE chromatography, using a buffer of triethylammonium bicarbonate, pH 8.0. CAIRs was collected and lyophilized as described previously (6).

Synthesis of CAIR— 100 mg of purified CAIRs was phosphorylated by the procedure of Yoshikawa et al. (69) as modified by Meyer et al. (5). After lyophilization, CAIR was dissolved in 10 mM CHES, pH 8.5, to prevent decarboxylation (62), and stored at –80 ºC.

The concentration of CAIR was determined by the stoichiometric conversion of NADH to NAD^+ using SAICAR synthetase and the coupling enzymes pyruvate kinase and lactate dehydrogenase and by chemical assays described previously (6). Both procedures indicated concentrations of CAIR within 3% agreement.

Construction of mutant SAICAR synthetases— Directed mutagenesis employed protocols from Stratagene using the Polymerase Chain Reaction (PCR), PfuTurbo DNA polymerase, 2′-deoxyribonucleoside triphosphates, template DNA (pET 28b vector containing the eSS insert with an N-terminal hexahistidyl tag), and primers and their reverse complements with the following sequences:

D175A, 5′-GGTCTGATTCTGGTCGCGTTCAAGCTGG-3′,

R199A 5′-CGGACGGTAGCGCCCTGTGGGACAAAGAAACG-3′;

R94A 5′-GGTTGAGTGTGTCGTGGCGAACCGTGCTGCTGG-3′;

S100A 5′-CCGTGCTGCTGGCGCTCTGGTGAAACGTC-3′;

K211A 5′-

GGACAAAGAAACGCTGGAGAAAATGGCGAAAGACCGTTTCCGCCAGAGC-3′;

R215A 5′-GGACAAAGACCGTTTCGCGCAGAGCCTCGGTGGCCTGATCG-3′.

D36N 5′-GATACGTCAGCAGGGAATGGCGCGCGCATTGAGCAG-3′;

D36A 5′-GATACGTCAGCAGGGGCGGGCGCGCGCATTGAGCAG-3′

S33A 5′-CCGCAATGATACGGCAGCAGGGGATGGCGCGCGC-3′

Del30 (G35P, A38G, Δ36-37) 5′-

CGAATTCCGCAATGATACGTCAGCACCGGGCCGCATTGAGCAGTTTGATCGC

-3′

A programmable thermocycler (BioRad iCycler) amplified mutant plasmids in a reaction volume of 50 μL. Incubation of the reaction mixture with 20 U of DpnI for 2 hrs at 37 °C removed the template plasmid. Cells were transformed into chemically competent E. coli DH5α cells and selected on Luria broth agar plates with kanamycin (30 μg/mL). Plasmid purification employed the QIAprep Spin Miniprep kit. Confirmation of all constructs was performed by sequencing of entire inserts by the Iowa State University DNA Synthesis and Sequencing Facility.

Purification of E. coli SAICAR Synthetase— Single colonies of plasmid-transformed E. coli strain BL21 (DE3) were used as inoculants of overnight cultures of Luria broth containing 30 μg/mL kanamycin sulfate. Each of 12 flasks containing 500 mL of Luria broth was inoculated with 5 mL of overnight culture and then grown with shaking (at 38 °C) to an A_{600} of 1.0. Cell cultures were cooled to 16 °C, induced with 0.25 mM isopropyl-β-D-thiogalactopyranoside (IPTG), and allowed to grow with shaking for an additional 16 hours before harvesting by centrifugation.

Harvested cell pellets were suspended in 80 mL of 20 mM KP_i, 500 mM NaCl, 10 mM imidazole, pH 8.0, and lysed with a French press at 20,000 psi. After centrifugation at 15,000xg for 45 minutes, the cell-free extract was loaded onto a Ni-nitrilotriacetic acid-agarose column and washed with 10 column volumes of lysis buffer (6). A second wash with 10 column volumes of lysis buffer containing 40 mM imidazole was followed by the elution of SAICAR synthetase with lysis buffer containing 250 mM imidazole. Protein purity and concentration was confirmed by sodium dodecylsulfate polyacrylamide gel electrophoresis (SDS-PAGE) and by Bradford assay, using bovine serum albumin as a standard (70).

Kinetic assays— Activity assays of each mutant used either a coupling system (5) or a direct assay (62). All assays were done in triplicate at 37 °C, in a total volume of 1 mL, using 10, 25, 2, 5, 2, 35, 2, 10, 50, 200, and 50 µg of wild-type, S33A, D36A, D36N, Del30, R94A, S100A, D175A, R199A, K211A, and R215A enzyme, respectively. 1 and 2 µg were used, respectively, to determine the K_m of CAIR for the D36N and S33A mutants. The assay buffer contained 50 mM Tris·HCl, pH 7.8, and 6 mM $MgCl_2$. The concentration of one substrate was varied from $0.2xK_m$ to $5xK_m$ while holding the other two substrates constant at $5xK_m$. Data were fit to the Michaelis-Menten equation with Grafit (71).

The determination of inhibition mechanisms of analogs of L-aspartate employed 5 concentrations of L-aspartate, varying from $0.2xK_m$ to $5xK_m$, and 5 concentrations of the analog, varying from 1.6–16 mM (for maleate), 20–100 mM (for L-malate), and 20–100 mM (for succinate). Concentrations of CAIR and ATP were $5xK_m$. Data were fit to models for competitive, noncompetitive, uncompetitive and mixed inhibition using Dynafit (72). The model with the best fit and fewest adjustable parameters determined the kinetic mechanism of inhibition.

Isolation of Sulfinate SAICAR Analog— Determination of mass of the product confirmed the enzyme-mediated reaction involving L-cysteine sulfinate. The coupled assay system drove to completion a reaction of 10 mM L-cysteine sulfinate, 2 mM CAIR, 2 mM ATP, and 50 µg eSS in a volume of 1 mL. After incubation with 1 U of alkaline phosphatase for 12 hrs at 37 °C, proteins were removed from the reaction mixture by the addition of 100 µL of chloroform, followed by centrifugation. Conversion of the nucleotides to their corresponding nucleosides by alkaline phosphatase enabled the chromatographic

resolution of product. The supernatant fraction was loaded onto Tosohaus Toyopearl DEAE 650m resin, washed with 150 mM ammonium bicarbonate and eluted with a gradient of 150–300 mM ammonium bicarbonate, monitoring the eluent at a wavelength of 260 nm. Pooled fractions were lyophilized, twice re-suspended in 10% ammonium hydroxide and lyophilized, and finally dissolved in 3 mL of de-ionized water and lyophilized again. The Proteomics Facility of the Iowa State University Plant Sciences Institute performed mass spectroscopic analyses.

Circular Dichroism— A Jasco J-710 spectropolarimeter provided CD spectra (190–260 nm) for mutant and wild-type enzymes. Proteins (5 µM) were in 5 mM KCl, 5 mM Tris·HCl, pH 7.8 (temperature and sample volume of 25 °C and 175 µL, respectively). Spectra from buffer without protein provided baseline corrections.

Dynamic Light Scattering— Concentrations of ADP, CAIR, and/or L-aspartate were 1, 0.5, and 5 mM, respectively, in solutions containing SAICAR synthetase (2 mg/ml), 6 mM $MgCl_2$, 10 mM Hepes, pH 7.8, and 1 mM dithiothreitol (DTT). Centrifugation of samples and rinse water in a high-speed bench-top centrifuge for 15 minutes removed dust. High baseline counts or large fluctuations over time indicated dust contamination and necessitated repeated washings of the cuvette with dust-free water. Data were collected from sample volumes of 12 µL using a Proteins Solutions Dynapro Light Scattering instrument. Acquisitions employed 100% laser power at 25 ºC with final mass calculations using between 113–884 scans. Data were analyzed using Dynamics V6 software assuming an isotropic sphere model. Anomalous scans were excluded prior to the calculation of mass. For each condition of ligation, final mass numbers came from triplicate runs performed on different days and from different protein preparations.

Crystallization— Crystals were grown by the method of hanging-drop vapor diffusion in VDX-plates (Hampton Research). For the maleate•CAIR•ADP•Mg^{2+} complex, 2 μL of protein solution (15 mg/mL protein, 15 mM Tris·HCl, 25 mM KCl, 100 mM $MgCl_2$, 50 mM ADP, 2 mM CAIR, 300 mM maleate, 5 mM dithiothreitol, and 5 mM EDTA, pH 8.0) were mixed with 2 μL of well solution (3.4–3.8 M sodium formate and 50 mM Tris·HCl, pH 8.5) and allowed to equilibrate against 0.5 mL of well solution. Single crystals of equal dimensions grew to 0.2–0.3 mm within 72 hrs. For the L-aspartate•sulfate•ADP•Mg^{2+} complex, 2 μL of protein solution (15 mg/mL protein, 15 mM Tris·HCl, 25 mM KCl, 50 mM $MgSO_4$, 25 mM ATP, 1.5 mM CAIR, 5 mM dithiothreitol, and 5 mM EDTA, pH 8.0) were mixed with 2 μL of well solution (24-33% PEG 8000, 0.7 M L-aspartate, 50 mM sodium cacodylate, pH 6.5) and allowed to equilibrate against 0.5 mL of well solution. Single crystals grew within five days.

Data Collection— Maleate•CAIR•ADP•Mg^{2+} Crystals were transferred to a cryoprotectant solution containing 4 M sodium formate, 50 mM Tris·HCl, pH 8.5, 100 mM $MgCl_2$, 25 mM ADP, 1 mM CAIR, 300 mM maleate and 10% (w/v) sucrose. L-aspartate•sulfate•ADP•Mg^{2+} crystals were transferred to well solution supplemented with 10% sucrose and the ligands present in the protein solution. After approximately 30 seconds of equilibration, crystals were plunged into liquid nitrogen. Data were collected at Iowa State University from a single crystal (temperature, 115 K) on a Rigaku R-AXIS IV++ rotating anode/image plate system using CuK_α radiation from an Osmic confocal optics system. Data were processed and reduced using the program package CrystalClear provided with the instrument. The CCP4 program TRUNCATE (73) converted intensities to structure factors.

Structure Determination and Refinement— Structure determination employed the CAIR•ADP•Mg^{2+} complex (PDB ascension identifier 2GQS, less ligands and water molecules) in molecular replacement phasing. Crystals of the L-aspartate•sulfate•ADP•Mg^{2+} complex, maleate• CAIR•ADP•Mg^{2+}, and CAIR•ADP•Mg^{2+} complex are isomorphous, having a complete dimer in the asymmetric unit. Inspection (using XTALVIEW(74)) revealed excellent agreement between electron density and model. Refinement without non-crystallographic restraints employed CNS (75) and simulated annealing (starting temperature of 500 K) with slow cooling in increments of 25 K to a final temperature of 300 K, followed by 100 steps of conjugate gradient energy minimization. Individual thermal parameters were refined after each cycle of simulated annealing and subject to the following restraints: bonded main-chain atoms, 1.5 $Å^2$; angle main-chain atoms, 2.0 $Å^2$; bonded side-chain atoms, 2.0 $Å^2$; and angle side-chain atoms, 2.5 $Å^2$. Water molecules were automatically added using CNS if a peak greater than 3.0σ was present in Fourier maps with coefficients $(F_{obs}–F_{calc})\ e^{i\alpha calc}$. Finally, a model for the ligands were fit to omit electron density. Refined water sites further than 3.2 Å from a hydrogen-bonding partner or with thermal parameters in excess of 50 $Å^2$ were eliminated The contribution of the bulk solvent to structure factors was determined using the default parameters of CNS. Constants of force and geometry for the protein came from Engh and Huber (76) and those for ADP, CAIR, and maleate from CNS resource files with appropriate modification of dihedral angles of the ribosyl moiety to maintain a 2′-endo ring conformation. Superposition of structures employed routines in the CCP4 suite of programs.

Results

Purity and conformational status of enzymes— Wild-type and mutant SAICAR synthetases were at least 95% pure on the basis of sodium dodecylsulfate polyacrylamide gel electrophoresis (SDS-PAGE). Circular dichroism spectra of the alanine mutations of Arg94, Ser100, Arg199, Lys211 and Arg215 are identical to that of the wild-type enzyme. The D175A enzyme, although active upon elution from Ni-nitrilotriacetic acid-agarose, precipitated during dialysis into a buffer suitable for recording a CD spectrum. Hence, changes in kinetic parameters due to the mutation at position 175 may be due to long-range perturbations in structure. CD spectra were not recorded for the D36N, D36A, S33A, or Del30 enzymes, but the D36N and S33A enzymes had k_{cat} values comparable to those of wild-type enzyme, and the D36A and Del30 enzymes crystallized under wild-type conditions and gave structures identical to the wild-type enzyme except in close proximity to the 30s loop[3]. Apparent masses of wild-type SAICAR synthetase decrease significantly with addition of saturating levels of CAIR and/or ADP, with or without L-aspartate (Table 2).

General Structural Features of Ligand Complexes of eSS— An eSS homodimer occupies the crystallographic asymmetric unit in the maleate•CAIR•ADP•Mg^{2+} and L-aspartate•sulfate•ADP•Mg^{2+} complexes reported here (Fig. 1). Statistics of data collection and refinement for the structures are in Table 1. The subunits are identical within the coordinate uncertainty. Electron density is not present for the hexahistidyl tag; however, observable electron density begins with M1 and continues to the C-terminal D237. The protein component of the four different complexes is nearly identical to that of the CAIR•ADP•Mg^{2+} structure (2GQS) (35). Superposition of all C_α positions of the

A subunit of each complex against the CAIR•ADP•Mg^{2+} structure gives root-mean-squared deviations of 0.3 Å for both structures. We focus here on the interactions of L-aspartate and maleate, referring the reader to the published CAIR•ADP•Mg^{2+} complex for additional information (35).

L-Aspartate•Sulfate•ADP•Mg^{2+} Complex— Electron density for ADP, sulfate (or phosphate), and Mg^{2+} in sites 1 and 3 are present in both subunits, but only in subunit A does electron density appear for L-aspartate. Under the conditions of crystallization, CAIR (approximately 1.5 mM) should go quantitatively to SAICAR, but L-aspartate (approximately 700 mM) is in great excess and evidently exchanges with SAICAR to give the observed complex. The α-carboxyl group of L-aspartate interacts with atom OG of Ser33 and the backbone amides of Gly35 and Asp36. One oxygen atom of the β-carboxyl group forms hydrogen bonds with the backbone amide of Gly35 and atom NE of Arg215. The α-amino group of L-aspartate interacts with the oxygen atom of the sulfate and with its own α-carboxyl group.

The superposition of the PAICAR•ADP•Mg^{2+} complex onto the L-aspartate•sulfate•ADP•Mg^{2+} complex (Figure 1) reveals sulfate in a location and orientation nearly identical to that of N-phosphoryl groups of PAICAR. PAICAR is an analogue of the putative phosphoryl intermediate of CAIR. Magnesium at site 3 in the L-aspartate complex has the same set of inner sphere ligands as in the PAICAR•ADP•Mg^{2+} complex except for a water molecule in place of the carbonyl group of PAICAR. Although no metal is present in site 2, the carboxyl group from Asp36 (30s loop) interacts with a water molecule coordinated with Mg^{2+} at site 3, analogous to interactions in the PAICAR complex. The α-amino of L-aspartate is 3.7 Å from the exocyclic amino

group, 2.6 Å from the carbon atom of the phosphoramide moiety of PAICAR, and ?? Å from the nitrogen atom of the phosphoramidate bond. The geometry is favorable for a nucleophilic attack of the α-amino group of L-aspartate on the carbon atom of a putative phosphoryl intermediate of CAIR.

Maleate•ADP•CAIR•Mg^{2+} Complex— Maleate binds near the 4-carboxyl group of CAIR. Donor-acceptor interactions involve one of its carboxyl groups with Arg215, the backbone amide of Asp36, and two water molecules near the 4-carboxyl group of CAIR. The other carboxyl group interacts with the backbone amide of Gly35 (Figure 2). Modeling L-aspartate onto the maleate molecule puts the α-amino group of the substrate some 4–5 Å from the carbon atom of the 4-carboxyl group of CAIR. Maleate in the crystal structure does not represent productively bound L-aspartate. The water molecules in proximity to the 4-carboxyl group of CAIR and the aforementioned carboxyl group of maleate partially block the L-aspartate pocket. A water-maleate complex then appears responsible for the competitive inhibition of SAICAR synthetase with respect to L-aspartate.

Kinetics of Wild-type and Mutant Synthetases— In the absence of CAIR, mutant and wild-type enzymes cause no significant hydrolysis of ATP; however, S33A, D36A, Del30, R94A, D175A, R199A, and K211A enzymes exhibit CAIR-dependent hydrolysis of ATP. CAIR-dependent ATP hydrolysis proceeds in the absence of L-aspartate, hence SAICAR cannot be formed. For some mutant enzymes (R94A, R199A, and K211A), the rate of CAIR-dependent hydrolysis of ATP is less than 5% of the rate of ATP hydrolysis in the presence of maximum substrate concentrations. Hence, for these and constructs that exhibit no measurable CAIR-dependent ATP hydrolysis (R215A, D36N, and wild-

type enzymes), determinations of K_m and k_{cat} employ coupled assays, assuming the equal molar formation of ADP and SAICAR (Table 3).

The rate of CAIR-dependent hydrolysis of ATP for the D175A enzyme is 50% of the rate of ATP hydrolysis in the presence of saturating substrates. The coupled assay then overestimates the rate of formation of SAICAR by the D175A enzyme, particularly at low concentrations of L-aspartate. Moreover, high apparent K_m values for CAIR and ATP for the Ala175 enzyme make the direct assay unfeasible, as optically-dense solutions mask increases in absorbance due to the formation of SAICAR. Hence, kinetic parameters in Table 3 for the Ala175 enzyme may be subject to systematic errors beyond those implied by their standard deviations.

Aside from the D175A enzyme, mutant SAICAR synthetases here show little change in their K_m values for ATP, the largest effect (3-fold increase) due to the R94A mutation. On the other hand, K_m values for CAIR increase 71-, 5-, and 14-fold for the R94A, S100A, and R199A enzymes, respectively. K_m values for L-aspartate increase 26-, 13-, 3-, 32-fold, for alanine mutations of Ser33 Arg94, Ser100, and Arg199, respectively, and K211A and R215A enzyme activities exhibit no signs of saturation up to 50 mM L-aspartate. (In assaying enzyme activity at high concentrations of L-aspartate, the coupled and direct assays are within 5% agreement in values for k_{cat} and K_m values for ATP and CAIR). At a concentration of 50 mM L-aspartate, the K211A and R215A enzymes show saturation kinetics at wild-type levels of CAIR and ATP (Table 3).

D36A and Del30 enzymes exhibit a peculiar phenomenon. In the direct assay, absorption at 282 nm increases in the presence of ATP and CAIR without L-aspartate. Addition of L-aspartate did not significantly alter the time-dependent increase in

absorption. Additionally, the D36A and Del30 enzymes exhibit CAIR-dependent hydrolysis of ATP in the absence of L-aspartate. With the addition of L-aspartate, the hydrolysis of ATP increases by less than 50%. Hence, neither the direct- nor coupled-assay could provide data free of systematic errors due to reactions that on the one hand consume ATP, but on the other lead to a UV-absorbing product that cannot be SAICAR.

The effect on k_{cat} varies significantly due to the mutations of the three side chains that hydrogen bond to the 5′-phosphoryl group of CAIR. The S100A enzyme exhibits a slight decrease in k_{cat} relative to the wild-type enzyme, whereas the R94A and R199A enzymes are less active by a 7- and 48-fold, respectively. The K211A and R215A synthetases have the least activity, exhibiting pseudo first-order rate constants (obtained in the presence of saturating concentrations of CAIR and ATP) of 60- and 120-fold lower, respectively, than k_{cat} for the wild-type enzyme. The D36N and S33A enzymes in the 30s loop had little effect on k_{cat}.

Kinetics of wild-type synthetase with analogs of L-aspartate—E. coli SAICAR synthetase cannot distinguish between L-aspartate and L-alanosine (Table 4, identical K_m and k_{cat} values within experimental uncertainty). L-cysteine sulfinic acid, having $–SO_2H$ in place of the β-carboxyl group of L-aspartate, exhibits a 12-fold increase in its K_m relative to that of L-aspartate, and a k_{cat} value identical (within experimental error) to that of L-aspartate. The reaction with L-cysteine sulfinic acid was verified by an alkaline phosphatase digest of the product, followed by purification and analysis by mass spectroscopy. The observed mass number of the nucleoside (395 amu) agrees with the expected mass number of the fully protonated $[MH]^+$ form of the nucleoside. Maleate, L-malate and succinate are competitive inhibitors with respect to L-aspartate, with maleate being the

most potent inhibitor (Table 4). Unlike the yeast enzyme, L-malate was not a substrate of the E. coli enzyme, producing no products even under prolonged incubation at concentrations of up to 100 mM. Fumarate does not inhibit the E. coli enzyme at concentrations up to 100 mM.

Discussion

SAICAR synthetase from E. coli has a Rapid Equilibrium Random kinetic mechanism (6). Under this model, the k_{cat} values presented in Table 3 are rate constants for the transformation of the enzyme-substrate complex into the enzyme-product complex, and the Michaelis constants for CAIR, ATP and L-aspartate are dissociation constants for each substrate from the complete substrate-enzyme complex. For rapid equilibrium mechanisms, changes in k_{cat} and K_m reflect changes in enzyme stabilization of the transition state and ligand affinity, respectively.

Mutations of Arg94, Ser100, and Arg199, each of which binds the 5′-phosphoryl group of CAIR, increase the dissociation of CAIR from the fully ligated enzyme and destabilize the transition state. Mutations at positions Arg94 and Arg199 also cause a relatively large increase in the K_m for L-aspartate, but the effect must be indirect because bound aspartate does not interact directly with Arg94 or Arg199. The binding of CAIR does appear to be important in the ordering the 30s loop, which interacts with L-aspartate extensively (35). Alanine mutations of Lys211 or Arg215 eliminate substrate saturation by L-aspartate. Mutations at five positions, then, elevate the K_m for L-aspartate, and three (Arg94, Arg199 and Arg215) of the four residues interact directly with CAIR. The most straightforward explanation is a CAIR-dependent association of L-aspartate: the 2′-

hydroxyl group of CAIR, (which directly binds to Arg215) may position Arg215 and Lys211 for the productive association of L-aspartate.

The role proposed for CAIR seems inconsistent with a Random kinetic mechanism for the wild-type enzyme (6). Random mechanisms have multiple pathways connecting the free enzyme to the complete enzyme-substrate complex. Flux through each of these pathways need not be equal. In the case of E. coli adenylosuccinate synthetase, for instance, IMP and GTP bind before L-aspartate in an overwhelming fraction of the turnovers (77). Hence, by analogy the binding of CAIR and ATP could precede the binding of L-aspartate in the vast majority of catalytic cycles. Human SAICAR synthetase interestingly adopts a Steady State Ordered mechanism in which CAIR binds first and L-aspartate last (78). In fact helix α5, which contains Lys211 Arg215, is disordered in crystal structures from Thermatoga maritima and Homo sapiens (11,12). This helix is a part of the CAIR binding pocket and interacts with the 30s loop and L-aspartate (35).

Nelson et al. (6) suggest a critical role for the α-amino group in the recognition of L-aspartate. Succinate should maintain the interactions of the carboxyl groups of the substrate without the steric repulsion of the α-amino group. Given the virtual absence of succinate inhibition of SAICAR synthetase (Table 4), interactions contributed by the α-amino group of L-aspartate must be critical to the stability of the ground-state complex. Indeed, the structure here seems rigid; the binding of succinate should create a one-atom void at the α-amino locus, easily sufficient to destabilize the complex (79). Bound L-malate would replace an amino group with a hydroxyl group, but also introduce a close contact involving the lone pair orbitals of that hydroxyl group and one of the Mg^{2+}-

coordinated water molecules. Hadacidin (N-formyl-N-hydroxyglycine), which retains only the β-carboxyl group of L-aspartate, diverges from L-aspartate at the α-amino and α-carboxyl groups. The N-hydroxyl group of hadacidin can bind either at the α-amino locus, and suffer the same poor non-bonded contact as the hydroxyl group of L-malate, or at one of the carboxyl loci, leaving a one-atom void at the α-amino locus. Hence, the lack of significant inhibition by hadacidin, succinate, and L-malate are attributable to improper fits to the α-amino locus.

The binding of L-aspartate as represented in the L-aspartate•sulfate•ADP•Mg^{2+} complex reveals how the amino acid substrate interacts with the protein. It demonstrates that the positioning of the α- and β-carboxyl groups is performed by the side chains of Ser33 and Arg215, as well as amides from the peptide linkages of the 30s loop. A model has been created superimposing the PAICAR•ADP•Mg^{2+} structure (an analogue of the proposed PCAIR intermediate) and the L-aspartate•sulfate•ADP•Mg^{2+}. The ADP molecule and magnesium ions map to identical positions in the PAICAR complex. The sulfate maps to the N-phosphoryl group of PAICAR. The result is a model of the fully-ligated SAICAR synthetase active site immediately preceding the attack by L-aspartate. The enzyme can enhance catalysis by pulling negative charge from the C4 atom of the phosphoryl intermediate of CAIR and by hydrogen bonding to the protons of the α-amino group of L-aspartate, positioning the lone-pair orbital for attack on the C4 atom. Mg^{2+} at sites 2 and 3 enhance the electrophilicity of the C4 atom. The phosphoryl group of the intermediate also acts to pull charge from the atom C4 through induction and provides a leaving group of low energy.

The model places the α-amino group of L-aspartate 2.6 Å away from the electrophilic C4 atom with a geometry favorable for the formation of a tetrahedral transition state. The α-amino of L-aspartate is 2.9 Å from nitrogen atom of the N-phosphoryl group of PAICAR, suggesting a possible path for proton transfer from the α-amino group of l-aspartate to the ester oxygen atom of the phosphoryl intermediate of CAIR. Alternatively, that same hydrogen atom from the α-amino group could participate in bifurcated hydrogen bond with one of the terminal oxygen atoms of the phosphoryl leaving group and the α-carboxyl group of L-aspartate.

As maleate is a competitive inhibitor with respect to L-aspartate (Table 4), it interacts with some of the elements that recognize the natural substrate. Its position overlaps the binding locus for the β-carboxyl group of L-aspartate. Maleate appears to bring in several water molecules that occupy the binding locus for the α-carboxylate of L-aspartate and interact with the C4 carboxyl group of CAIR.

The expected mass of a hexahistidyl-tagged subunit is 29.5 kDa, and hence the dimer observed in crystals structures should exhibit a mass of 59 kDa. Data from light scattering are consistent with a dimer in the absence of ligands, but indicate a decrease in apparent mass and radius of gyration in response to the addition of ligands. These changes in apparent mass and size are consistent with a conformational transition from an expanded dimer in the absence of ligands to a more compact dimer in the presence of ligands. As noted in the results section, the SAICAR-synthetase dimer of T. maritima, and now more recently the human bifunctional enzyme (12), is conformationally open relative to the ligated dimer of eSS (11,12,35). Hence, the reduction in the radius of

gyration of eSS could reflect a transition from a loosely folded state much like ligand-free tSS to a more compact and organized structure.

The properties of the Ala175 mutant protein suggest an important role for this residue in stabilizing the enzyme. More significantly perhaps is the CAIR-dependent/L-aspartate-independent hydrolysis of ATP exhibited by S33A, D36A, Del30, R94A, D175A, R199A, and K211A enzymes. Firstly, these enzymes do not hydrolyze ATP in the absence of CAIR, but require CAIR to enable ATP hydrolysis. For these mutant enzymes bound CAIR activates catalysis, but either allows water to compete with the 4-carboxyl group of CAIR for the γ-phosphoryl group of ATP or allows hydroxide to attack the carbonyl phosphate of CAIR. Conceivably, an analog of CAIR could activate the catalytic machinery of the synthetase, resulting in the unproductive hydrolysis of ATP. Such an analog would be harmful to cells both as an inhibitor of purine nucleotide biosynthesis and by depleting ATP.

SAICAR synthetase and adenylosuccinate synthetase from E. coli have Rapid Equilibrium Random kinetic mechanisms (6,77). For adenylosuccinate synthetase, L-aspartate binds last in the preferred pathway of substrate addition (54), and quite likely SAICAR synthetase also favors kinetic pathways in which L-aspartate binds last. The two enzymes in all likelihood catalyze the transfer of the γ-phosphoryl group of a nucleoside triphosphate (GTP for adenylosuccinate synthetase and ATP for SAICAR synthetase) to a nucleotide acceptor to form phosphoryl intermediates (6-phosphoryl-IMP and the carbonyl phosphate of CAIR in the former and latter systems, respectively) (6,48). Crystallographic structures and directed mutations of adenylosuccinate synthetase indicate a significant role for the 5′-phosphoryl group of IMP in organizing the active site

of the enzyme (52,80-82). Activation of the catalytic machinery by the binding of the nucleotide acceptor would in principle reduce unproductive hydrolysis of the nucleoside triphosphate. Work here suggests that CAIR could also organize the active site of SAICAR synthetase. Finally, the 2′-hydroxyl group of bound IMP interacts with an arginyl side chain (residue 303 in E. coli adenylosuccinate synthetase) essential to the recognition of L-aspartate (82,83). Similarly, SAICAR synthetase uses the 2′-hydroxyl group of CAIR to localize an arginyl side chain (Arg215) that is essential for the binding of L-aspartate (35).

These similarities probably have not come about through divergent evolution from a common primordial ancestor: the folds of the polypeptide chains for adenylosuccinate synthetase and SAICAR synthetase differ significantly, suggesting the pre-existence of a chemical mechanism that was recognized in early times by at least two different proteins. Perhaps initially, these proteins did little more than bind unstable phosphoryl intermediates, protecting them from unproductive hydrolysis. In these primordial systems, the recognition of L-aspartate may have begun through a fortuitous hydrogen bond with the 2′-hydroxyl group of the phosphoryl intermediate.

References

1. Lukens, L. N., and Buchanan, J. M. (1959) J Biol Chem 234(7), 1791-1798
2. Miller, R. W., and Buchanan, J. M. (1962) J Biol Chem 237, 485-490
3. Patey, C. A., and Shaw, G. (1973) Biochem J 135(3), 543-545
4. Firestine, S. M., and Davisson, V. J. (1994) Biochemistry 33(39), 11917-11926
5. Meyer, E., Leonard, N. J., Bhat, B., Stubbe, J., and Smith, J. M. (1992) Biochemistry 31(21), 5022-5032
6. Nelson, S. W., Binkowski, D. J., Honzatko, R. B., and Fromm, H. J. (2005) Biochemistry 44(2), 766-774

7. Antonyuk, S. V., Grebenko, A. I., Levdikov, V. M., Urusova, D. V., Melik-Adamyan, V. R., Lamzin, V. S., and Wilson, K. S. (2001) Crystallography Reports 46(4), 687-691
8. Levdikov, V. M., Grebenko, A. I., Barynin, V. V., Melik-Adamyan, W. R., Lamzin, V. S., and Wilson, K. S. (1996) Crystallography Reports 41(2), 275-286
9. Levdikov, V. M., Barynin, V. V., Grebenko, A. I., Melik-Adamyan, W. R., Lamzin, V. S., and Wilson, K. S. (1998) Structure 6(3), 363-376
10. Urusova, D. V., Antonyuk, S. V., Grebenko, A. I., Lamzin, V. S., and Melik-Adamyan, V. R. (2003) Crystallography Reports 48(5), 763-767
11. Zhang, R., Skarina, T., Evdokimova, E., Edwards, A., Savchenko, A., Laskowski, R., Cuff, M. E., and Joachimiak, A. (2006) Acta Crystallograph Sect F Struct Biol Cryst Commun 62(Pt 4), 335-339
12. Li, S. X., Tong, Y. P., Xie, X. C., Wang, Q. H., Zhou, H. N., Han, Y., Zhang, Z. Y., Gao, W., Li, S. G., Zhang, X. C., and Bi, R. C. (2007) J Mol Biol 366(5), 1603-1614
13. Batova, A., Diccianni, M. B., Omura-Minamisawa, M., Yu, J., Carrera, C. J., Bridgeman, L. J., Kung, F. H., Pullen, J., Amylon, M. D., and Yu, A. L. (1999) Cancer Res 59(7), 1492-1497
14. Levenberg, B., and Buchanan, J. M. (1957) J Biol Chem 224(2), 1019-1027
15. Hartman, S. C., and Buchanan, J. M. (1958) J Biol Chem 233(2), 451-455
16. Hartman, S. C., and Buchanan, J. M. (1959) J Biol Chem 234(7), 1812-1816
17. Kappock, T. J., Ealick, S. E., and Stubbe, J. (2000) Curr Opin Chem Biol 4(5), 567-572
18. Zalkin, H., and Dixon, J. E. (1992) Prog Nucleic Acid Res Mol Biol 42, 259-287
19. Nygaard, P., and Smith, J. M. (1993) J Bacteriol 175(11), 3591-3597
20. Thoden, J. B., Firestine, S., Nixon, A., Benkovic, S. J., and Holden, H. M. (2000) Biochemistry 39(30), 8791-8802
21. Marolewski, A., Smith, J. M., and Benkovic, S. J. (1994) Biochemistry 33(9), 2531-2537
22. Gots, J. S., Benson, C. E., Jochimsen, B., and Koduri, K. R. (1977) Ciba Found Symp (48), 23-41
23. Gots, J. S., Benson, C. E., Jochimson, B., and Koduri, K. R. (1976) Purine and Pyrimidine Metabolism, Elsevier, Amsterdam
24. Mueller, E. J., Meyer, E., Rudolph, J., Davisson, V. J., and Stubbe, J. (1994) Biochemistry 33(8), 2269-2278
25. Tyagi, A. K., and Cooney, D. A. (1980) Cancer Res 40(12), 4390-4397
26. Anandaraj, S. J., Jayaram, H. N., Cooney, D. A., Tyagi, A. K., Han, N., Thomas, J. H., Chitnis, M., and Montgomery, J. A. (1980) Biochem Pharmacol 29(2), 227-245
27. Casey, P. J., and Lowenstein, J. M. (1987) Biochem Pharmacol 36(5), 705-709
28. Illei, P. B., Rusch, V. W., Zakowski, M. F., and Ladanyi, M. (2003) Clin Cancer Res 9(6), 2108-2113
29. Batova, A., Diccianni, M. B., Nobori, T., Vu, T., Yu, J., Bridgeman, L., and Yu, A. L. (1996) Blood 88(8), 3083-3090
30. Efferth, T., Gebhart, E., Ross, D. D., and Sauerbrey, A. (2003) Biochem Pharmacol 66(4), 613-621

31. Li, W., Su, D., Mizobuchi, H., Martin, D. S., Gu, B., Gorlick, R., Cole, P., and Bertino, J. R. (2004) Oncol Res 14(7-8), 373-379
32. Efferth, T., Miyachi, H., Drexler, H. G., and Gebhart, E. (2002) Blood Cells Mol Dis 28(1), 47-56
33. Thoden, J. B., Kappock, T. J., Stubbe, J., and Holden, H. M. (1999) Biochemistry 38(47), 15480-15492
34. Mathews, II, Kappock, T. J., Stubbe, J., and Ealick, S. E. (1999) Structure 7(11), 1395-1406
35. Ginder, N. D., Binkowski, D. J., Fromm, H. J., and Honzatko, R. B. (2006) J Biol Chem 281(30), 20680-20688
36. Ostanin, K. V., Alenin, V. V., Domkin, V. D., and Smirnov, M. N. (1989) Biokhimiia 54(8), 1265-1273
37. Alenin, V. V., Ostanin, K. V., Kostikova, T. R., Domkin, V. D., Zubova, V. A., and Smirnov, M. N. (1992) Biokhimiia 57(6), 845-855
38. Firestine, S. M., Misialek, S., Toffaletti, D. L., Klem, T. J., Perfect, J. R., and Davisson, V. J. (1998) Arch Biochem Biophys 351(1), 123-134
39. Schmuke, J. J., Davisson, V. J., Bonar, S. L., Gheesling Mullis, K., and Dotson, S. B. (1997) Yeast 13(8), 769-776
40. Minet, M., and Lacroute, F. (1990) Curr Genet 18(4), 287-291
41. Chen, Z. D., Dixon, J. E., and Zalkin, H. (1990) Proc Natl Acad Sci U S A 87(8), 3097-3101
42. Schild, D., Brake, A. J., Kiefer, M. C., Young, D., and Barr, P. J. (1990) Proc Natl Acad Sci U S A 87(8), 2916-2920
43. Iwahana, H., Honda, S., Tsujisawa, T., Takahashi, Y., Adzuma, K., Katashima, R., Yamaoka, T., Moritani, M., Yoshimoto, K., and Itakura, M. (1995) Biochim Biophys Acta 1261(3), 369-380
44. Som, I., Mitsch, R. N., Urbanowski, J. L., and Rolfes, R. J. (2005) Eukaryot Cell 4(10), 1725-1735
45. Litchfield, G. J., and Shaw, G. (1971) J Chem Soc (B), 1474-1484
46. Honzatko, R. B., Stayton, M. M., and Fromm, H. J. (1999) Adv Enzymol Relat Areas Mol Biol 73, 57-102, ix-x
47. Lieberman, I. (1956) J Biol Chem 223(1), 327-339
48. Fromm, H. J. (1958) Biochim Biophys Acta 29(2), 255-262
49. Honzatko, R. B., and Fromm, H. J. (1999) Arch Biochem Biophys 370(1), 1-8
50. Poland, B. W., Bruns, C., Fromm, H. J., and Honzatko, R. B. (1997) J Biol Chem 272(24), 15200-15205
51. Choe, J. Y., Poland, B. W., Fromm, H. J., and Honzatko, R. B. (1999) Biochemistry 38(21), 6953-6961
52. Iancu, C. V., Borza, T., Fromm, H. J., and Honzatko, R. B. (2002) J Biol Chem 277(30), 26779-26787
53. Bass, M. B., Fromm, H. J., and Rudolph, F. B. (1984) J Biol Chem 259(20), 12330-12333
54. Cooper, B. F., Fromm, H. J., and Rudolph, F. B. (1986) Biochemistry 25(23), 7323-7327
55. Markham, G. D., and Reed, G. H. (1978) J Biol Chem 253(17), 6184-6189

56. Chipperfield, J. R., Humble, R. W., Iveson, G., Kadir, K., Mackenzie, G., and Shaw, G. (1987) Nucleosides and Nucleotides 6(1&2), 353-358
57. Chipperfield, J. R., Humble, R. W., Iveson, G., Kadir, K., Mackenzie, G., and Shaw, G. (1988) Nucleosides and Nucleotides 7(5&6), 571-576
58. Groziak, M. P., Bhat, B., and Leonard, N. J. (1988) Proc Natl Acad Sci U S A 85(19), 7174-7176
59. Groziak, M. P., Huan, Z. W., Ding, H., Meng, Z., Stevens, W. C., and Robinson, P. D. (1997) J Med Chem 40(21), 3336-3345
60. Constantine, C. Z., Starks, C. M., Mill, C. P., Ransome, A. E., Karpowicz, S. J., Francois, J. A., Goodman, R. A., and Kappock, T. J. (2006) Biochemistry 45(27), 8193-8208
61. Hoskins, A. A., Morar, M., Kappock, T. J., Mathews, II, Zaugg, J. B., Barder, T. E., Peng, P., Okamoto, A., Ealick, S. E., and Stubbe, J. (2007) Biochemistry 46(10), 2842-2855
62. Firestine, S. M., Poon, S. W., Mueller, E. J., Stubbe, J., and Davisson, V. J. (1994) Biochemistry 33(39), 11927-11934
63. Perfect, J. R., Toffaletti, D. L., and Rude, T. H. (1993) Infect Immun 61(10), 4446-4451
64. Donovan, M., Schumuke, J. J., Fonzi, W. A., Bonar, S. L., Gheesling-Mullis, K., Jacob, G. S., Davisson, V. J., and Dotson, S. B. (2001) Infect Immun 69(4), 2542-2548
65. Cheville, N. F., Olsen, S. C., Jensen, A. E., Stevens, M. G., Florance, A. M., Houng, H. S., Drazek, E. S., Warren, R. L., Hadfield, T. L., and Hoover, D. L. (1996) Infect Immun 64(7), 2431-2439
66. Gale, G. R., and Smith, A. B. (1968) Biochem Pharmacol 17(12), 2495-2498
67. Baillon, J., Tauc, P., and Herve, G. (1985) Biochemistry 24(25), 7182-7187
68. Srivastava, P. C., Mancuso, R. W., Rousseau, R. J., and Robins, R. K. (1974) J Med Chem 17(11), 1207-1211
69. Yoshikawa, M., Kato, T., and Takenishi, T. (1967) Tetrahedron Lett 50, 5065-5068
70. Bradford, M. M. (1976) Anal Biochem 72, 248-254
71. Leatherbarrow, R. J. (2001) Grafit. In., 5 Ed., Erithacus Software Ltd.
72. Kuzmic, P. (1996) Anal Biochem 237(2), 260-273
73. 4, C. C. P. N. (1994) Acta Crystallogr D Biol Crystallogr 50, 760-763
74. McRee, D. E. (1992) J Mol Graph 10(44-46)
75. Brunger, A. T., Adams, P. D., Clore, G. M., DeLano, W. L., Gros, P., Grosse-Kunstleve, R. W., Jiang, J. S., Kuszewski, J., Nilges, M., Pannu, N. S., Read, R. J., Rice, L. M., Simonson, T., and Warren, G. L. (1998) Acta Crystallogr D Biol Crystallogr 54, 905-921
76. Engh, R. A., and Huber, R. (1991) Acta Crystallogr A47, 392-400
77. Rudolph, F. B., and Fromm, H. J. (1969) J Biol Chem 244(14), 3832-3839
78. Binkowski, D. J., Ginder, N. D., Fromm, H. J., and Honzatko, R. B. (2008) Biochemistry Submitted for publication
79. Iancu, C. V., Zhou, Y., Borza, T., Fromm, H. J., and Honzatko, R. B. (2006) Biochemistry 45(38), 11703-11711

80. Hou, Z., Wang, W., Fromm, H. J., and Honzatko, R. B. (2002) J Biol Chem 277(8), 5970-5976
81. Kang, C., Sun, N., Poland, B. W., Gorrell, A., Honzatko, R. B., and Fromm, H. J. (1997) J Biol Chem 272(18), 11881-11885
82. Poland, B. W., Fromm, H. J., and Honzatko, R. B. (1996) J Mol Biol 264(5), 1013-1027
83. Thompson, J. D., Higgins, D. G., and Gibson, T. J. (1994) Nucleic Acids Res 22(22), 4673-4680
84. Kraulis, P. J. (1991) J Appl Crystallogr 24, 946-950

Table I. Statistics of Crystallographic Data Collection and Refinement

Ligand Complex	Maleate, CAIR, ADP, Mg^{2+}	L-aspartate, CAIR, ADP, Mg^{2+}
Space Group	$P2_12_12_1$	$P2_12_12_1$
Unit Cell Parameters	a=59.29, b=67.18, c=145.83	a=59.31, b=67.67, c=148.36
Resolution	61.02 – 2.07 (2.18 – 2.07)	61.57 – 2.30 (2.48 – 2.30)
Reflections	201,911	189,939
Unique Reflections	33,423	27,228
% Completeness	92.3 (64.4)	99.9 (99.9)
R_{merge} [a]	0.080 (0.243)	0.073 (0.243)
No. of atoms	4,216	4,075
No of solvent sites	283	194
R_{factor} [b]	21.6	20.8
R_{free} [c]	26.0	25.0
Mean B for protein ($Å^2$)	30.2	26.0
Mean B for ligands ($Å^2$)	27.4	30.7
Mean B for waters ($Å^2$)	31.7	32.0
Bond lengths (Å)	0.006	0.007
Bond angles (deg.)	1.2	1.3
Dihedral angles (deg.)	22.7	22.8
Improper angles (deg.)	0.73	1.41

Table II. Footnotes.

[a] $R_{merge} = \Sigma_j\Sigma_i \mid I_{ij} - \langle I_j \rangle \mid / \Sigma_i\Sigma_j I_{ij}$, where i runs over multiple observations of the same intensity, and j runs over all crystallographically unique intensities.

[b] $R_{factor} = \Sigma \mid\mid F_{obs} \mid - \mid F_{calc} \mid\mid / \Sigma \mid F_{obs} \mid$, where $\mid F_{obs} \mid > 0$.

[c] R_{free} based upon 10% of the data randomly culled and not used in the refinement.

Table 2. Variation of radius of gyration and apparent molecular weight with ligation of ***E. coli*** SAICAR synthetase.

Ligands	Radius (nm)	Molecular weight (kDa)
none	3.55±0.01	65.1±0.4
ADP	3.43±0.02	60.2±0.6
CAIR	3.38±0.01	58.6±0.9
CAIR, L-aspartate	3.39±0.04	59±2
ADP, CAIR	3.36±0.04	58.0±2
ADP, CAIR, L-aspartate	3.38±0.04	58±2

Table 3. Kinetic Parameters of wild-type and mutant SAICAR synthetases.

Construct	K_m ATP (μM)	K_m CAIR (μM)	K_m L-aspartate (mM)	k_{cat}[c] (s^{-1})
Wild-type	50 ± 5	4.1 ± 0.8	0.72 ± 0.06	6.2 ± 0.2
Arg94→Ala	150 ± 10	290 ± 50	9 ± 3	0.9 ± 0.1
Ser100→Ala	46 ± 6	19 ± 2	2.06 ± 0.05	5.9 ± 0.2
Asp175→Ala[a]	420 ± 20	380 ± 30	0.6 ± 0.1	3.00 ± 0.07
Arg199→Ala	50 ± 7	58 ± 5	23 ± 3	0.13 ± 0.01
Arg215→Ala[a]	26 ± 2	5.2 ± 0.5	NA	0.094 ± 0.002
Lys211→Ala[a]	23 ± 3	6.0 ± 0.6	NA	0.049 ± 0.002
Asp^{36}→Asn	38 ± 4	2.3 ± 0.5	0.9 ± 0.1	3.5 ± 0.1
Asp^{36}→Ala[b]	NA	NA	NA	NA
Del30[b]	NA	NA	NA	NA
Ser^{33}→Ala[b]	65 ± 2	4.8 ± 0.8	19 ± 6	4.4 ± 0.4

Table 3. Footnotes.

[a]Psuedo first-order in L-aspartate from 1–50 mM with ATP and CAIR at concentrations of 260 and 50 μM, respectively. The parameter k_{cat} for this mutant enzyme is the slope of the linear variation of initial velocity vs. the concentration of L-aspartate with ATP and CAIR at concentrations of 260 and 50 μM, respectively. K_m values for CAIR and ATP are determined at an L-aspartate concentration of 50 mM.

[b]ΔA_{282} observed when in the presence of ATP and CAIR alone.

[c]Values for k_{cat} come from data taken at saturating CAIR and ATP, and varied concentrations of L-aspartate.

Table 4. Recognition of L-aspartate analogs by wild-type SAICAR synthetase from E. coli.

Substrate/Inhibitor	K_m or K_i (mM)
L-Aspartate[a]	0.77±0.08
L-Alanosine[a]	0.83±0.05
L-Cysteine sulfinate[a]	5.6±0.3
L-Malate[b]	20±1
Maleate[b]	1.6±0.3
Succinate[b]	64±5

Table 4. Footnotes.
[a]k_{cat} value identical (within experimental error) to that of the wild-type enzyme in Table 3.
[b]Linear competitive inhibitor with respect to L-aspartate.

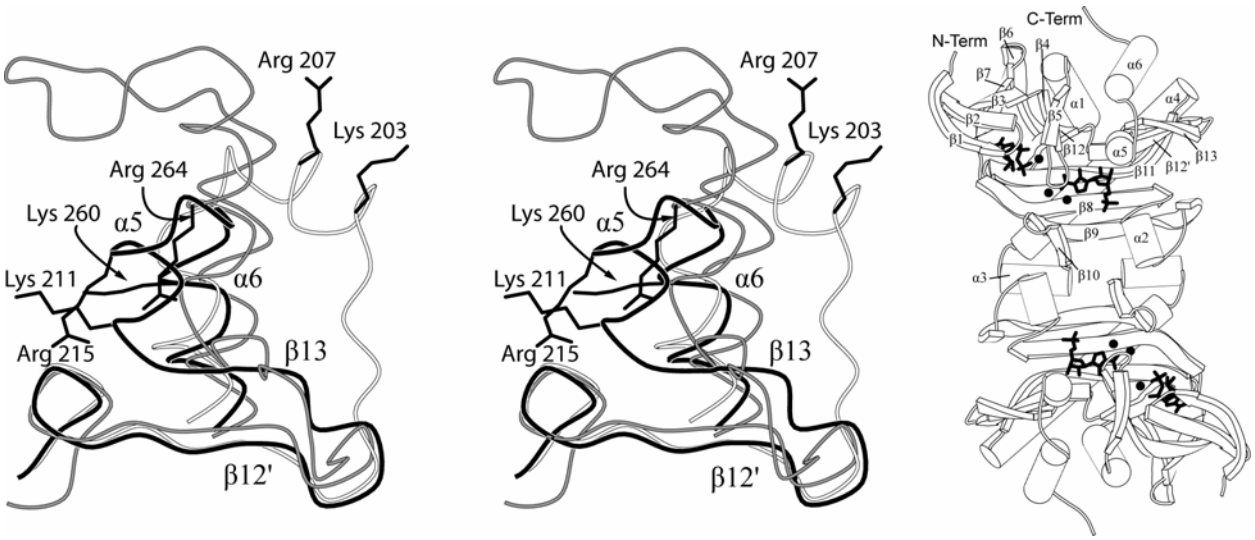

Figure 1. Structural and conformational variation in microbial SAICAR synthetases. Stereoview of elements putatively involved in the binding of L-aspartate for the synthetases from E. coli (PDB identifier 2GQS, black trace with residues 211&215), S. cerevisiae (PDB identifier 1OBG, grey trace with residues 260&264), and T. maritima (PDB identifier 1KUT, white trace with residues 203&207) (left). Helix α5 specifically exhibits significant conformational variation. Overview of the synthetase from E. coli, placing regions of conformational change in the context of the ADP•CAIR-ligated dimer (right).

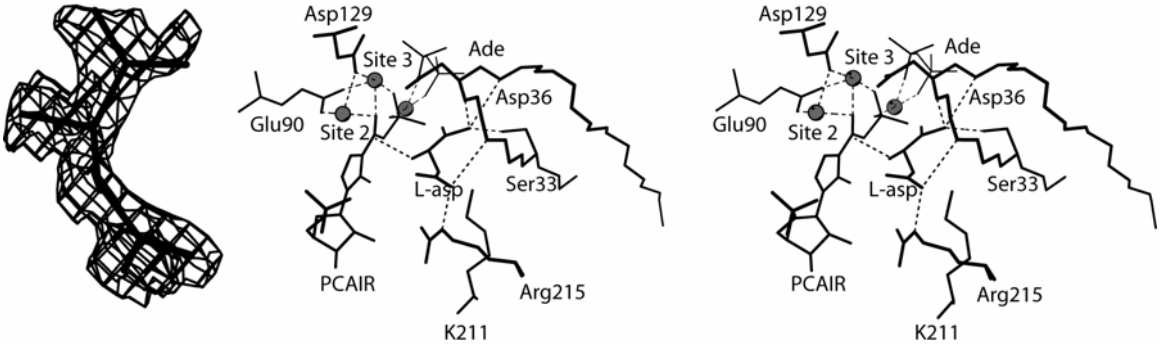

Figure 2. Stereoview of the productive binding of L-aspartate to the active site of ***E. coli*** SAICAR synthetase. Dashed lines indicate donor–acceptor interactions, with L-aspartate labeled L-asp. Mg^{2+} ions are grey-shaded spheres. Magnesium site 1 is not labeled for clarity. This figure was draw with MOLSCRIPT (84)

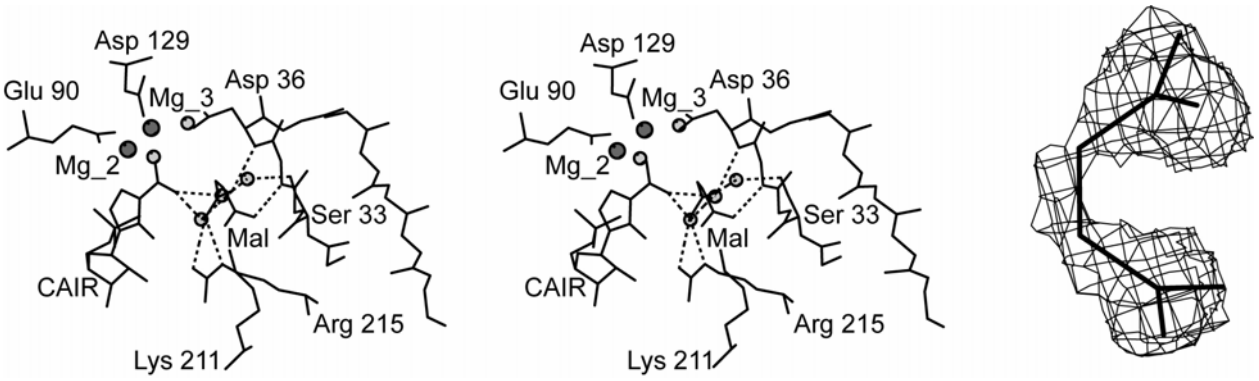

Figure 3. Crystal structure of the maleate•ADP•CAIR complex of ***E. coli*** SAICAR synthetase. Stereoview of maleate (labeled MAL) in the active site (left). Mg^{2+} ions are grey-shaded spheres and water molecules open spheres. Dashed lines indicate donor–acceptor interactions involving maleate. This image was draw with MOLSCRIPT (84). Omit electron density associated with bound maleate contoured at 1σ with a cutoff radius of 1 Å (right). This image was draw by XTALVIEW (74).

Chapter VI. General Conclusions

Studies described here mark a significant expansion of our understanding of the reaction of SAICAR synthetase. Prior to this work, little was understood about the substrate binding of CAIR, and L-aspartate. Some information was present for the binding of adenine nucleotide and Mg^{2+} at site 1, but there was ambiguity as to what the correct binding mode was. Additionally, significant conformational differences existed in regions near portions of the enzyme proposed to be the active site.

This work was the first to demonstrate CAIR binding in the enzyme and revealed the interaction of two previously unknown Mg^{2+} ions with this substrate. The residues interacting with Mg^{2+} ions are conserved and, along with the C7 carboxyl oxygen of CAIR, define two binding sites, known as sites 1 and 2. The structure of CAIR, Mg^{2+}, and ADP formed the basis for a phosphoryl transfer model. This model presented inline geometry between the carboxyl carbon of CAIR and the oxygen leaving group of the β-phosphoryl group of ATP. Extensive metal interactions of good geometry as well as three lysines from the protein stabilize the charge on the modeled phosphoryl intermediate. The identity of the CAIR binding site was confirmed kinetically by the significant increase of K_m observed in mutations of residues that interacted with 5′-phosphoryl group of CAIR in the crystal structure.

The co-crystallization of SAICAR synthetase with CAIR analogues, AICAR and IMP, and adenine nucleotides revealed the N-linked phosphoryl intermediates, PAICAR and 1-PIMP. These intermediates were phosphorylated at positions structurally analogous to the carboxyl position of CAIR modeled in the previous phosphoryl transfer model. Although a phosphoryl-CAIR intermediate could not be trapped, these

intermediates demonstrated that similar compounds could be formed by the enzyme. Perhaps their persistence in the active site is related to an intrinsically more stable N-P bond linkage. The interactions of the phosphoryl group were similar to that of the phosphoryl intermediate that was modeled as described above, except Lys^{123} was not found to interact with the phosphoryl intermediate and the base of the phosphorylated intermediate was tilted relative to the substrate.

Evidence for the formation of a PCAIR intermediate was demonstrated using positional isotope exchange (PIX). If bond cleavage happens between the β- and γ-phosphoryl groups and a stable intermediate is formed when enzyme is mixed with γ-^{18}O-ATP, PIX can be observed. This is caused by the rotation around any of the remaining phosphoryl group bonds of ADP moving the bridging ^{18}O into a non-bridging position and an ^{16}O into the bridging position. If the system is at equilibrium and the ATP is in significant exchange with the bulk solvent, significant isotope scrambling can be observed. The two species, ^{18}O in the bridging position or ^{16}O in the bridging position, have different chemical shifts in ^{31}P NMR. When γ-^{18}O-ATP or a mixture of L-aspartate and γ-^{18}O- ATP are mixed with enzyme, no scrambling occurs. When γ-^{18}O-ATP is mixed with CAIR and enzyme, scrambling is observed, indicating that CAIR is necessary for a phosphoryl intermediate to be formed.

Finally, the L-aspartate binding site was observed through crystal structures as well as site-directed mutagenesis. Co-crystallization of the E. coli enzyme with CAIR, ATP, $MgSO_4$, and L-aspartate yielded ADP, Mg^{2+}, sulfate, and L-aspartate in the active site. The sulfate group superimposes where the phosphoryl groups of PAICAR and 1-IMP are within coordinate uncertainty. This revealed extensive interactions with the 30s

loop, as well as the contribution of binding from residues Lys^{211} and Arg^{215} of the α5 helix. Site directed mutations in those regions revealed a functional impact on L-aspartate binding.

Prior to the commencement of this work, the kinetic mechanism of E. coli SAICAR synthetase was determined by members from the lab. It was found to be Sequential Rapid Equilibrium Random. Work on the kinetic mechanism of the human homologue commenced thereafter. Human SAICAR synthetase activity is paired on a single polypeptide with AIR carboxylase activity, therefore the decomposition of CAIR to AIR competes for substrate when trying to characterize the SAICAR synthetase reaction. In order to prevent this NAIR (a nitro analogue of CAIR) which potently and specifically inhibits the AIR carboxylase reaction was used. Another strategy for removing AIR carboxylase activity was also explored by creating the mutant enzyme K304A. Based upon homology modeling against the isozyme from E. coli, this was predicted to be a critical residue for binding CAIR. Indeed, activity was reduced to the non-catalyzed rate of decarboxylation of CAIR. Unlike the E. coli enzyme, human SAICAR synthetase was found to have a Sequential Steady State Ordered mechanism, with CAIR binding first, ATP second, and L-aspartate last. The K_m for CAIR was found to be ~10 μM for the NAIR-inhibited enzyme and ~1μM for the K304A enzyme. None of the other kinetic parameters changed significantly. K_a's for steady state mechanisms are combinations of elementary kinetics constants. All of the k's comprising the K_m of CAIR are present in other kinetics terms except for k_1, which is, therefore, the most likely cause of the difference between the two systems. This term is associated with the binding rate of CAIR to the unligated enzyme. Since NAIR is observed kinetically and

structurally to compete for the same site as CAIR for the AIR carboxylase domain, it is reasonable to conclude that the site is occupied during the measurement of the SAICAR synthetase reaction. Since K304A is directed at a site that has been demonstrated to interact with the binding of the 5′ phosphoryl group, it is likely shutting down the enzyme by preventing binding and not by merely blocking catalysis. Thus the K304A mutant likely represents a system where nothing is bound in the CAIR pocket of AIR carboxylase. This implicates a communication between the status of ligation of the binding site and the on-rate of CAIR to the SAICAR synthetase active site.

This information represents a step forward in our basic understanding of SAICAR synthetase to the de novo purine biosynthesis pathway. This fundamental enzymology lays the groundwork necessary for future work in drug design or protein engineering. Since de novo purine biosynthesis is central to cell proliferation, it can be a point of control for the rapidly dividing cells of tumors or microbial infections. As computational methods for calculating inhibitor binding to proteins improves, it is likewise important to present the best beginning protein models. The structural basis for ligand binding presented here can give clues as to which functional groups and what distances should be considered when designing scaffolds for drugs. Additionally the various states of ligation can provide understanding of the volume constraints necessary to maximize Vander Waals interactions. It also represents a developed and well-characterized system in which the effectiveness of these compounds can be tested. Kinetic differences apparent between the E. coli and human homologues adds to the possibility that significant differences do exist between the enzymes and that this difference might be exploited to selectively inhibit microbial forms of the enzyme. In the case of the human system, the

results of studying the kinetic mechanism shows how a bifunctional enzyme can be used to kinetically regulate the flux through a system. This presents an alternate line of explanation to that of substrate-channeling which had been suggested previously.